(4)

David Taylor Research Center

Bethesda, Maryland 20084-5000

AD-A217 253

DTRC/SHD-1223-05 December 1989

Ship Hydromechanics Department
Research and Development Report

Nonlinear Subharmonic Roll Response of a SWATH Ship in Regular Beam Seas

by
Christopher J. Hart

DTRC/SHD-1223-05 Nonlinear Subharmonic Roll Response of a SWATH Ship in Regular Beam Seas

MAJOR DTRC TECHNICAL COMPONENTS

CODE 011 DIRECTOR OF TECHNOLOGY, PLANS AND ASSESSMENT

12 SHIP SYSTEMS INTEGRATION DEPARTMENT

14 SHIP ELECTROMAGNETIC SIGNATURES DEPARTMENT

15 SHIP HYDROMECHANICS DEPARTMENT

16 AVIATION DEPARTMENT

17 SHIP STRUCTURES AND PROTECTION DEPARTMENT

18 COMPUTATION, MATHEMATICS & LOGISTICS DEPARTMENT

19 SHIP ACOUSTICS DEPARTMENT

27 PROPULSION AND AUXILIARY SYSTEMS DEPARTMENT

28 SHIP MATERIALS ENGINEERING DEPARTMENT

DTRC ISSUES THREE TYPES OF REPORTS:

1. **DTRC reports, a formal series,** contain information of permanent technical value. They carry a consecutive numerical identification regardless of their classification or the originating department.

2. **Departmental reports, a semiformal series,** contain information of a preliminary, temporary, or proprietary nature or of limited interest or significance. They carry a departmental alphanumerical identification.

3. ***Technical memoranda*, an informal series,** contain technical documentation of limited use and interest. They are primarily working papers intended for internal use. They carry an identifying number which indicates their type and the numerical code of the originating department. Any distribution outside DTRC must be approved by the head of the originating department on a case-by-case basis.

NDW-DTNSRDC 5602/51 (Rev 2-88)

UNCLASSIFIED

SECURITY CLASSIFICATION OF THIS PAGE

REPORT DOCUMENTATION PAGE

Form Approved OMB No. 0704-0188

1a. REPORT SECURITY CLASSIFICATION: UNCLASSIFIED	1b. RESTRICTIVE MARKINGS
2a. SECURITY CLASSIFICATION AUTHORITY	3. DISTRIBUTION / AVAILABILITY OF REPORT: Approved for public release; distribution is unlimited.
2b. DECLASSIFICATION / DOWNGRADING SCHEDULE	
4. PERFORMING ORGANIZATION REPORT NUMBER(S): DTRC/SHD-1223-05	5. MONITORING ORGANIZATION REPORT NUMBER(S)
6a. NAME OF PERFORMING ORGANIZATION: David Taylor Research Center / 6b. OFFICE SYMBOL (If applicable): Code 1562	7a. NAME OF MONITORING ORGANIZATION
6c. ADDRESS (City, State, and Zip Code): Bethesda, MD 20084-5000	7b. ADDRESS (City, State, and Zip Code)
8a. NAME OF FUNDING / SPONSORING ORGANIZATION: ONR / 8b. OFFICE SYMBOL (If applicable)	9. PROCUREMENT INSTRUMENT IDENTIFICATION NUMBER
8c. ADDRESS (City, State, and Zip Code): Office of the Chief of Naval Research, Arlington, VA 22217-5000	10. SOURCE OF FUNDING NUMBERS: PROGRAM ELEMENT NO. 61153N / PROJECT NO. / TASK NO. / WORK UNIT ACCESSION NO. 509006

11. TITLE (Include Security Classification): Nonlinear Subharmonic Roll Response of a SWATH Ship in Regular Beam Seas

12. PERSONAL AUTHOR(S): Hart, Christopher J.

13a. TYPE OF REPORT	13b. TIME COVERED	14. DATE OF REPORT (Year, Month, Day)	15. PAGE COUNT
Final	FROM _____ TO _____	1989 December	107

16. SUPPLEMENTARY NOTATION

17. COSATI CODES			18. SUBJECT TERMS (Continue on reverse if necessary and identify by block number)
FIELD	GROUP	SUB-GROUP	SWATH Seakeeping, Nonlinear Rolling, Mathieu Instability, Parametric or Subharmonic Roll Response

19. ABSTRACT (Continue on reverse if necessary and identify by block number)

One of the primary virtues of a Small Waterplane Area Twin Hull (SWATH) ship is its low motion characteristics in severe seas. By varying the appropriate inertial and geometric parameters, designers can 'de-tune' a SWATH ships' motion responses for a particular expected operating environment. Using model test data and linearly based motion prediction simulations, the effects of various design changes on motions can be studied. The occurrence of subharmonic roll motion has been observed in several past SWATH experiments and is not predicted using linear techniques. This nonlinear response has generally occurred on designs where the natural roll frequency is roughly half of the natural heave frequency. However, the extent of the boundaries of this instability, has not been well defined for a SWATH ship.

The objective of this investigation, therefore, is to provide experimental results defining the stability boundary for the roll motion of a SWATH drifting in beam seas and to study the possible cause of this phenomenon using a nonlinear math model of the coupled heave-roll response. Presented are the results of wave tank tests conducted on a model representing a 2900 ton SWATH ship drifting at zero speed in 'regular'

20. DISTRIBUTION / AVAILABILITY OF ABSTRACT: ☐ UNCLASSIFIED/UNLIMITED ☒ SAME AS RPT ☐ DTIC USERS	21. ABSTRACT SECURITY CLASSIFICATION: UNCLASSIFIED
22a. NAME OF RESPONSIBLE INDIVIDUAL: Christopher J. Hart	22b. TELEPHONE (Include Area Code): 202-227-1554 / 22c. OFFICE SYMBOL: Code 1562

DD Form 1473, JUN 86 *Previous editions are obsolete.*

SECURITY CLASSIFICATION OF THIS PAGE

UNCLASSIFIED

(Block 19 Continued)

(monochromatic) beam waves. Regular wave (linear) transfer functions are presented along with natural periods and damping characteristics. The amplitude and frequency envelope in which the subharmonic response occurs is provided along with a qualitative description of the combined motion characteristics near the stability boundaries. Also presented are results using a theoretical model based on a Mathieu-like expression of the heave-coupled roll response. The experimental results are compared with the theoretical model, with reasonable qualitative correlation.

PREFACE

(To Report # DTRC/SHD-1223-05)

This report presents the contents of a thesis submitted to the George Washington University (GWU) School of Engineering and Applied Science in partial satisfaction of the degree requirements of the Ocean and Marine Engineering Masters Degree Program, which is sponsored by the Ship Hydromechanics Department at David Taylor Research Center (DTRC). The thesis, entitled "Nonlinear Subharmonic Roll Response of a SWATH Ship in Regular Beam Seas," is being presented as a departmental report in order that the information receive greater distribution and be more readily available to the research community. This report is simply a reproduction of the manuscript presented to GWU and no effort has been made to further edit or reformat the document. As such, it does not entirely conform to the usual editorial requirements or format of a typical Departmental report.

While this project was initiated and performed primarily on personal time, the completion of the research (particularly the analytical modeling and documentation stages) was made possible by (and may not have been possible without) funding provided under the Applied Hydrodynamic Research (AHR) program of the Office of Naval Research (ONR). This program is managed at ONR by Mr. Jim Fein and administered at DTRC by Mr. Vincent Monacella, of Code 1504. The author wishes to express his appreciation to both these gentlemen for their interest and support.

It is hoped that the lessons learned, and the information presented in this report on the subharmonic rolling behavior of Small Waterplane Area Twin Hull (SWATH) Ships will be of benefit to those working in the area of SWATH ship dynamics.

Christopher John Hart

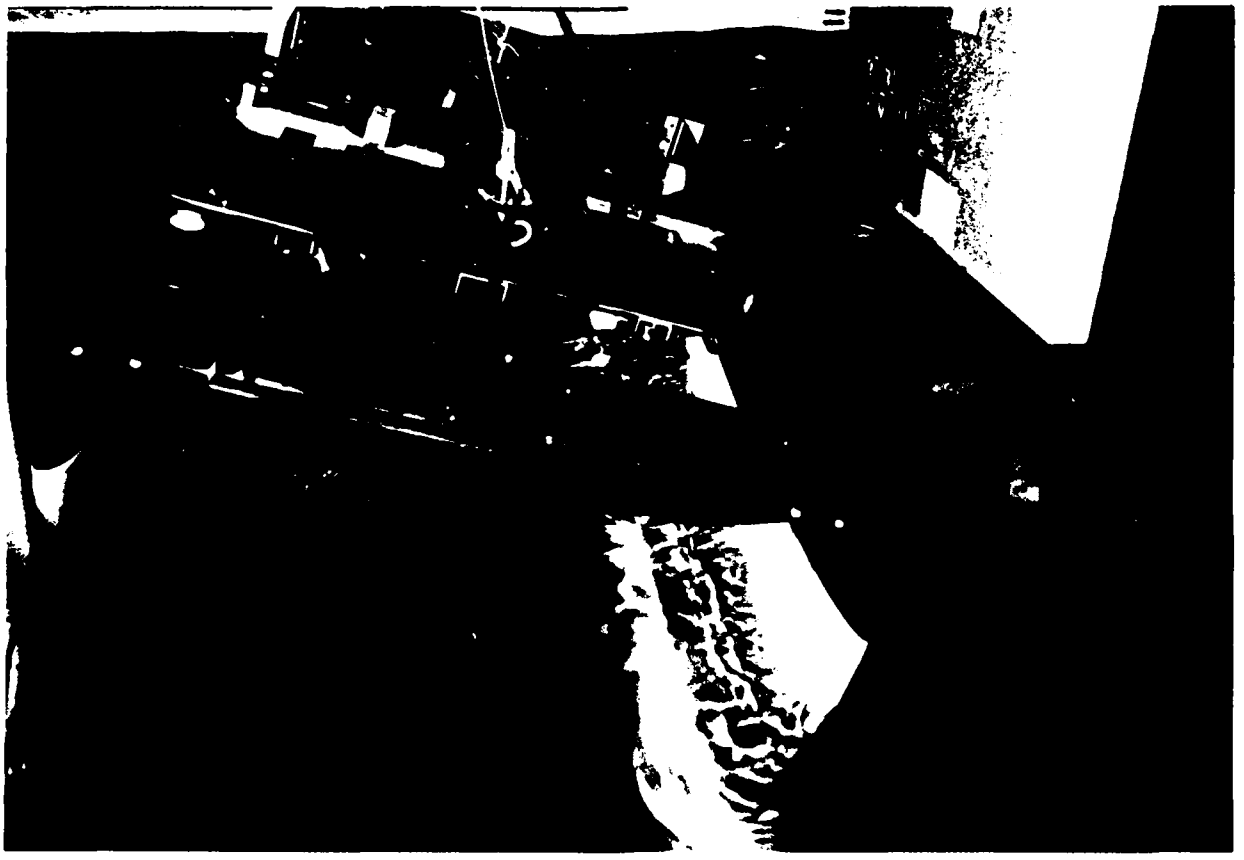

Frontispiece: SWATH model during extreme rolling in DTRC experiments.

ABSTRACT

One of the primary virtues of a Small Waterplane Area Twin Hull (SWATH) ship is its low motion characteristics in severe seas. By varying the appropriate inertial and geometric parameters, designers can 'de-tune' a SWATH ships' motion responses for a particular expected operating environment. Using model test data and linearly based motion prediction simulations, the effects of various design changes on motions can be studied. The occurrence of subharmonic roll motion has been observed in several past SWATH experiments and is not predicted using linear techniques. This nonlinear response has generally occurred on designs where the natural roll frequency is roughly half of the natural heave frequency. However, the extent of the boundaries of this instability, has not been well defined for a SWATH ship.

The objective of this investigation, therefore, is to provide experimental results defining the stability boundary for the roll motion of a SWATH drifting in beam seas and to study the possible cause of this phenomenon using a nonlinear math model of the coupled heave-roll response. Presented are the results of wave tank tests conducted on a model representing a 2900 ton SWATH ship drifting at zero speed in 'regular' (monochromatic) beam waves. Regular wave (linear) transfer functions are presented along with natural periods and damping characteristics. The amplitude and frequency envelope in which the subharmonic response occurs is provided along with a qualitative description of the combined motion characteristics near the stability boundaries. Also presented are results using a theoretical model based on a Mathieu-like expression of the heave-coupled roll response. The experimental results are compared with the theoretical model, with reasonable qualitative correlation.

CONTENTS

CONTENTS (continued)

FIGURES

FIGURES (continued)

Page

FIGURES (continued)

Page

FIGURES (continued)

Page

TABLES

NOTATION

Abbreviations

DTRC	David Taylor Research Center
GMt	Transverse metacentric height
KG	Vertical distance from keel to VCG
LCG, VCG	Longitudinal and vertical centers of gravity
SWATH	Small waterplane area twin hull
RPM	Revolutions per minute

Symbols

a	Wave amplitude
B	Roll damping coefficient (N/I)
α, α_m	Maximum surface wave slope (ka, or $\frac{\omega^2 a}{g}$)
α_e	Effective wave slope.
δ	Logarithmic decrement (Chap. 5)
δ	Coefficient of Mathieu eq. (Chap. 6)
ε_1, ε_2	Constants in modified roll equation
g, G	Gravitational constant (32.155 ft/sec^2, at DTRC)
η	Surface wave profile
$H(\omega)$, $\zeta(\omega)$	Magnitude and phase of the heave motion transfer function
I	Roll moment of inertia
$\ddot{\phi}$, $\dot{\phi}$, ϕ	Roll angular acceleration, velocity , and displacement.
φ	Nondimensional roll angle
k	Wave number, $=\frac{\omega^2}{g}$
N	Roll damping coefficient
θ	Pitch angle
T_B	Depth of the model center of buoyancy below the waterline
ω	Wave frequency (radians per second)
ω_e	Wave encounter frequency
$\omega_{\phi n}$, ω_r	Roll natural (or resonant) frequency
ω_n, ω_d	Undamped, and damped natural frequency (Chap. 5)
$\omega_{\theta n}$, $\omega_{z n}$	Pitch and heave natural frequencies, respectively
x, y, z	Surge, sway and heave
ζ	Damping ratio, $\cong\frac{\delta}{2\pi}$ (Chap. 5)
$\lvert R(\omega)\rvert$, $\varepsilon_r(\omega)$	Magnitude and phase of the relative heave motion transfer function
Δ	Ship or model displacement

CHAPTER 1. INTRODUCTION

Small Waterplane Area Twin Hull (SWATH) ships are primarily recognized for their seakeeping capabilities. Because SWATH ships can be designed with markedly reduced motion characteristics in rough seas, the U.S. Navy has conducted extensive research and development of the SWATH concept. The Navy's first SWATH ship class will be the 3400 LT, T-AGOS-19, for which the contract design was completed in the latter part of 1986. The SWATH TAGOS is scheduled to begin Military Sealift Command operation in the fall of 1989 as the first Navy designed SWATH to be built for auxiliary ship type use. A SWATH design was chosen for this mission primarily because of its ability to remain operational in extreme seas. Based on analytical predictions and model experimental results, SWATH technology is being considered for use in future auxiliary and combatant designs.

Ship designers currently use data from model scale seakeeping experiments, as well as linearly based ship motion computer simulation results to study the effects of design variations on seakeeping performance. Parameters such as, waterplane area, strut thickness, strut separation, and control surface size and location, can be varied to *de-tune* the motion responses of the ship to a particular wave environment. In general, longer natural periods can be achieved on a SWATH than for a monohull of the same displacement. Since SWATH ships are primarily designed for missions requiring low motions, it is therefore of great importance that the designer be able to predict SWATH motion responses in the expected operational sea conditions. The development of prediction capability (tools) is also therefore of great importance.

Roll is probably one of the most undesirable ship motion characteristics (causing hull stresses, crew discomfort, shifting cargo, etc.). Roll is referred to as a *lateral plane* motion, along with sway and yaw. In beam seas, a ship primarily experiences roll, sway, and heave. Roll is the least predictable, as well as the most nonlinear mode of motion. Though roll and

sway are linearly coupled, all couplings of heave into the lateral modes of motion are nonlinear.

The occurrence of subharmonic rolling has been observed in both regular and irregular wave SWATH seakeeping experiments for certain designs. Sub- or half-harmonic roll response refers to roll motion at a frequency lower than or at half of the wave excitation frequency, and is not predicted in linear theory, where response and excitation must occur at the same frequency. In 1981, the Navy sponsored model experiments at the Davidson Lab, where Numata[1*] documented the occurrence of this 'instability' for several variations of SWATH geometries in beam seas. He found that half-harmonic rolling occurred for all geometries when excited by waves at or near twice the natural roll frequency. This subharmonic motion appeared only for some wave amplitudes and it was recommended that further tests be conducted to define the boundaries of its occurrence.

This type of instability has been observed in other dynamic systems. Timoshenko[2] discusses the occurrence of similar instability regions in mechanical vibrations as a consequence of a fluctuating or time dependent spring stiffness. He showed that large vibrations could be built up in systems with variable spring characteristics for certain frequencies of stiffness fluctuation. By including spring stiffness as a periodic function of time in the differential equation of motion, he demonstrated good agreement with experiments in defining the boundaries of instability, and found that spring stiffness fluctuation at the natural frequency and half the natural frequency was of the most practical significance. This is also characteristic behavior of a Mathieu-like instability. This thesis explores an analogy to SWATH ships, in that the roll restoring moment, treated as a constant in the roll equation of motion in linear theory, may be varying as a consequence of heave and therefore acting as a periodic spring stiffness.

---

* References are listed on page 97.

In the Fall of 1985, Numata's single strut SWATH model was obtained from the Davidson Lab and beam sea regular wave experiments were conducted in the 140 Foot Towing Basin at the David Taylor Research Center (DTRC).* The single strut model configuration was used because it best demonstrated half-harmonic response in Numata's experiments, both in regular and irregular waves. Model motions were recorded over an extended range of wave frequencies and heights representative of ocean waves to define linear response as well as the occurrence and boundaries of the instabilities. Strong subharmonic rolling motion was observed and recorded over a range of wave frequencies and heights sufficient to define boundaries of its occurrence. A comparison of similar test conditions [linear transfer functions] with Numata's results shows good correlation. A harmonic analysis program that computes the amplitudes of the fundamental and the half-harmonic responses was to be used to identify the occurrence and magnitude of subharmonic rolling. Several difficulties arose with the proposed method of data analysis since many of the responses were unsteady (i.e. exhibited various growth rates, transitions from responses at the fundamental, shifting to a subharmonic motion). Therefore, the analysis presented is of a more qualitative description of the observed subharmonic behavior than originally intended.

To provide a theoretical model, an expression was determined representing a periodic fluctuation of roll stiffness (i.e. variation in transverse metacentric height, or GMt, due to heaving motion), and substituted into the restoring term of a simplified linear differential equation for roll. In its final form, this expression (linear with periodic coefficients) resembles a Mathieu equation. The boundaries of instability computed from this math model are compared to the experimental results. This model was used to explore the mechanism of

* Formerly the David W. Taylor Naval Ship Research and Development Center (DTNSRDC). The name was officially changed to David Taylor Research Center (DTRC) in September, 1987.

subharmonic roll response, and was used in an evaluation of whether the relative or absolute heave motion provides the more significant correlation.

Presented are the experimental results, including regular wave transfer functions from harmonic analysis, static roll stability, natural frequency and damping calculations. The amplitude and frequency envelope in which the subharmonic response occurred is provided along with a qualitative description of the combined motion characteristics (such as, roll growth rates and maximum roll amplitudes) near the stability boundaries. The mechanism of the subharmonic roll has been explored by comparing experimental results with theoretically derived responses and stability boundaries.

CHAPTER 2. DESCRIPTION OF MODEL AND TEST EQUIPMENT

MODEL

The model used in these experiments was borrowed from the Stevens Institute's Davidson Laboratory and was the same model (#4571A) used in the experiments conducted by Numata [1]. The model was refurbished and ballasted to the *low KG* or *high GM* variant of Numata's series. This configuration was chosen because it was the only one of Numata's configurations for which the subharmonic roll was noted to be absent at both very low wave amplitudes, and at higher amplitudes, but with a subharmonic region in between. This variant also exhibited subharmonic response in Numata's irregular waves experiments, as well.

A photograph of the model is shown in Fig. 1. At a scale ratio of 35.17, the model corresponds to a full scale SWATH ship of approximately 2900 long tons, and is similar to the SWATH 6 series design, which has been tested extensively at DTRC. The lower hulls are cylindrical with an elliptical nose, parallel middle body, and a parabolic tail section. The struts are also elliptical from the leading edge to a parallel mid-section, and are parabolic to the trailing edge. Details of the model geometry are given in Figure 2. Principal characteristics of the model as tested are listed in Table 1a, and a comparison with Numata's *as tested* model characteristics is provided in Table 1b.

The model is constructed of high density foam, and covered with a 1/32nd inch thick layer of fiberglass. The center section of each strut is hollow, allowing the placement of ballast weights below the waterline to achieve the proper distribution of mass. Each half (port/stbd) is of one piece (hull/strut) construction and is connected by bridging structure of aluminum channel at four longitudinal locations. The model has four control surfaces on the inboard sides of the lower hulls. The canards (forward fins) and stabilizers (aft fins) were set to zero angle of attack for these experiments.

As mentioned above, the model was ballasted to the *low KG* or *high GM* variant of Numata's series. The ballast consisted of the measurement transducers, precision ground ballast weights, and a special track with movable inclining weights for performing ballasting tasks. Model weight was verified using an NCI Model #5400 digital electronic platform scale, with a range and accuracy of 200±.02 lb, respectively. The model was placed on a knife edge, at the longitudinal center of gravity (LCG) and an inclining test in air was performed to obtain the vertical center of gravity (VCG). The model was then oscillated in air and ballast weights were moved to obtain the desired roll and pitch gyradii. The model was also inclined in water to measure the transverse metacentric height, GM_t .

While some difference in the model inertial characteristics would be expected (between these and Numata's tests) due to the sensitivity of the ballasting procedure, a discrepancy arose in the model displacement at the design waterline. The model needed 4 pounds of additional ballast weight (~3% increase) to float at the design waterline. Calculations (including correction for differences in scaling from saltwater to fresh water densities) were checked and rechecked, as were the model dimensions and the waterline marks. Model weight was checked using 3 separate scales. A possible explanation for this difference is that the model volume below the waterline (as constructed) may be 3% over the design (i.e. 1.4% in terms of linear dimensions). At the time of Numata's experiments, the Davidson Lab did not have a scale wide enough to weigh an assembled SWATH model and Numata may have ballasted the model to the waterline and then calculated the necessary locations for the ballast weights. In any case, the model characteristics between these tests and Numata's are nearly identical, in every other aspect.

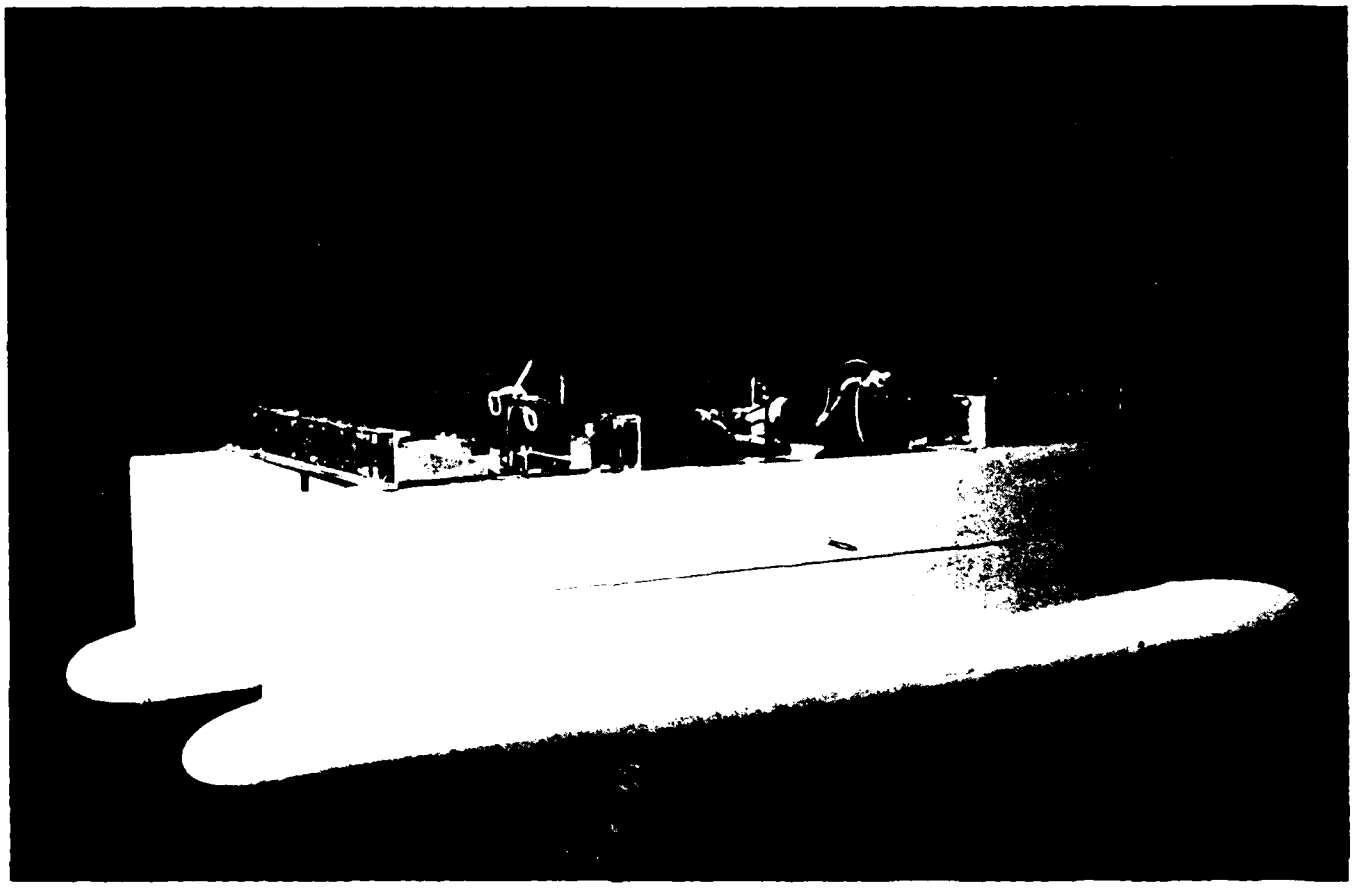

Fig. 1. Photograph of the 1/35.17 scale Davidson Lab SWATH model used in tests.

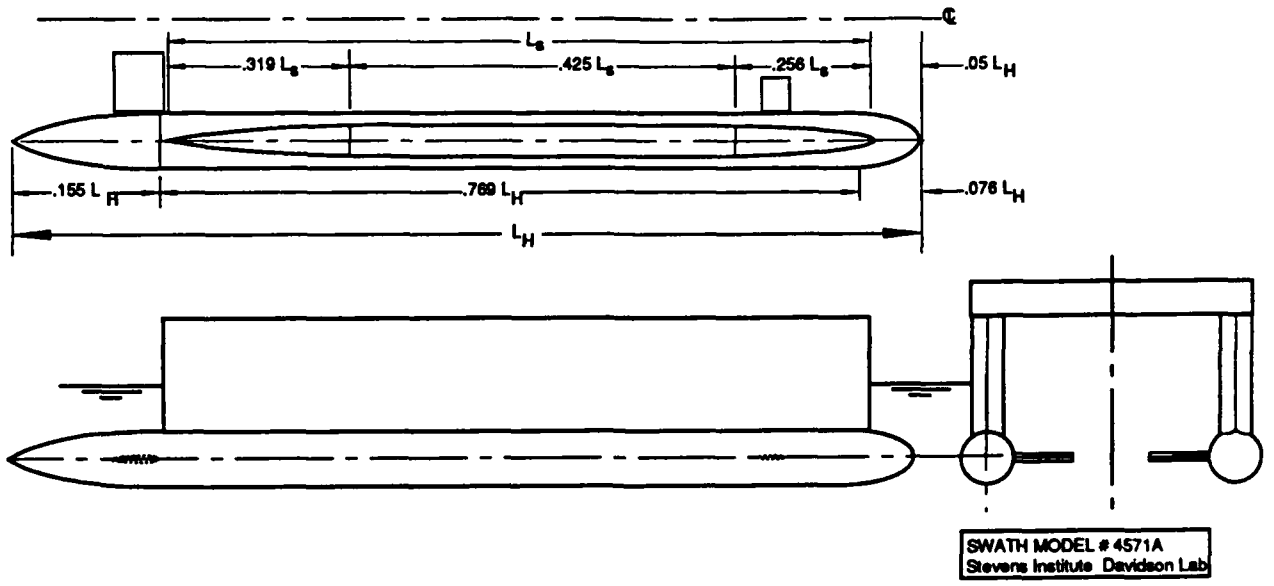

2.a Linear dimensions as a percentage of lower hull length, L_H, and strut length, L_S.

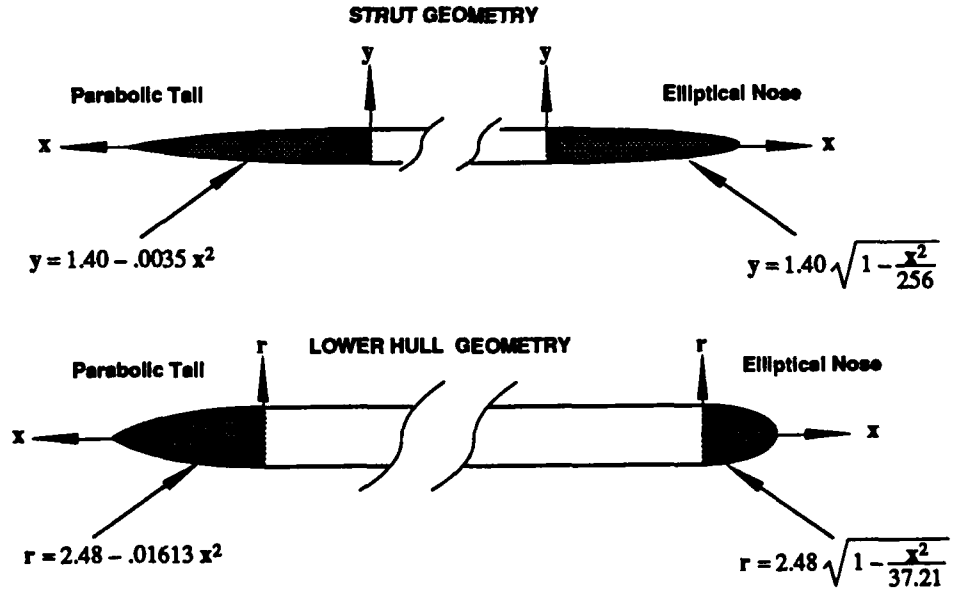

(Where x is longitudinal distance and y and r are the vertical half-breadth or radius of each section in model scale inches, respectively.)

2.b. Equations for lower hull and strut shapes.

Fig. 2. Details of the model geometry.

Table 1. Model characteristics.

Table 1a. Model characteristics, in English and SI or metric units..

Characteristic (Model Scale Ratio = 35.17)	ENGLISH		METRIC	
	Ship	Model	Ship	Model
Hull Length	234.5 ft	80.0 in.	71.5 m	203.3 cm
Hull Centerline Spacing	64.5 ft	22.00 in.	19.7 m	55.9 cm
Hull Diameter	14.6 ft	4.98 in.	4.5 m	12.7 cm
Draft to Keel	26.5 ft	9.04 in.	8.1 m	23.0 cm
Deck to DWL	17.6 ft	6.00 in.	5.4 m	15.2 cm
Strut Length	183.5 ft	62.61 in.	55.9 m	159.0 cm
Strut Thickness	8.2 ft	2.80 in.	2.5 m	7.1 cm
Strut Setback from Hull Nose	11.7 ft	4.00 in.	3.6 m	10.2 cm
Fwd. Fins (Canards)-Chord	7.4 ft	2.52 in.	2.3 m	6.4 cm
Fwd. Fins (Canards)-Span	9.0 ft	3.07 in.	2.7 m	7.8 cm
Fwd. Fins- LE from Hull Nose	33.6 ft	11.46 in.	10.2 m	29.1 cm
Aft Fins (Stabilizer)-Chord	12.9 ft	4.40 in.	3.9 m	11.2 cm
Aft Fins (Stabilizer)-Span	15.6 ft	5.32 in.	4.8 m	13.5 cm
Aft Fins- LE from Hull Nose	196.7 ft	67.11 in.	60.0 m	170.5 cm
Prismatic Coefficient	0.902	0.902	0.902	0.902
Waterplane Coefficient	0.839	0.839	0.839	0.839
Displacement- appended*	2994.7 ltsw	150.0 lb	3042.8 mtsw	68.0 kg
- unappended	2965.6 ltsw	148.5 lb	3013.2 mtsw	67.4 kg
LCB & LCG from hull nose	108.4 ft	37.00 in.	33.04 m	93.98 cm
VCG above DWL	0.81 ft	0.275 in.	0.25 m	0.70 cm
VCG above Keel, KG	27.3 ft	9.32 in.	8.32 m	23.66 cm
Transverse GM	9.7 ft	3.31 in.	2.96 m	8.42 cm
Longitudinal GM	-	-	-	-
Roll Gyradius	32.04 ft	10.9 in.	9.77 m	27.69 cm
as% hull spacing	49.7	49.7	49.7	49.7
Natural Roll Period, sec	15.00	2.53	15.00	2.53
Natural Roll Frequency	0.418 rad/s	2.48 rad/s	0.418 rad/s	2.48 rad/s
Pitch Gyradius	47.98 ft	16.4 in.	14.62 m	41.57 cm
as% hull length	20.5	20.5	20.5	20.5
Natural Pitch Period, sec	13.1	2.2	13.1	2.2
Natural Pitch Frequency	0.480 rad/s	2.86 rad/s	0.480 rad/s	2.86 rad/s
Natural Heave Period, sec	8.5	1.44	8.5	1.44
Natural Heave Frequency	0.739 rad/s	4.36 rad/s	0.739 rad/s	4.36 rad/s

* Model weight discrepancy of approx. 4. lbs -see text

Table 1. (Continued)

Table 1b. Comparison with Numata's Low KG model configuration.

Characteristic (Model Scale Ratio = 35.17)	HART		NUMATA	
	Ship	Model	Ship	Model
Hull Length	234.5 ft	80.0 in.	same	same
Hull Centerline Spacing	64.5 ft	22.00 in.	"	"
Hull Diameter	14.6 ft	4.98 in.	"	"
Draft to Keel	26.5 ft	9.04 in.	"	"
Deck to DWL	17.6 ft	6.00 in.	"	"
Strut Length	183.5 ft	62.61 in.	"	"
Strut Thickness	8.2 ft	2.80 in.	"	"
Strut Setback from Hull Nose	11.7 ft	4.00 in.	"	"
Fwd. Fins (Canards)-Chord	7.4 ft	2.52 in.	"	"
Fwd. Fins (Canards)-Span	9.0 ft	3.07 in.	"	"
Fwd. Fins- LE from Hull Nose	33.6 ft	11.46 in.	"	"
Aft Fins (Stabilizer)-Chord	12.9 ft	4.40 in.	"	"
Aft Fins (Stabilizer)-Span	15.6 ft	5.32 in.	"	"
Aft Fins- LE from Hull Nose	196.7 ft	67.11 in.	"	"
Prismatic Coefficient	0.902	0.902	"	"
Waterplane Coefficient	0.839	0.839	"	"
Displacement- appended*	2994.7 ltsw	150.0 lb	2921.0 ltsw	146.3 lb
- unappended	2965.6 ltsw	148.5 lb	2900.0 ltsw	145.3 lb
LCB & LCG from hull nose	108.4 ft	37.00 in.	same	same
VCG above DWL	0.81 ft	0.275 in.	1.1 ft	0.36 in.
VCG above Keel, KG	27.3 ft	9.32 in.	27.6 ft	9.40 in.
Transverse GM	9.7 ft	3.31 in.	9.6 ft	3.28 in.
Longitudinal GM	-	-	36.0 ft	12.28 in.
Roll Gyradius	32.0 ft	10.9 in.	31.5 ft	10.8 in.
as% hull spacing	49.7	49.7	49	49
Natural Roll Period, sec	15.00	2.53	14.90	2.51
Natural Roll Frequency	0.418 rad/s	2.48 rad/s	0.422 rad/s	2.50 rad/s
Pitch Gyradius	48.0 ft	16.4 in.	not reported	not reported
as% hull length	20.5	20.5	not reported	not reported
Natural Pitch Period, sec.	13.1	2.2	13.7	2.31
Natural Pitch Frequency	0.480 rad/s	2.86 rad/s	0.459 rad/s	2.72 rad/s
Natural Heave Period	8.5	1.44	8.2	1.38
Natural Heave Frequency	0.739 rad/s	4.36 rad/s	0.766 rad/s	4.55 rad/s

* Model weight discrepancy of approx. 4. lb -see text

TEST EQUIPMENT

Test Facility

Tests were conducted at The David Taylor Research Center in the 140 Foot Towing Basin. The 140 Foot Towing Basin is 10 ft.(3 m) wide, 5.0 ft.(1.5 m) deep, and is 140 ft. (42.7 m) long (actually 131 ft. from lip of Wavemaker to Beach).* An electric powered carriage, mounted on a set of overhead rails running the length of the basin, can be operated in either direction at various speeds up to 6 knots. This facility is equipped with a pneumatic wavemaker at one end and a wave absorbing *beach* at the other.

The wavemaker consists of a partially submerged dome which spans the width of the tank, and is connected via ducting, to a centrifugal blower and a set of oscillating *gate valves*. The valves are arranged so that the centrifugal blower alternately pumps air from the atmosphere into the dome, and from the dome into the atmosphere. Thus, waves are produced by cycling the dome air pressure and consequently, the water surface under the dome. Control of wave height is achieved by adjusting the speed of the 'varidrive' blower motor (*blower rpm*), thus varying the maximum pressures in the dome. Wavelength (or wave frequency) is controlled by varying the speed of the motor-driven hydraulic coupler on the oscillating gate valves. A magnetic pick-up and rotating gear on the coupler provide a signal which was calibrated in terms of the required rpm (referred to as *flap rpm*) for a desired wave frequency.

The wave absorbing beach, made from layers of wire mesh, has a 10 degree slope and spans the width of the basin. Because of the somewhat deteriorated condition of the beach, an experiment was conducted to evaluate the extent of wave reflections. After some refurbishing of the beach, the reflection coefficient was measured over the expected range of

* By comparison, the Davidson Lab facility at Stevens Institute of Technology is 12 ft.(3.66 m) wide, 5.5 ft.(1.68 m) deep, and is 313 ft. (95.4 m) long.

test wave frequencies and amplitudes. From these results, it became evident that reflections from the beach would still be significant and needed to be avoided.

Model Instrumentation

A summary of the specific measurements, including the location, calibration factor, and type of transducer used in data collection is given in Table 2. Wave height, sway and heave were measured using Westmar ultrasonic level transducers. These transducers were used instead of direct attachments such as string-potentiometers, in order to eliminate any influence on the model motions which might be caused by the contact or tension in the string. Also, by providing large styrofoam "targets" for heave and sway, the model was free to drift, relative to the carriage, without compromising the accuracy of the measurements. This would not be the case for a string pot, which would be required to remain vertical.

Table 2. Measurement transducers.

Channel	Measurement	Transducer	*Calibration* units/volt	Location
1	Wave Height	Ultrasonic	1.0 in/v (2.54 cm/v)	12.21 ft to Stbd (of model C.L.)
2	Drift (displacement)	String Potentiometer	20.0 in/v (12.7 cm/v)	drift range of 12 ft
3	Sway	Ultrasonic	1.0 in/v (2.54 cm/v)	on model LCG, to Port
4	Heave	Ultrasonic	1.0 in/v (2.54 cm/v)	Model LCG, on C.L.
5	Roll	Roll/ Pitch Gyro	2.0 deg/v	
6	Pitch	Roll/ Pitch Gyro	2.0 deg/v	
7	Wavemaker Flap RPM	Magnetic Pick-Up (60 tooth gear)	100 rpm/v	
8	Wavemaker Blower RPM	Magnetic Pick-Up (slotted disk)	600 rpm/v	
9	Heave CG Acceleration	Accelerometer	0.1 g/v	2" aft of LCG on model C.L.

C.L. = center line

Unfortunately, problems did occur using the sonic transducers. For test conditions involving large roll angles, sonic *drop-out* occurred. That is, the echo from the target was lost and the signal was corrupted with spikes (noise). This was due, in part to the limitations

of the beam width or cone angle of the sonic transducer. While several sonic heads with various beam angles up to 16 degrees were tried, the drop-outs could not be avoided. A heave accelerometer was added to the model (after run #57), to provide some quantitative information on heave, particularly during large subharmonic rolling. The vertical accelerometer used was a 0.5g, Systron-Donner (model #4310), force balance servo type, and was mounted 2 inches (5.08 cm) aft of midships, on the model centerline.

Pitch and roll were measured using a Honeywell vertical aircraft pitch/roll gyro. The gyro has a resolution/accuracy of between 1/4th to 1/8th of a degree. Figure 3 shows a close-up of the model deck, and the layout of the some of the instrumentation. Not pictured are the inclinometer and bubble level, mounted on the foredeck, which were used in ballasting and checking the model trim.

Drift speeds of the model were below that which could be read by the carriage speed transducer, so a string-potentiometer was rigged up to a 4:1 pulley system to monitor the position of the carriage in the basin over a range of about 12 feet. Frequency to voltage converters were calibrated to convert the outputs of the optical slotted disk and 60 tooth magnetic pick-up, into RPM readings of the wavemaker blower and flap rpm settings, respectively.

Test Set-Up

A sketch of the experimental set-up is shown in Fig. 4. The model was positioned transversely in the basin, under the center of the towing carriage. Light elastic restraining lines were attached at the bow and stern to provide slight restoration in yaw, in order to maintain a 90 degree heading to the waves. The tension in the lines was adjusted to provide minimal affect on the motion responses. With the exception of the use of a smaller towing tank and sonic transducers, this test set up was nearly identical to Numata's. The model was positioned approximately 44 ft (13.41 m) from the wavemaker, with the wave probe mounted

on the centerline of the towing carriage, 12.21 ft.(3.72 m) upwave of the model (see Fig.4b.). An electric winch was mounted on the towing carriage and used for raising the model out of the water between runs and when *waves only* data were being collected. The umbilical (data) cables to the transducers were suspended from the carriage with light elastic line, allowing plenty of slack to account for model motions, as can be seen in the photograph in Fig.5.

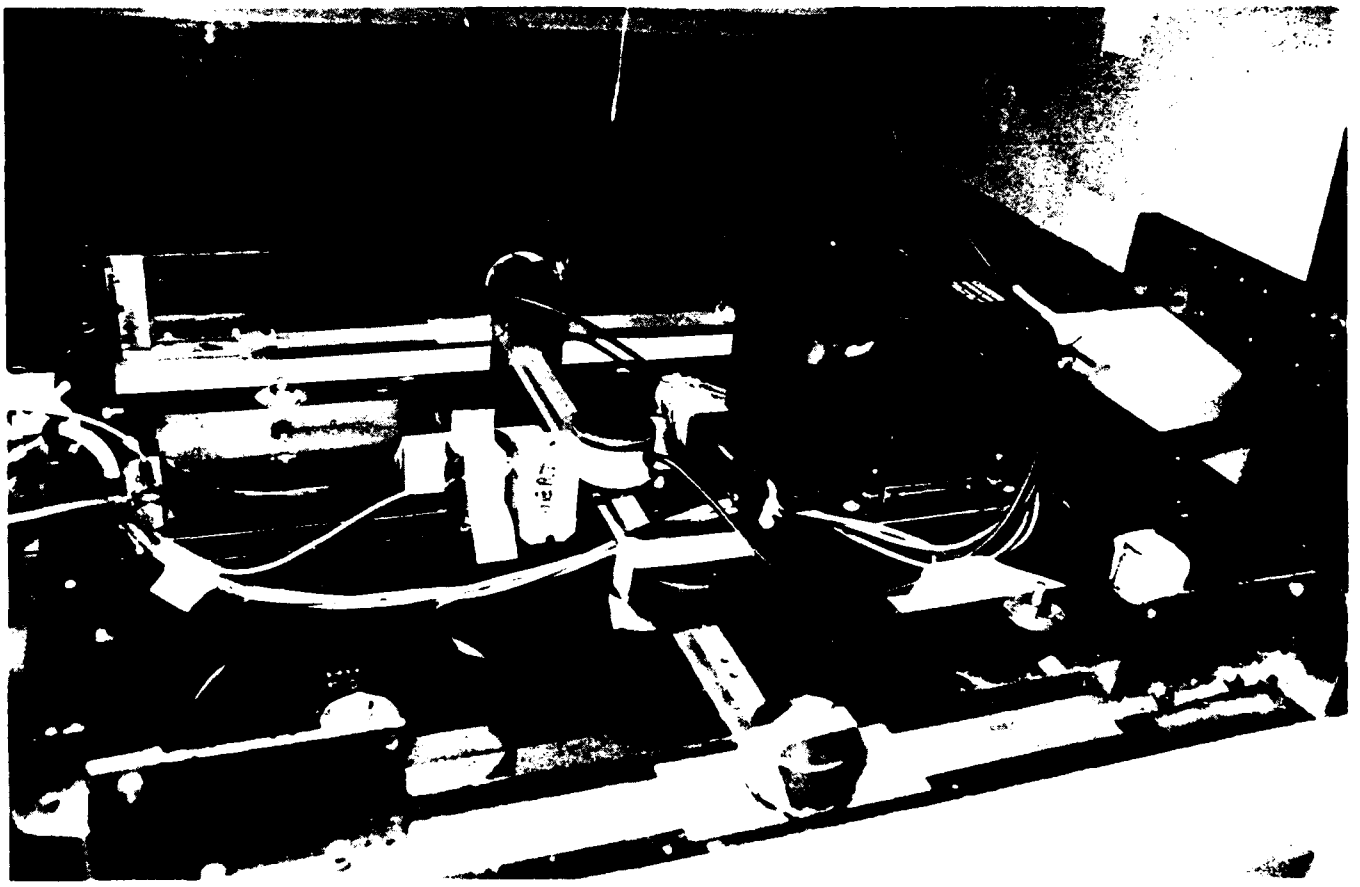

Fig. 3. Photograph of test instrumentation on model deck.

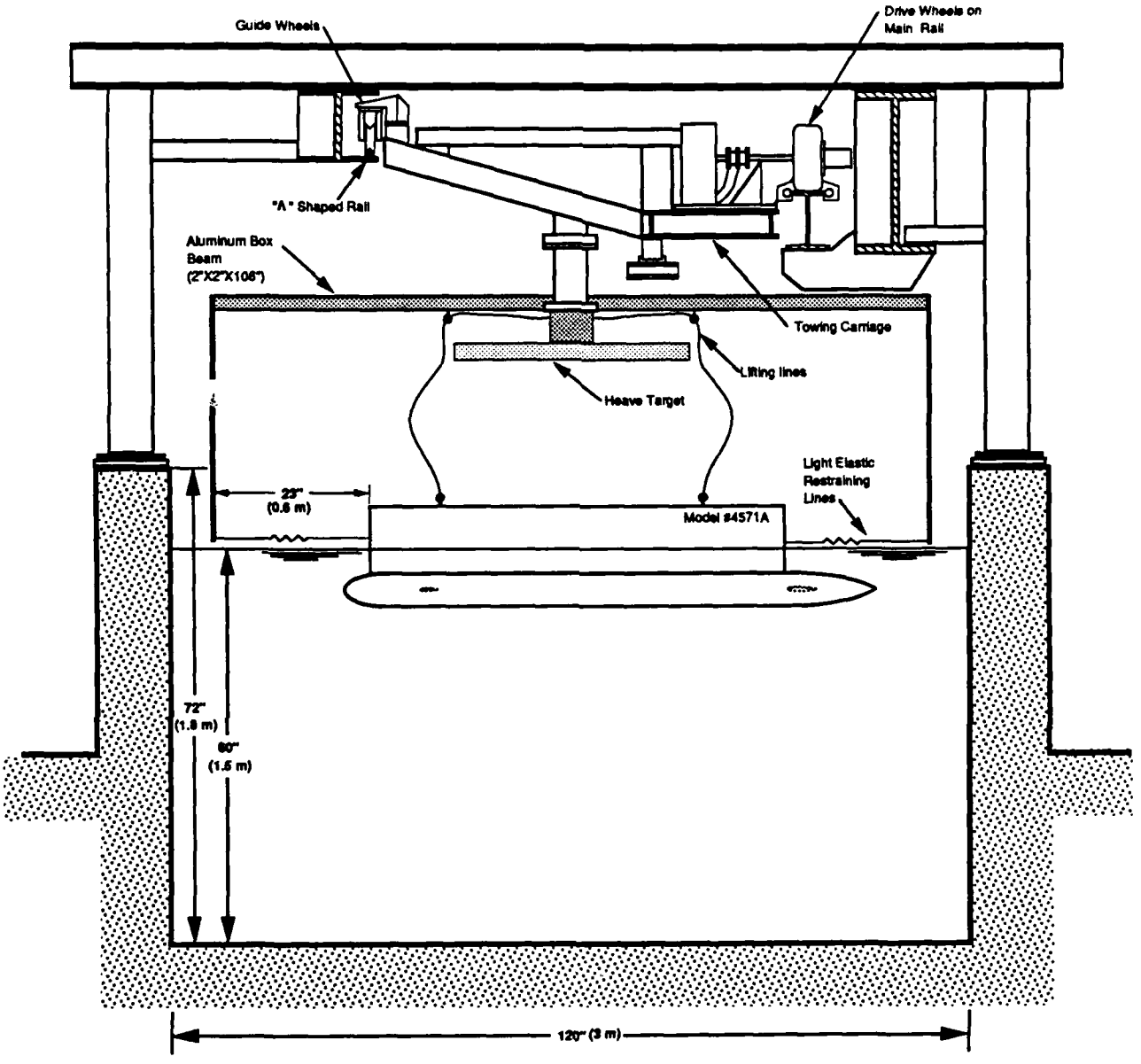

Fig. 4a. Test set-up: model in basin (cross-sectional view).

Fig. 4. Experimental set-up.

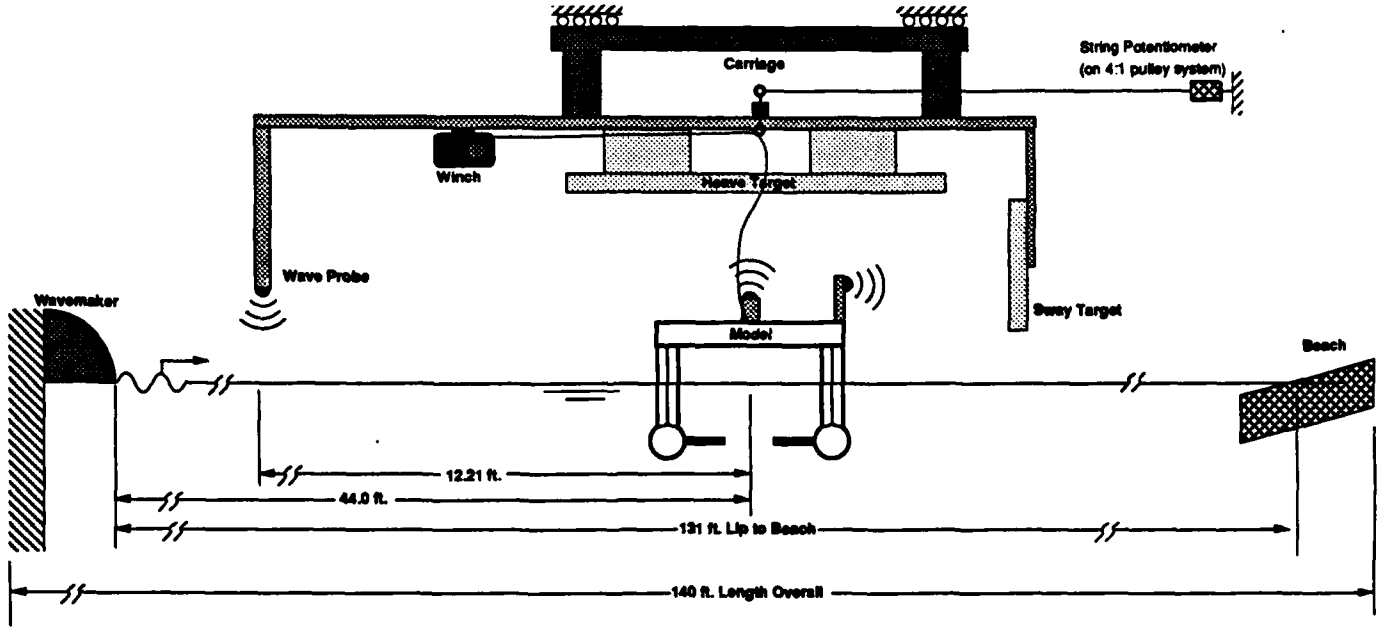

Fig. 4b. Test set-up: model in basin (side view).

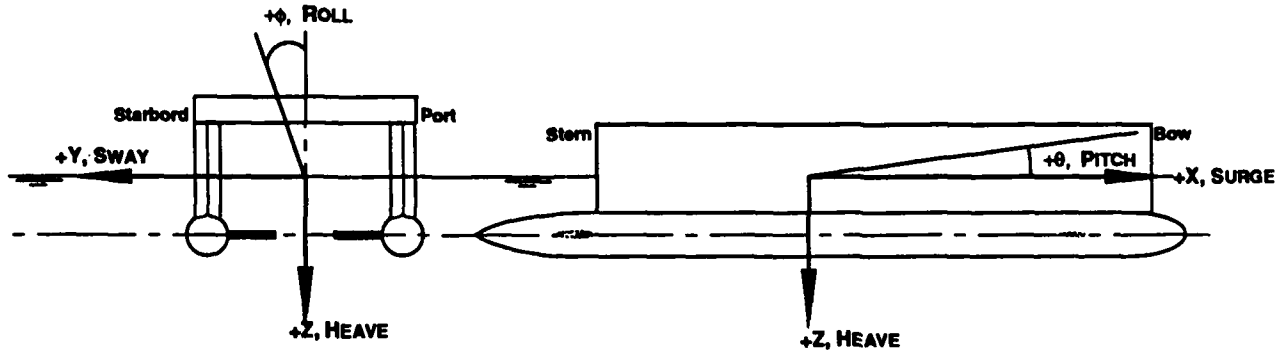

Fig. 4c. Coordinate system.

Fig. 4. (Continued).

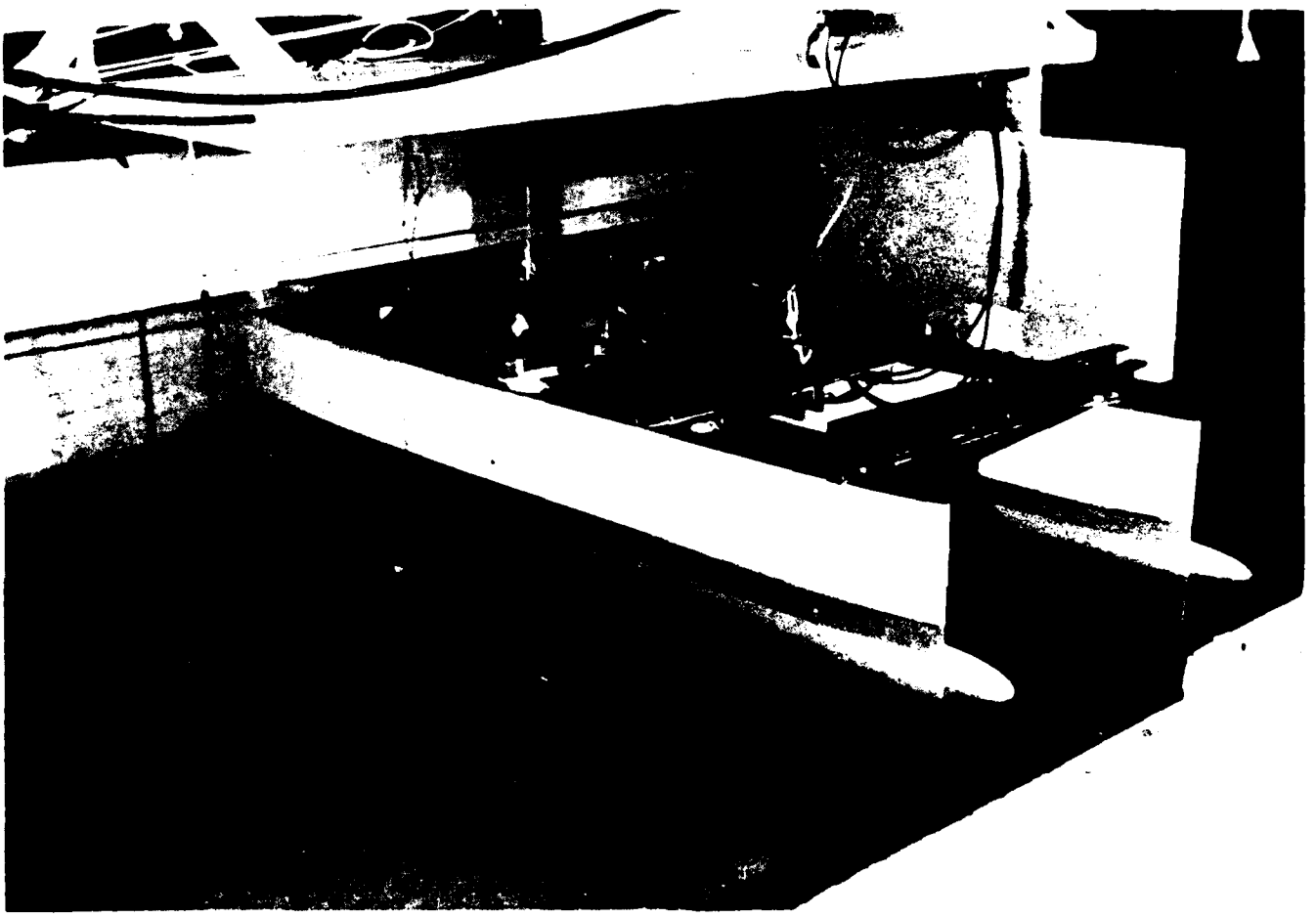

Fig. 5. Photograph of the model in 140 Foot Basin.

CHAPTER 3. TEST PROGRAM AND PROCEDURE

Tests were conducted in three phases: Calm water free oscillations, to obtain natural periods and damping characteristics; regular wave tests to obtain linear transfer functions; and regular wave tests over a matrix of amplitudes and frequencies in the region of subharmonic roll , to characterize the stability boundaries. An overall summary of the test matrix is given in Table 3.

Table 3. Outline of test conditions.

A. Natural Periods and Damping Characteristics From Free Decay Tests
Pitch, Roll and Heave; with model restraints
Pitch, Roll and Heave; without restraints

B. Regular Wave Transfer Functions (non subharmonic region)
Ranging in encounter frequency ,ω_e, from 2 to 4.5 rad/s (model), .3 to .76 rad/s (ship),
Target wave height 5% of the overall ship length (4 in. model scale, 11.7 ft full scale)
Wave slope corrected for bottom effects

C. Parametric Excitation (subharmonic roll)
Frequencies ranging from 10% below to 25% above 2x natural roll frequency, $\omega_{\phi n}$.
Ranging in ω_e from 4.7 to 6.3.rad/s (model), 0.8 to 1.1rad/s (ship)
Wave amplitudes from .2 to 2 in. model,0.6 to 5.6 ft, full scale

The natural periods and damping factors were obtained from free decay oscillations in calm water. These tests were conducted both with and without the yaw restraints attached.

The regular wave transfer functions of heave, roll, pitch, and sway were defined in the linear (non subharmonic) region to provide both the linear characteristics of the motions and a comparison to Numata's results as a check. The criteria for wave height was based on Numata's target of 5% of ship length, which corresponds to a target wave height of 4 inches (10.2 cm), model scale. Therefore, a minimal calibration of the wavemaker was conducted, over a range of frequencies and amplitudes, to obtain the approximate wavemaker settings for the target wave height at each test condition.

Since the roll and heave transfer functions were of particular interest, data were taken at smaller frequency intervals, near the resonant frequencies, in order to better define the

peaks. At each frequency, data were collected over 10 cycles where possible; but at low frequencies, fewer cycles were collected to avoid reflected waves. Knowing that the wave reflections from the beach were a potential problem, Table 4 was used as a guide to timing the data collections. Calculations in Table 4 include the effects of water depth on wavelength and celerity. That is, deep water simplifications were *not* assumed in these wave calculations, but rather the intermediate depth form of the wave equations were used [see Dean & Dalrymple[3]]. Time 1, in Table 4 refers to the time for waves to travel past the model, to the beach and back to the model. Time 2 refers to the time for the waves to travel from the model to the beach, back to the wavemaker and then reflect back to the model. It should be noted that at the time of the experiments, only the waves reflected by the beach were considered to be important. Waves reflecting off of the model, traveling to the wavemaker and back to the model, may in fact, have been more significant in these experiments than originally anticipated.

The general procedure for the regular wave tests are detailed below. First, the desired wave frequency was set on the wavemaker. Then the blower *revolutions per minute* (rpm) was set, based on information from the earlier calibration. Next, the model was lowered into the water, the waves were started, and the analog stripchart recorder started. When the waves reached the model, a timer was started to track the time remaining before reflected waves from the beach were to be anticipated (at the model). Digital data collection was then initiated, and if the model drifted, the carriage speed was adjusted to match the model drift velocity.

In the subharmonic region, the parametric excitation (subharmonic roll) tests were conducted over a matrix of wave frequencies and heights, sufficient to define boundaries of the instability. Table 5 presents a detailed test matrix of the conditions for the subharmonic tests. Since the unstable region was expected to occur at a frequency near or equal to twice the natural roll frequency, the input wave frequencies are expressed as a frequency ratio

defined as, $\omega_e/2\omega_{\phi n}$, where ω_e is the wave encounter frequency, and $\omega_{\phi n}$ is the natural roll frequency.

The procedure for runs in the subharmonic region was as follows. First the desired wave frequency was set up on the wavemaker. Then waves were sent at a low wave height, and the roll response was measured, as described above for the linear response. Run lengths were generally longer (typically around 50 sec.) to monitor the roll behavior, as the model drifted. The basin was allowed to settle between runs. The blower setting was then increased, thereby increasing the wave height, while maintaining a constant wave frequency setting for the next run. In this manner, data were collected for several waveheights at each wave frequency. In Table 5, the *lines* of constant wave frequencies are given letter designations, A-J, for frequency ratios ranging from 0.94 to 1.27 . As either wave height or frequency were increased, the model drift rate tended to increase, thus reducing the wave encounter frequency, as will be seen in the data.

Table 4. Wave reflection calculations for a position of 46 ft. (14 m) from the wavemaker.

Wavelength L, ft	Wave Number K, 1/ft	Frequency Omega, r/s	Period T, sec	Celerity C, ft/sec	Depth Factor, n	Group Velocity Cg, ft/sec	Time 1, sec (177 ft/Cg)	Time 2, sec (347 ft/Cg)
2.0	3.142	10.058	0.625	3.201	0.500	1.601	110.573	216.774
3.0	2.094	8.212	0.765	3.921	0.500	1.961	90.283	176.995
4.0	1.571	7.112	0.883	4.528	0.500	2.264	78.187	153.281
5.0	1.257	6.361	0.988	5.062	0.500	2.531	69.927	137.088
6.0	1.047	5.807	1.082	5.545	0.500	2.774	63.803	125.084
7.0	0.898	5.375	1.169	5.989	0.501	3.001	58.978	115.623
8.0	0.785	5.027	1.250	6.401	0.503	3.220	54.973	107.772
9.0	0.698	4.737	1.326	6.785	0.506	3.437	51.505	100.973
10.0	0.628	4.490	1.400	7.145	0.512	3.657	48.406	94.898
11.0	0.571	4.275	1.470	7.483	0.519	3.883	45.583	89.364
12.0	0.524	4.084	1.538	7.800	0.528	4.118	42.987	84.273
13.0	0.483	3.914	1.605	8.098	0.538	4.360	40.593	79.581
14.0	0.449	3.759	1.672	8.376	0.550	4.611	38.391	75.263
15.0	0.419	3.617	1.737	8.636	0.564	4.867	36.371	71.303
16.0	0.393	3.487	1.802	8.879	0.577	5.126	34.527	67.688
17.0	0.370	3.365	1.867	9.105	0.592	5.388	32.849	64.398
18.0	0.349	3.252	1.932	9.316	0.606	5.650	31.327	61.414
19.0	0.331	3.146	1.997	9.513	0.621	5.910	29.949	58.713
20.0	0.314	3.046	2.063	9.696	0.636	6.167	28.703	56.272
21.0	0.299	2.952	2.129	9.866	0.651	6.418	27.578	54.066
22.0	0.286	2.863	2.195	10.024	0.665	6.664	26.562	52.073
23.0	0.273	2.779	2.261	10.172	0.679	6.902	25.643	50.272
24.0	0.262	2.699	2.328	10.309	0.692	7.134	24.812	48.643
25.0	0.251	2.623	2.395	10.436	0.705	7.357	24.059	47.167
26.0	0.242	2.551	2.463	10.555	0.717	7.572	23.376	45.828
27.0	0.233	2.482	2.531	10.666	0.729	7.778	22.755	44.611
28.0	0.224	2.417	2.600	10.769	0.741	7.976	22.191	43.504
29.0	0.217	2.354	2.669	10.866	0.752	8.166	21.676	42.494
30.0	0.209	2.295	2.738	10.956	0.762	8.347	21.205	41.571

Table 5. Test matrix for the subharmonic region.

Lines of Constant Wave Period	Input Wave Period sec, model	Input Wave Frequency rad/sec, model	Frequency Ratio $\omega_0/2\omega_1$	Input Wave Period sec, ship	Input Wave Frequency rad/sec, ship	Run Number Range
A	1.34	4.69	0.94	7.95	0.79	93 - 98
B	1.29	4.87	0.98	7.65	0.82	99 - 101
C	1.26	4.99	1.00	7.47	0.84	74 - 80
D	1.25	5.03	1.01	7.41	0.85	55-57, 58-62, 110
E	1.21	5.19	1.05	7.18	0.88	81 - 87, 111
F	1.17	5.37	1.08	6.94	0.91	44,45,47-52,54
G	1.14	5.51	1.11	6.76	0.93	65 - 71, 73
H	1.08	5.82	1.17	6.40	0.98	103 - 109
I	1.05	5.98	1.20	6.23	1.01	88 - 92
J	1.00	6.28	1.27	5.93	1.06	63 - 64, 113

CHAPTER 4. DATA COLLECTION AND REDUCTION

An Analogic 15 bit analog-to-digital (A-D) converter and an Interdata Model 70 computer were used to digitize and record time histories of all channels to magnetic tape at a sample rate of 30/channel/second. Analog signals were filtered prior to digitizing using 6 hz, 6 pole Butterworth low pass filters, and were monitored throughout the test using an analog strip chart recorder. Figure 6 shows a block diagram of the data acquisition equipment, and a photograph of the data acquisition hardware set-up is shown Fig. 7.

At the end of each run, the analysis software provided both a "minimum" analysis (means, standard deviations and $\sqrt{2}$ x standard deviation†), and harmonic analysis of the data channels, as shown in Fig. 8. A sample of the minimum analysis page is given in Fig. 8a and the corresponding harmonic analysis output is shown in Fig. 8b. Wave encounter frequency, wave slope, and wave celerity are output on each page. Some of the items are listed under the following headings:

FE, ωE = frequency of wave encounter
FO, ωO = wave frequency
TE = period of wave encounter
TO = wave period
LAMBDA = wave length
CELERITY = wave phase speed

In Fig.8a, the MEAN is a "D.C. level", and the SDDEV is the root mean square (RMS) about the mean. In Fig. 8b, the harmonic analysis provides the half harmonic, fundamental, and first harmonic amplitudes and phases. The amplitude of the fundamental (AMP2) is used to calculate the nondimensional transfer functions, as follows.

a. angular measurements: angle/ α
b. displacement measurements: displacement/ a

† For sinusoidal response, $\sqrt{2}$ x standard deviation (or 'ROOTQ0,' as it appears on the printout), is the single amplitude.

c. acceleration measurements: acceleration/ $a\omega_e^2/G$

where α= maximum wave slope, a= wave amplitude, and G= gravity.

Digital time histories of the data stored on magnetic tape were generated after the experiments with a program called THRPDC (time history reproduce) to examine the data at specific time slices of each run. Figure 9 shows the digitized time history of the same data summarized in Fig. 8. The digitized data could then be examined for signal noise, sonic 'dropouts,' and other effects which would void harmonic analysis results of that time segment. Harmonic analysis was then further used to analyze various time segments of runs. These outputs, in conjunction with the use of analog stripchart output, provided the necessary means to study the overall test results. All three forms of output: digital time history, analog chart recordings, and harmonic analysis of specific time segments of each run were necessary to study and to characterize the motion responses of each run.

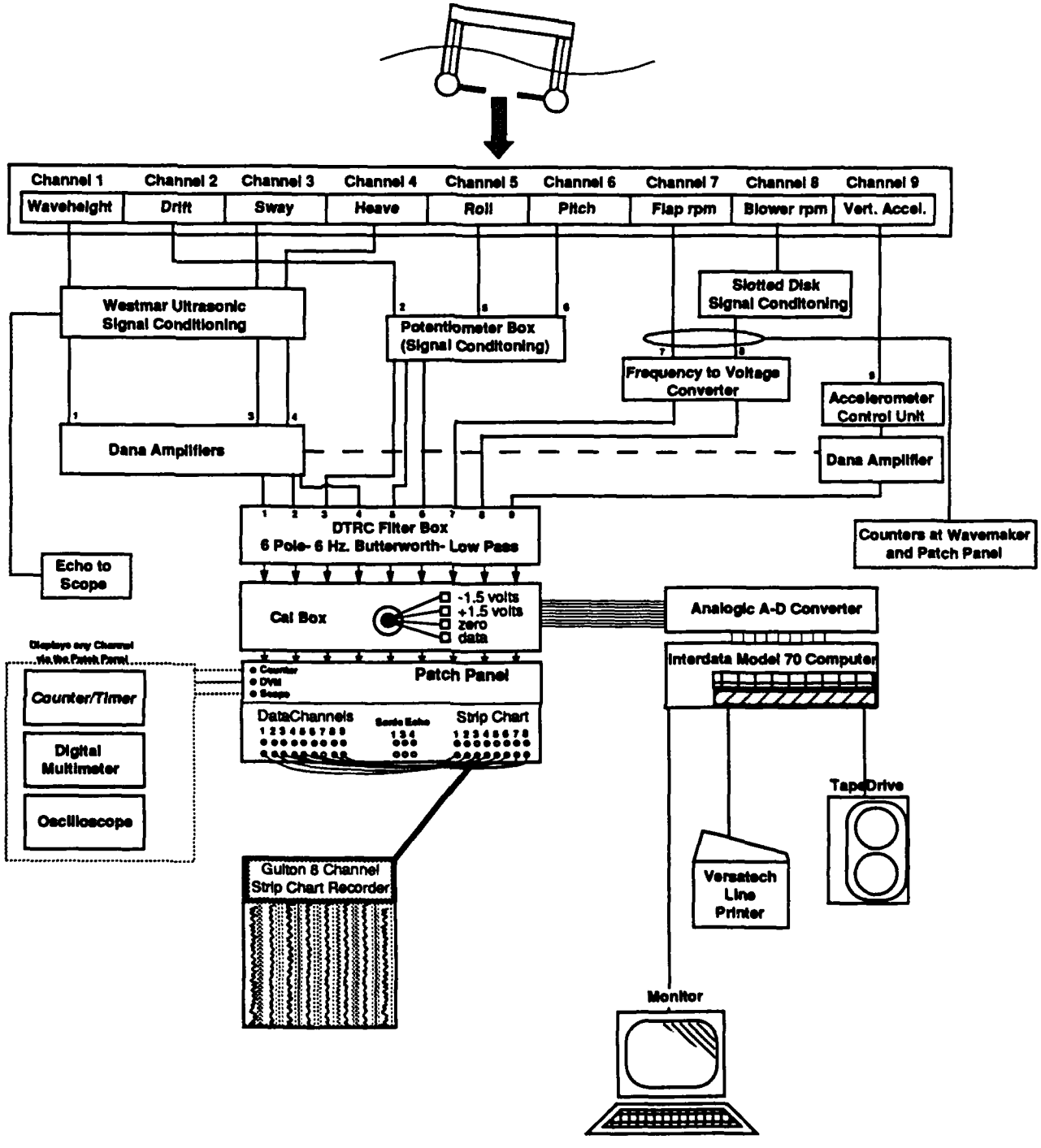

Fig. 6. Block diagram of instrumentation, signal conditioning and data collection equipment.

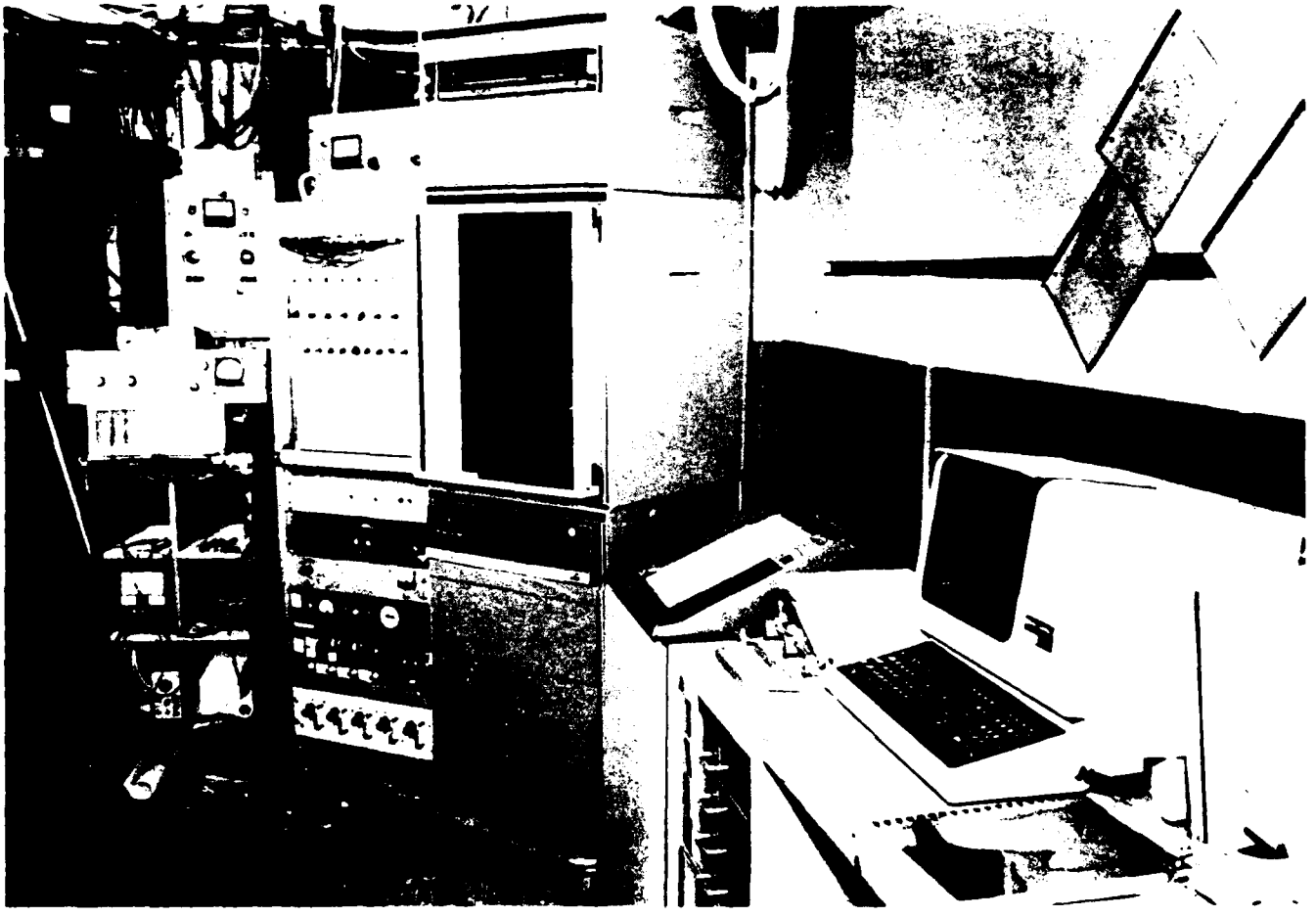

Fig. 7. Photograph of test instrumentation rack, and data acquisition computer.

140 FT BASIN SWATH BEAM SEA ROLL STUDY - SUBHARMONIC RESPONSE 21 DECEMBER '85

BASIN DEPTH, FT. : 5.0000

Fe =	0.429 hz	We =	2.696 rad/sec	Te =	2.331 sec
F0 =	0.429 hz	W0 =	2.696 rad/sec	T0 =	2.331 sec
Lambda =	27.820 ft	Wave Slope =	2.877 deg	Celerity =	7.072 kt
Lambda/L =	4.171	Wave Steep =	0.012	Lambda/H =	86.646

Heading : 90.0 deg

Runs : 31.: 0.000 - 27.970

	Channel		Calib	Gain	Mean	StdDev	Root0
1	WAVE HT	in	1.000E+00	1.000E+00	-1.993E-03	1.362E+00	1.926E+00
2	DRIFT	in	-5.000E+00	1.000E+00	3.469E+00	2.441E-03	3.453E-03
3	SWAY	in	-1.000E+00	1.000E+00	-1.443E+00	2.825E+00	2.864E+00
4	HEAVE	in	-1.001E+00	1.000E+00	1.563E-01	1.445E+00	2.844E+00
5	ROLL	deg	2.004E+00	1.000E+00	-2.598E-01	2.702E+00	3.821E+00
6	PITCH	deg	1.004E+00	1.000E+00	9.574E-02	1.179E+00	1.667E+00
7	FLAP	rpm	1.000E+02	1.000E+00	1.299E+02	2.736E+00	3.869E+00
8	BLOWER	rpm	1.000E+02	1.000E+00	2.297E+02	2.762E-01	3.906E-01

Fig. 8a. Minimum analysis page.

140 FT BASIN SWATH BEAM SEA ROLL STUDY - SUBHARMONIC RESPONSE 21 DECEMBER '85

BASIN DEPTH, FT. : 5.0000

Fe =	0.429 hz	We =	2.696 rad/sec	Te =	2.331 sec
F0 =	0.429 hz	W0 =	2.696 rad/sec	T0 =	2.331 sec
Lambda =	27.820 ft	Wave Slope =	2.877 deg	Celerity =	7.072 kt
Lambda/L =	4.171	Wave Steep =	0.012	Lambda/H =	86.646

Heading : 90.0 deg

Runs : 31.: 0.000 - 27.970

FFBB MULTIBIB				015		110		210	
Frequency (rad/sec)				1.348		2.696		5.391	
# of cycles				6		12		24	
Channel		Root0	Amp2/R00	Trn Fun	Amp1	Phase	Amp2	Phase	Amp3	Phase
1 WAVE HT	in	1.926E+00	9.91E-01	1.00E+00	5.182E-02	161.9	1.908E+00	0.0	1.445E-01	134.0
3 SWAY	in	2.864E+00	7.17E-01	1.00E+00	1.539E-01	84.5	2.854E+00	94.1	6.613E-02	-59.5
4 HEAVE	in	2.844E+00	9.91E-01	1.00E+00	2.832E-02	132.8	2.825E+00	149.3	4.524E-02	5.6
5 ROLL	deg	3.821E+00	9.01E-01	1.02E+00	4.693E-02	-38.9	3.749E+00	151.1	1.495E-01	146.0
6 PITCH	deg	1.667E+00	9.00E-01	0.00E-01	3.935E-02	139.1	1.647E+00	45.9	1.014E-01	113.1

Fig. 8b. Harmonic analysis page.

Fig. 8. Sample output from the real time data analysis, (run #31).

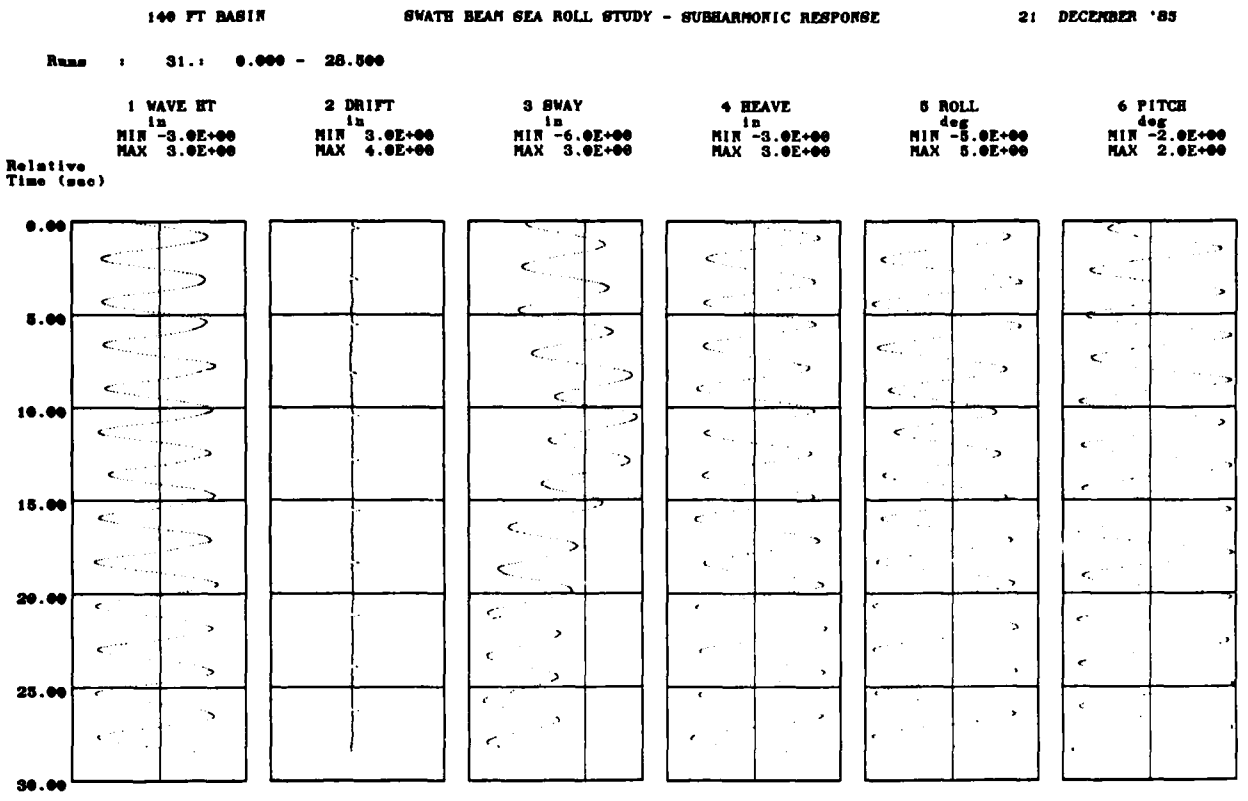

Fig. 9. Sample output from THRPDC (time history reproduce), for run #31.

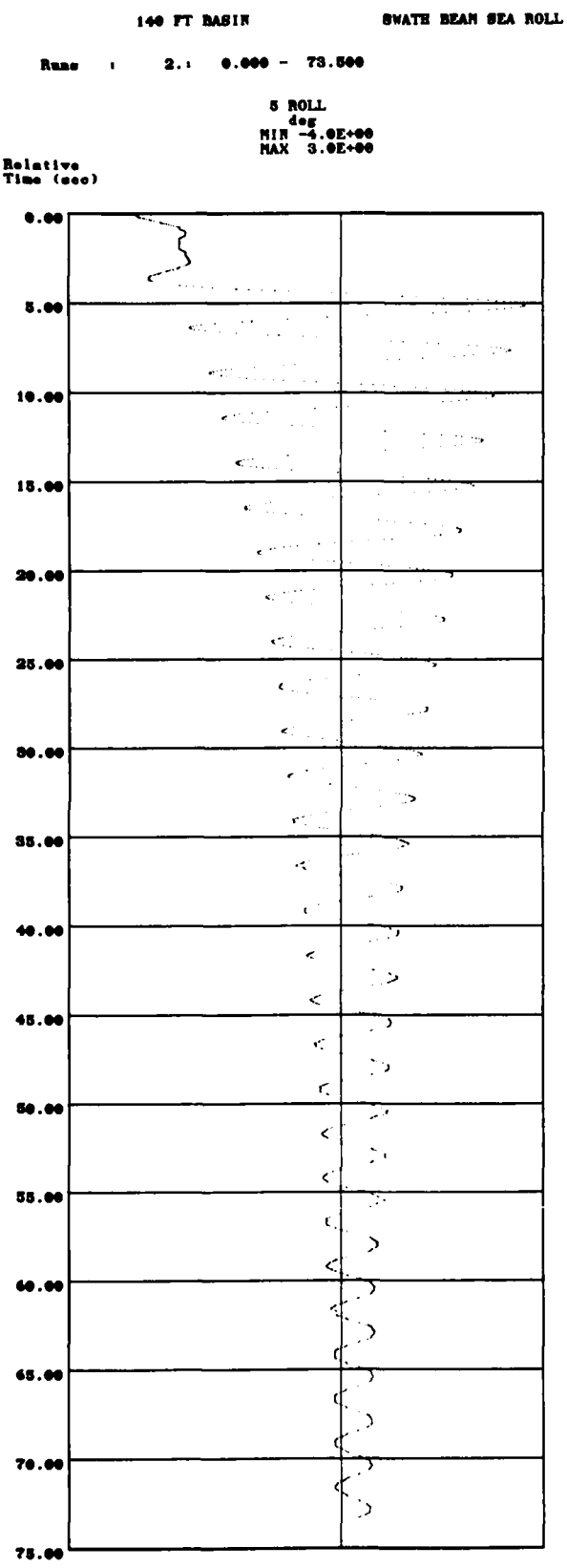

Fig. 10. Sample time history of the roll oscillation in calm water.

CHAPTER 5. PRESENTATION AND DISCUSSION OF RESULTS

NATURAL PERIODS AND DAMPING

Natural frequency and damping coefficients were determined from free oscillation experiments in calm water, as described below. The rate of decay of motion in a damped linear system is approximately exponential and can be determined from the ratio of successive amplitudes. The *logarithmic decrement* , δ, a commonly used measure of decay, is defined as the natural logarithm of the ratio of amplitudes n cycles apart, such that,

$$\delta = \frac{1}{n} \ln\left[\frac{z_i}{z_{i+n}}\right] \tag{5.1}$$

where z_{i+n} is the amplitude n cycles after z_i. The logarithmic decrement is related to the damping factor by

$$\delta = \frac{2\pi\zeta}{\sqrt{1-\zeta^2}} \tag{5.2}$$

and thus for small damping, the damping ratio, ζ, can be determined from

$$\delta \cong 2\pi\zeta \tag{5.3}$$

$$\zeta = \frac{\delta}{2\pi} \ . \tag{5.4}$$

Since the *damped natural frequency* , ω_d, is measured in the free oscillation, and is defined as,

$$\omega_d = \omega_n \sqrt{1-\zeta^2} \tag{5.5}$$

the undamped natural frequency, ω_n, can then be calculated from Eq. 5.5. Note that the damping was so low in these experiments that the difference between the damped and undamped natural frequency, using Eq. 5.5, is two orders of magnitude below that which could be measured with the test apparatus.

Figure 10 shows a sample of the roll natural decay time history. The mean roll was not exactly zero so the mean offset needed to be extracted. This was also the case for heave. A method of fairing the half-amplitude peaks and extracting the mean offset was adapted from Roberts[4]. Roberts[4] uses a spline fit of the decay of the overall envelope and then interpolates for the estimated half-cycle peaks and troughs, as shown in Fig. 11a. The resulting peaks and troughs are shown with the corrected mean in Fig. 11b. For simplicity, a straight line interpolation between peaks was used to define the envelope, rather than the spline fit . While not as precise as the spline, this technique greatly reduced the scatter in the estimation of the half-cycle amplitude decay. Figure 12 shows a sample of the corrected versus the uncorrected peaks in the roll decay. The absolute values of the peak amplitudes were then plotted versus half cycles, on a semi-log scale. The slopes of the straight lines drawn through these data as shown in Figure 13 are equivalent to the log decrement, given by Eq. 5.1.

Table 6 presents a summary of the natural periods in both model and ship scale, and the damping factors [Eq. 5.4] expressed as a percent of the critical damping. Since there was a noticeable decrease in the damping after the first 5 cycles for both roll and heave oscillations, the damping factors are presented separately for the initial 5 cycles, as well as for the whole run. The drop after the first 5 cycles was more significant for heave, however, the damping in all cases was considered to be small. While damping was treated as linear in this study, an evaluation of the effects of higher order damping terms could be applied using these data in the future. Dalzell[5] and Spouge[6], provide methods in which the data could be used to determine the extent of higher order, nonlinear damping coefficients such as the linear-plus-quadradic or linear-plus-cubic forms. The observed nonlinearity (first 5 cycles) may well be fit by one of these forms.

Also shown in Table 6 are the standard deviations of the natural periods. As can be seen in the data, the effects of the restraints were negligible. As might be expected, the

restraining lines only caused a slight increase in the damping (roll and heave), and appeared not to have an effect on the natural frequencies, other than to slightly decrease the standard deviation of the heave period.

Strong heave-pitch coupling was observed in the attempts to get a clean pitch oscillation in calm water, for the pitch damping. Therefore, only the period is reported for pitch.

Table 6. Natural periods and damping factors

Mode	Natural Periods		Damping Factors	
	Model sec	Ship sec	First 5 cycles % critical	All cycles % critical
Roll-as tested	2.53 ± .02	15.0 ± 0.1	1.9	1.7
Roll-no restraints	2.53 ± .02	15.0 ± 0.1	2.1	1.7
Heave-as tested	1.44 ±.03	8.5 ± 0.2	3.6	1.6
Heave-no restraints	1.44 ± .05	8.5 ± 0.3	3.8	1.8
Pitch-as tested	2.2 ± 0.4	13.1 ± 2.4	- Not Applicable-	- Not Applicable-

It is interesting to note that of the four configurations tested by Numata[1], the two that had the most subharmonic response (Deep Draft & Low KG*) had ratios of heave to roll natural frequency, very close to two, and that of the two, the Deep Draft configuration had greater subharmonic roll amplitudes.

* The *Low KG* (or *High* GM_t) configuration is the one modeled in this study.

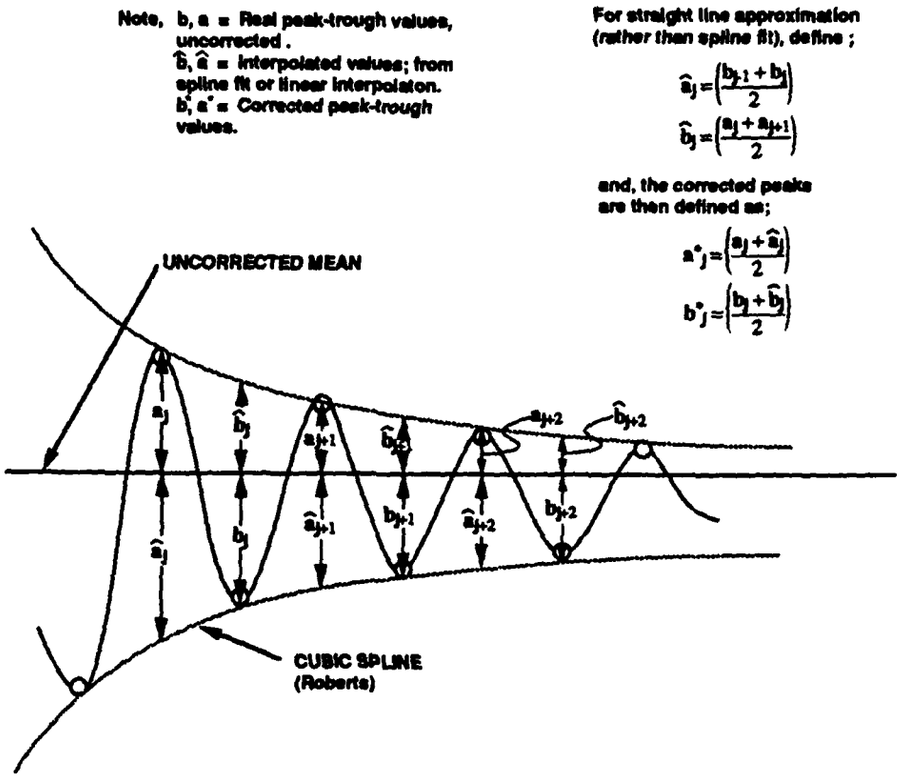

(a) Spline fit to positive and negative peaks.

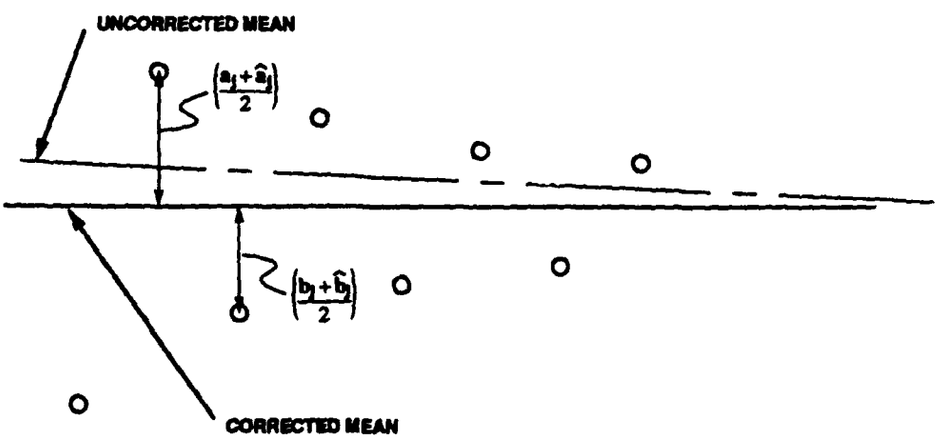

(b) Mean corrected peaks.

Fig. 11. Method of drift removal and mean offset correction to roll decay trace from calm water experiments.

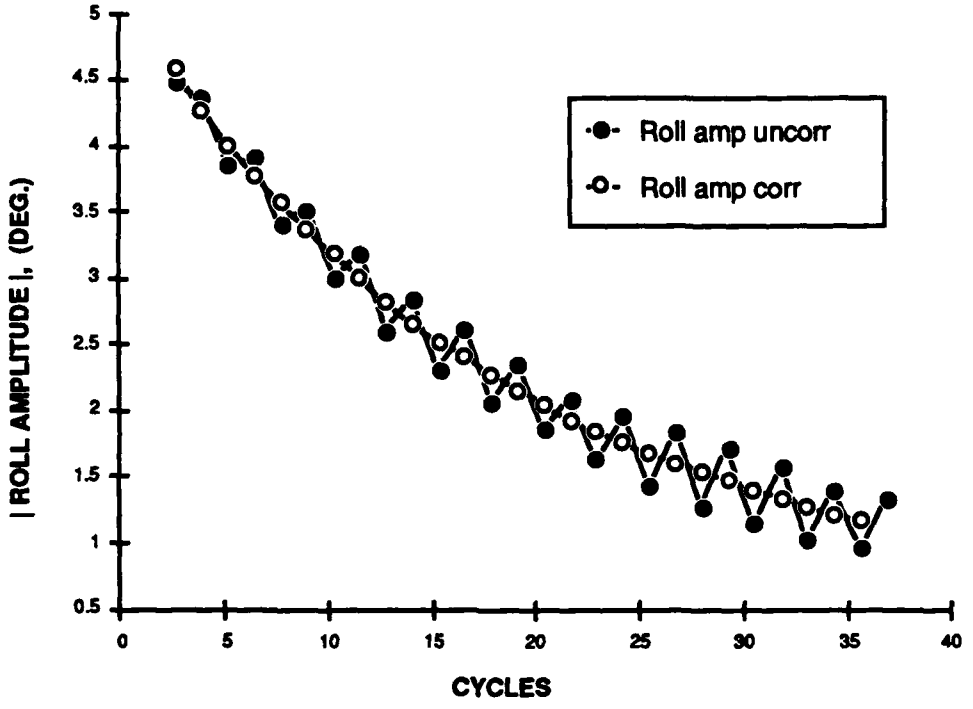

Fig. 12. Sample plot of the corrected and uncorrected peaks of roll amplitude decay.

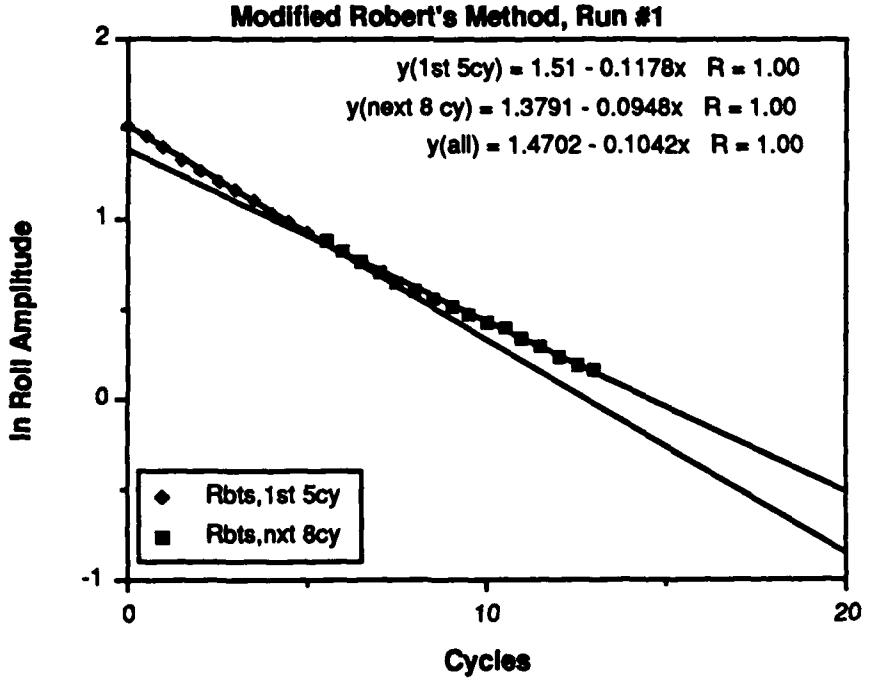

Fig. 13. Log decrement plot for roll damping calculation.

REGULAR WAVE TRANSFER FUNCTIONS

Presented in Figures 14a. -14d., are the regular wave transfer functions of Sway, Heave, Roll , and Pitch (as defined in previous chapter). The resonant (natural) frequencies are marked and Numata's regular wave data[1] are included for comparison. The correction for shallow water effects was applied to the wave slopes used to calculate the Roll and Pitch transfer functions.

The transfer functions generally exhibit the proper asymptotic shape. That is, at high frequency they tend toward zero, and at low frequency toward unity, with peak responses at or near the resonance points (with the exception of pitch, as expected). In beam seas, the pitch transfer function is expected to be small, however the effects of heave coupling can be seen. The double peaks in the pitch transfer function, correspond to the pitch and heave resonance points. The asymmetry of the fins, fore and aft (larger fins aft) may also contribute to the heave coupling. Still, the magnitude is below 1, which is to be expected in beam seas. A somewhat lower Roll transfer function peak was observed, as compared to Numata's data, but the shape agrees qualitatively (Fig. 14c).

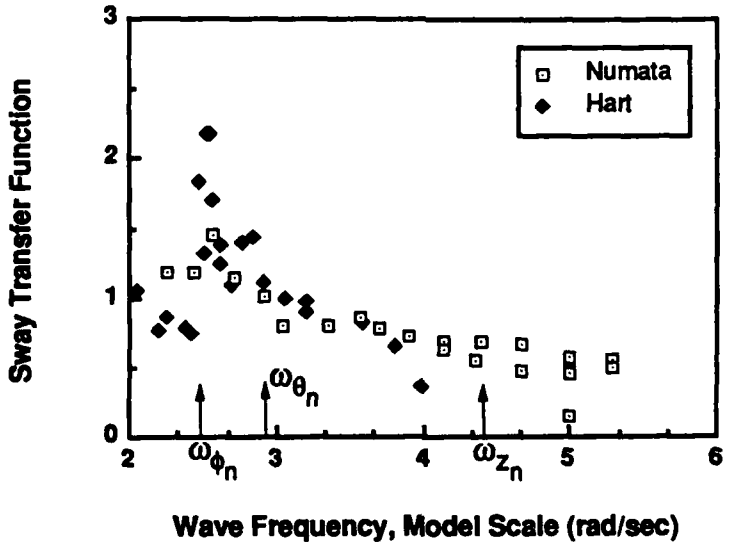

Fig. 14a. Sway transfer function.

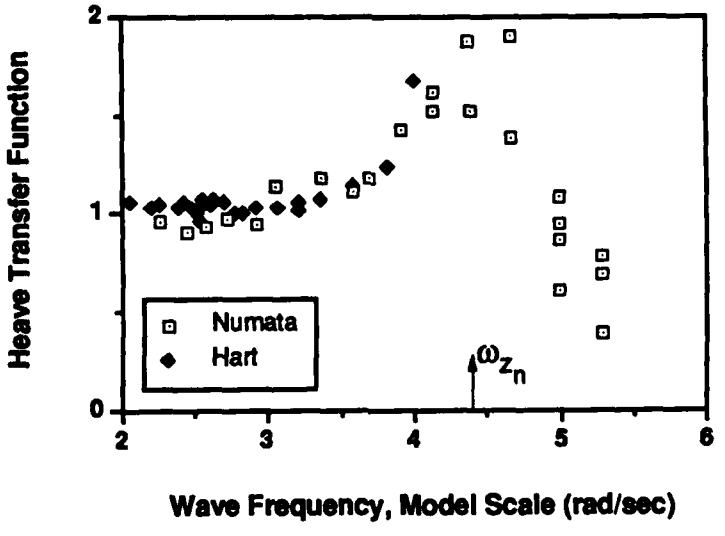

Fig. 14b. Heave transfer function.

Fig. 14. Linear transfer functions with comparison to Numata's results.

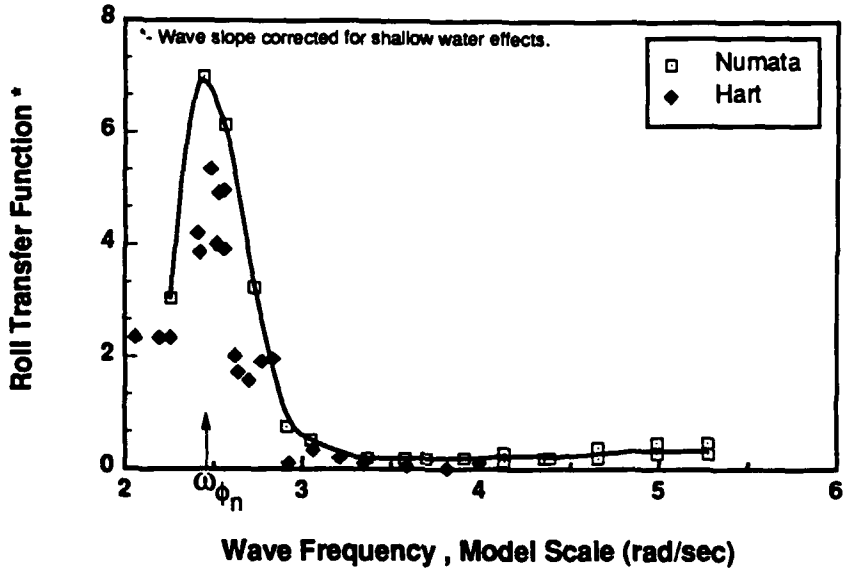

Fig. 14c. Roll transfer function.

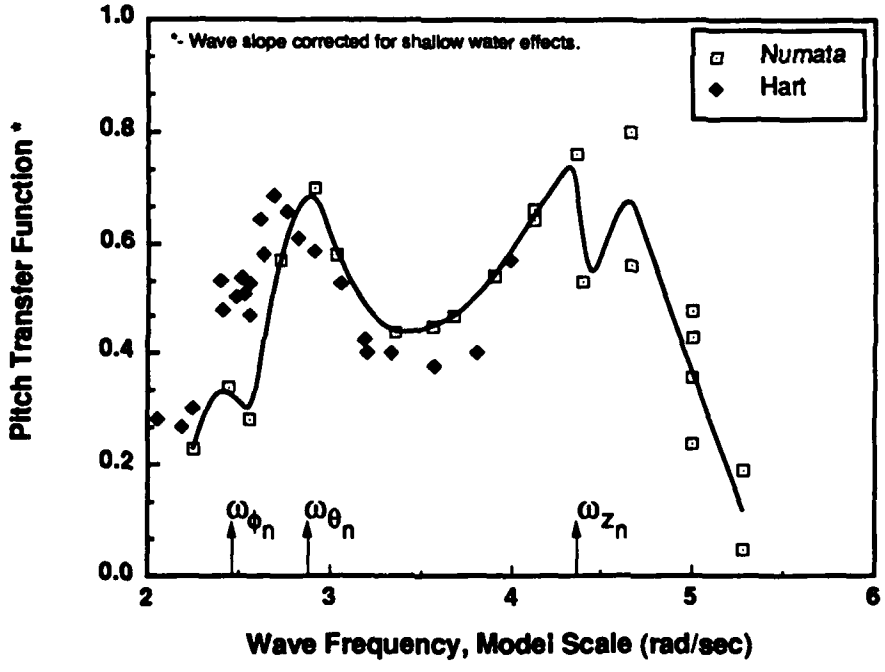

Fig. 14d. Pitch transfer function.

Fig. 14. (Continued)

SUBHARMONIC ROLL RESPONSE

Stability Diagram

The results of tests conducted to determine the subharmonic roll characteristics of this model, are presented in Fig. 15. This figure presents an overall picture of the types of responses which occurred in this region. First, it should be noted that the ordinate is in model scale units of wave amplitude, while the abscissa is given as a nondimensional frequency ratio of the wave encounter frequency to twice the natural roll frequency. As mentioned earlier, the objective of this experiment was to characterize the stability boundary of the occurrence of subharmonic rolling. This stability diagram (Fig.15) represents both quantitative and qualitative information. It serves as a sort of map of the type of responses that were observed, as well.

There were basically four types of roll response identified in this wave frequency region. They are denoted on the figure as *No*, for no subharmonic response; *Slight* , for a small, but detectable component of subharmonic roll; *Combined*, which represents runs that clearly exhibited distinct components of each; and *Yes* which refers to the occurrence of pure (large amplitude) subharmonic rolling.

The stability boundary is basically defined by the linear (*no*) responses, which occurred at both the low and high wave amplitudes, and at wave frequencies above and below the resonant frequency of $\omega_e/2\omega_{\phi n}=1$. These points are denoted with the open circles. The "U" shaped line drawn on the diagram is just a freehand approximation of the boundary between the stable and unstable regions.

The occurrence of *slight* subharmonic response, denoted by the shaded circles, was typical mostly of the low frequency side of the boundary. This type of response was characterized by an unsteady roll motion of low magnitude. These runs, while typically

having a small but detectable component of subharmonic response, often started out as linear and then became unsteady (perhaps chaotic).

The *Combined* runs, denoted with the split black and white circles, typically exhibited strong subharmonic response. These runs often started out as linear roll, then transitioned to subharmonic response while growing in amplitude, often to large subharmonic roll amplitudes. Combined responses most often occurred on the high frequency side and top of the stability boundary.

The runs noted as *Yes* in Fig. 15 with the solid circles, typically exhibited a pure subharmonic roll response of large amplitude. In most cases, the roll motion started out with a low amplitude subharmonic response growing to appreciable subharmonic roll amplitudes.

While the responses could generally be classified into one of these four categories, several other interesting forms of behavior were observed, some of which made the distinction between categories unclear. For example, the growth rate of roll as a function of wave amplitude and frequency may have been the main difference observed between a *combined* run and a *yes* run classification for some runs. The rate at which the roll transitioned from one mode to another (ex. linear to combined) also varied with the specific test conditions. Other interesting observations were that the model's drift rates often varied during a given run, as a function of the motions. Also, large steady tilt angles (i.e. large mean roll angles) occurred at the larger wave amplitudes, both inside and outside of the stability boundary. The maximum roll angles achieved in a given run also varied throughout the region. All of these variations, while being interesting, made the task of analyzing and categorizing the data extremely difficult. These observations will be discussed further in the following sections.

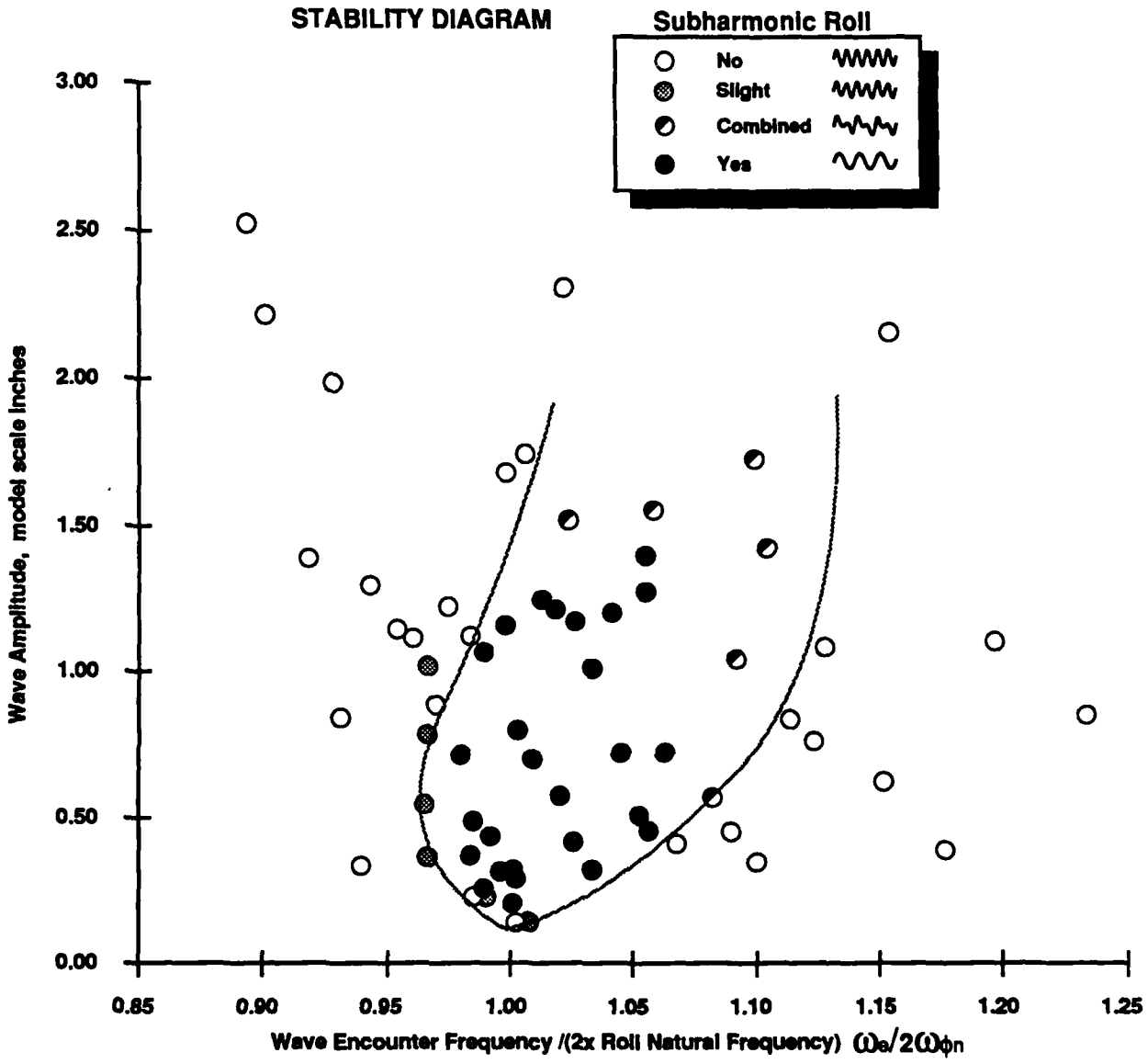

Fig. 15a. Stability diagram with data points and boundary.

Fig. 15. Stability diagram of the occurrence of subharmonic roll in experiments.

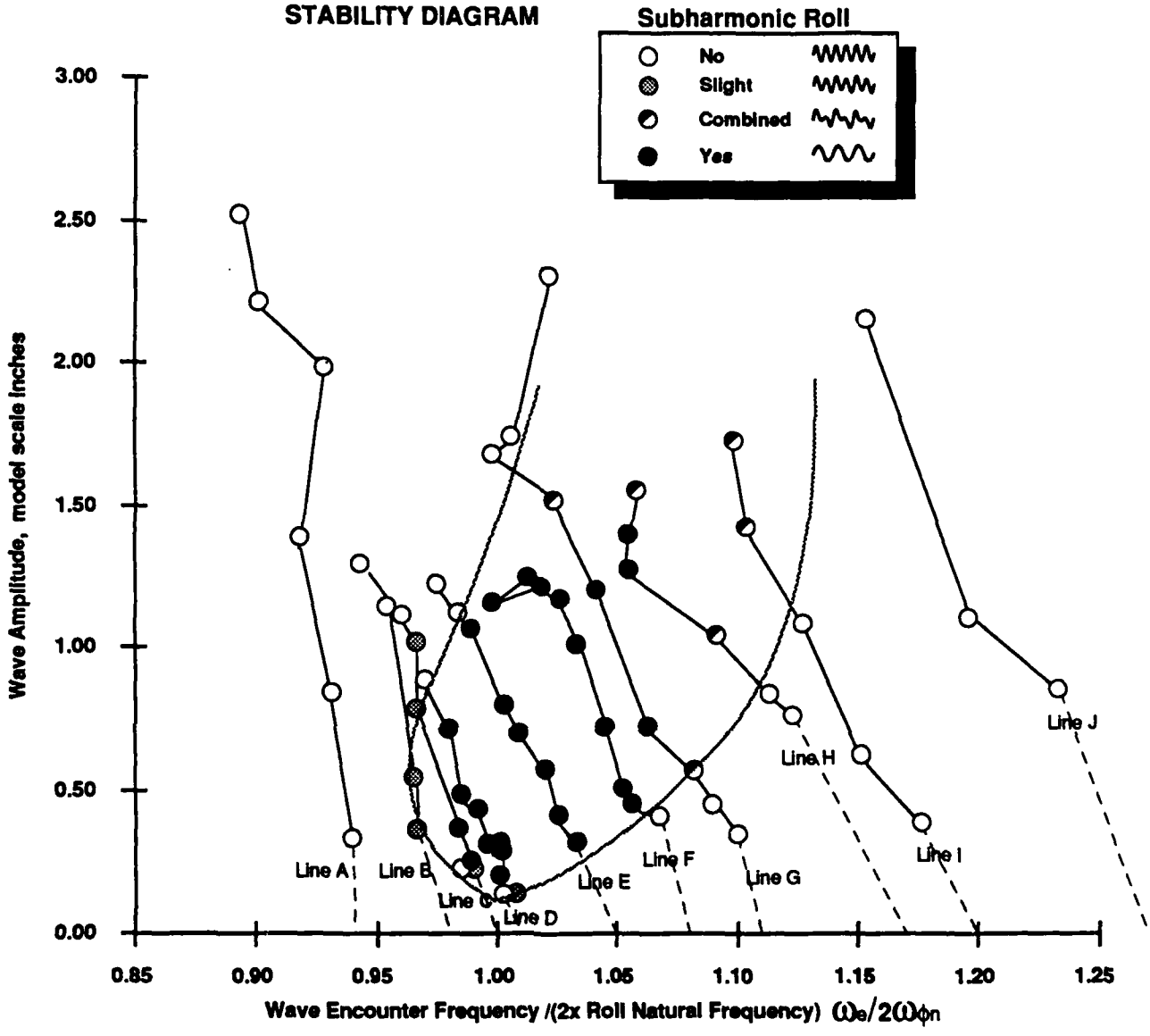

Fig. 15b. Stability diagram with lines of constant wave frequency marked.

Fig. 15. (Continued)

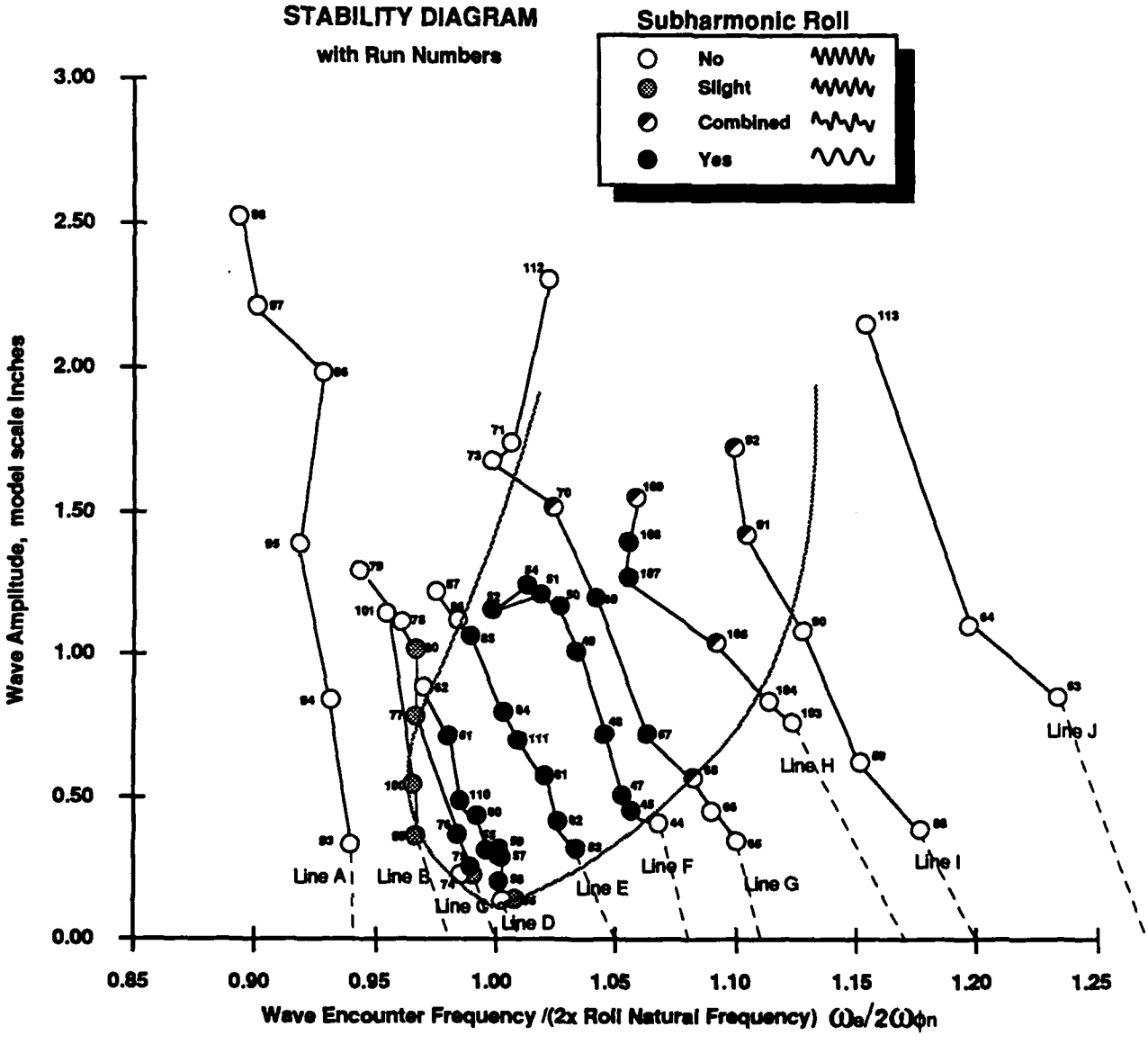

Fig. 15c. Stability diagram with run numbers marked

Fig. 15. (Continued)

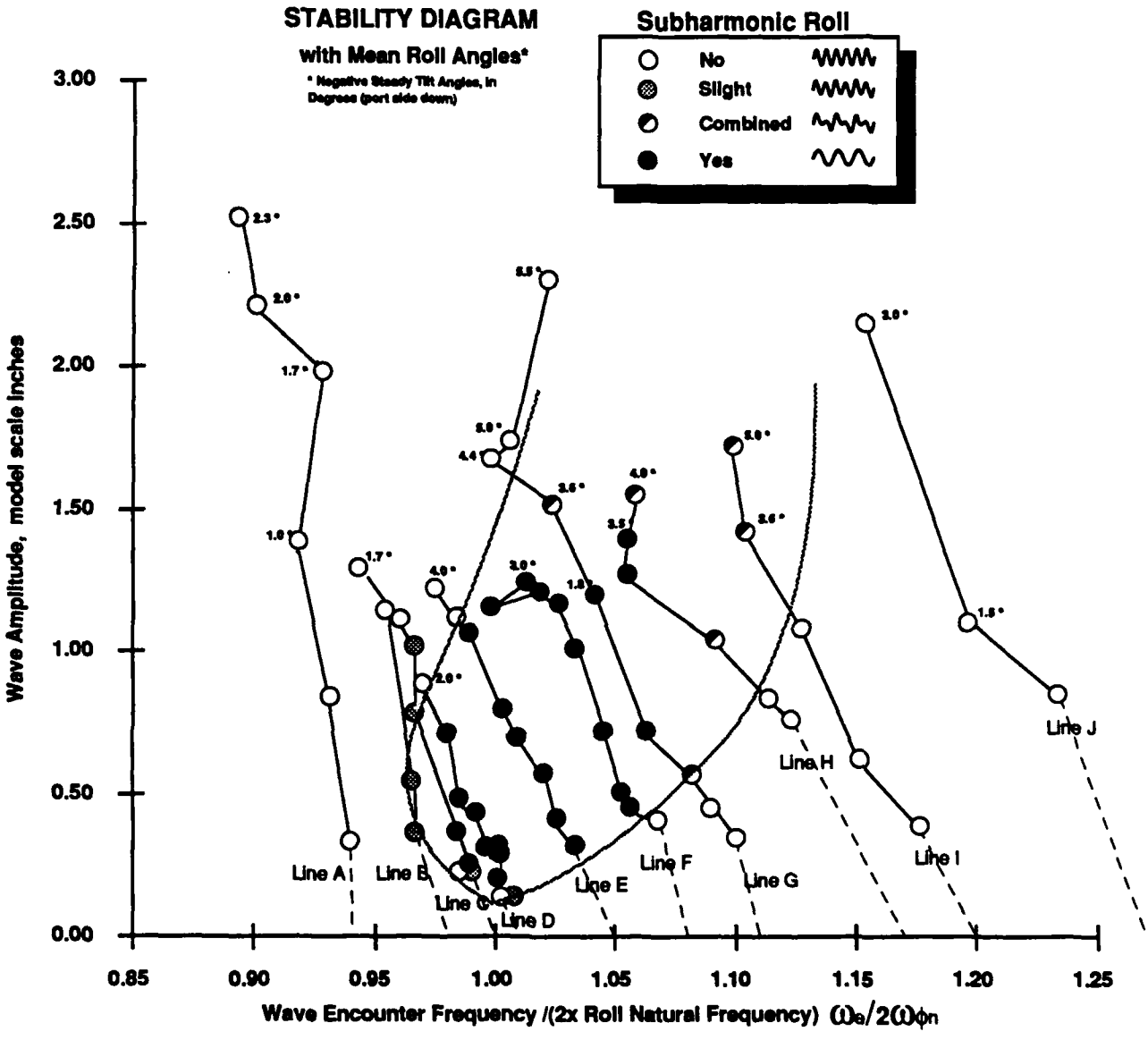

Fig. 15d. Stability diagram with with steady tilt angles marked.

Fig. 15. (Continued)

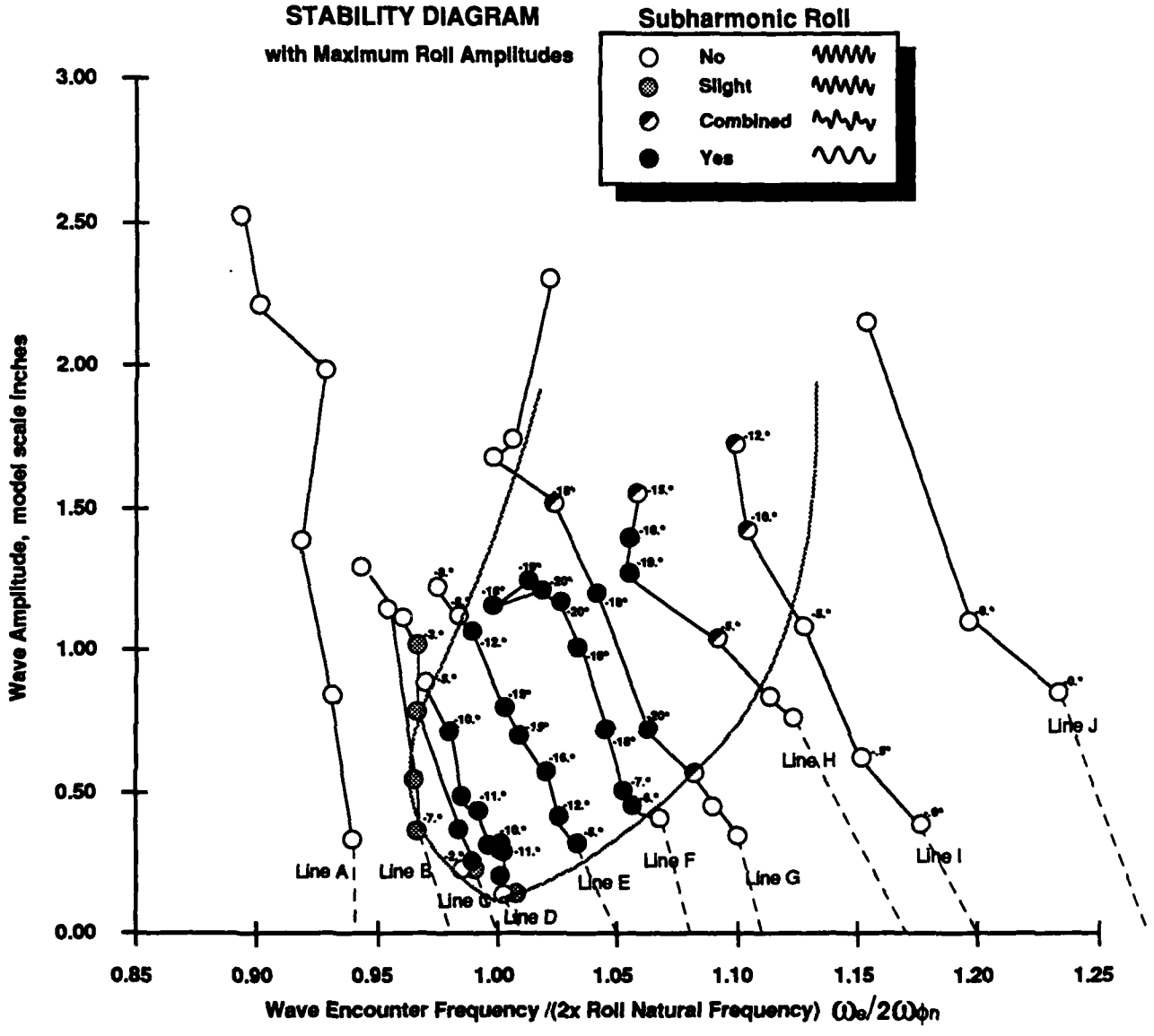

Fig. 15e. Stability diagram with maximum roll angles (single amplitude) marked.

Fig. 15. (Continued)

Lines of Constant Wave Frequency

In Figure 15b. *Lines* A through J are added to the stability diagram and correspond to the lines of constant wave frequency, previously referred to in the test matrix in Table 5. The specific run numbers for each point on the stability diagram are provided in Fig. 15c. While the dashed lines from the abscissa denote the wave frequency for each *Line* on the stability diagram, each point reflects the model's encounter frequency. It can be seen by the way each line is swept toward lower frequencies at higher wave amplitudes, that the model drifted in nearly all of the runs in this region (thereby reducing the frequency of encounter between the model and the waves). In *Line G*, for example, at low wave amplitude, the roll response is linear (runs 65 & 66). As wave height was increased, the model drift rate increased, causing the encounter frequency to be reduced to a point where the model begins to respond in a subharmonic manner (runs 67 to 70). As the wave height was raised further, the response again became linear, as the encounter frequency was no longer in the unstable region (runs 71,73,112). Therefore, in Line G at a constant wave frequency, by merely increasing the wave amplitude, the model transitioned through the various boundaries (or modes of response) in the stability diagram.

Subharmonic roll occurred at the lowest wave amplitudes for runs having wave frequencies nearest to the resonance point of $\omega_e/2\omega_{\phi_n}=1$. In general, the rate of growth of roll amplitude increased with wave amplitude, but there appears to be a cap, or maximum wave height above which the roll returns to linear motion. The Lines A and J bounded the stability diagram, showing no subharmonic tendencies at wave frequency ratios of .94 and 1.27, respectively.

Measures of Nonlinear Roll Response

Summarized in Figures 15d and 15e are estimates of the steady tilt and the maximum roll angle, plotted on the stability diagram for the various runs. Since these results may be

dependent on the length of the run (e.g. time to build up to a steady maximum roll angle), they should probably be viewed as a qualitative data summary of the test results, or general description rather than quantitative fact. As can be seen in Fig 15d, steady tilt reached angles on the order of -5. degrees, generally increased with wave amplitude, and was not confined to subharmonic rolling region– although the larger angles occurred in the unstable region. Figure 15e shows the maximum roll angles amplitudes measured throughout the subharmonic region.

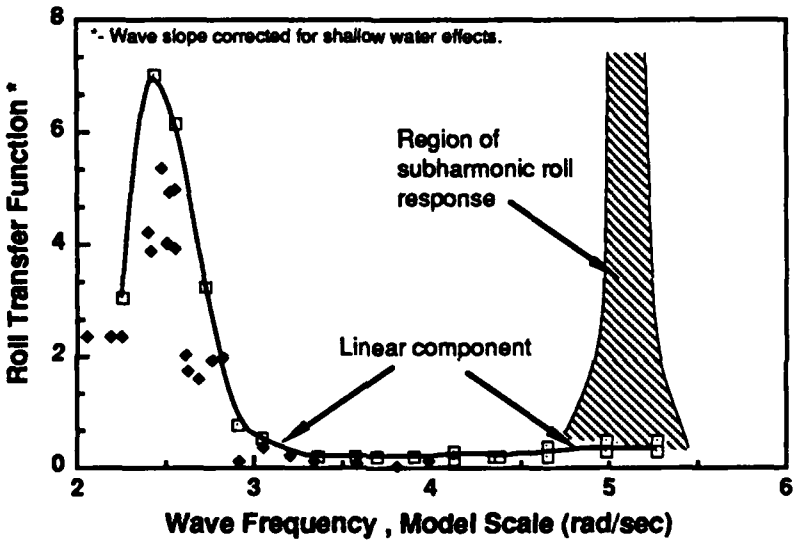

Fig. 16. Roll transfer function showing region of roll instability.

The overall significance of the subharmonic response can be seen in Fig. 16, where the general region of the subharmonic roll is shown with the expected response from linear theory. Although the linear response is expected to be minimal in this region, the subharmonic component of roll has potential to produce significant and unexpected roll angles. The maximum roll angles, however, appeared to be capped at amplitudes of approximately –20 degrees, and the frequency range of the subharmonic roll was relatively narrow.

Sample Time Histories

To further illustrate the types of responses observed in these experiments, several representative time histories are presented and discussed below (Figs. 17-28). These time histories were generated using the THRPDC program, from the digitized data on tape. Each page presents the time histories of wave height, drift, sway, heave, roll, pitch, and vertical acceleration (Z ACC CG) given in model dimensional units. Care should be taken in comparing the responses from run to run since the plots were scaled automatically and thus the scales are not necessarily the same in each figure. Also, the phase relationship between the motions and the wave height channel cannot be directly applied in these plots since the phase of the wave data has not been corrected for the fact that the wave probe was 12.21 feet upstream of the model. The polarity of the wave height signal is also reversed in these time histories (corrections were made in the analysis but not to the digitized raw data). In viewing the responses, note that the mean sway indicates the model's position relative to the carriage, where positive sway is to starboard or toward the wavemaker. The drift channel basically shows the carriage position as a function of time, and goes from positive to negative, as the carriage is drifted with the model toward the beach.

In Fig. 17, the time history of run 56 (of Line D in Figure 15c) shows the transition of the roll motion from linear to subharmonic at a very low wave amplitude. Over the first 13 seconds, the model has started drifting (see sway channel), while the carriage is initially stationary. Looking at the drift channel, it can be seen that the carriage is then started and moved to follow the model's approximate rate of drift. At the time of the experiment, the roll motion in this run was not evident to the eye (or on the analog strip chart), and it was originally thought that there was little or no subharmonic response. However, with the roll amplitude scale blown up to ±0.4 degrees, the transition from linear to subharmonic roll is clearly evident. Figure 18 shows how the response changes in run 58, the next run on Line D, for an increase in wave height of less than a tenth of an inch (model scale). Here the roll

is clearly subharmonic and grows steadily to a single amplitude of over 10 degrees. Run 84 (Fig. 19) from Line E has roughly the same encounter frequency, but occurs at a higher wave amplitude, and exhibits an even faster build up of the subharmonic roll. These time histories are fairly typical of the *Yes* runs in Fig. 15.

Figure 20 (run 80, Line C) is an example of a typical *slight* run type, having a low amplitude, unsteady roll response with some evidence of the subharmonic component of roll. Figure 21 (run 91, Line I) shows a typical combined response, where at the high wave amplitude and frequency boundary of the stability diagram, large roll amplitudes in both the linear (fundamental) and subharmonic (half-harmonic) frequencies can be seen.

The digital time histories for runs 65 to 71 of Line G are given in Figures 22 to 28. Figures 22, 23, and 28 (runs 65,66, and 71) provide examples of linear response (*no*) run types for two of the boundaries of the stability diagram, and Figures 24 to 27 (runs 67 to 70) illustrate the effect of increasing wave height, at a constant wave frequency. In Fig. 22 (run 65), a slight subharmonic transient can be seen in the first 7 to 8 cycles that appears to die out. While the roll amplitudes are hardly steady over the course of the run, the frequencies were basically linear (i.e. matched the wave frequency) for both runs 65 and 66 (Fig. 22 & 23). The roll amplitudes were less than 1 degree in these runs, which may account in part for the apparent unsteady roll.

In Fig. 24, run 67, the roll build up can be seen as it starts as linear low amplitude rolling, and then transitions to combined, and then finally pure subharmonic rolling. It takes approximately 18 to 20 cycles to transition from linear to subharmonic, before reaching a maximum amplitude of nearly 15 degrees (30 deg. peak to peak). While pitch also transitions to a subharmonic response, the maximum amplitudes are relatively small (1 to 1.5 degrees.).

Figure 25 shows the time history for run 68, which was in a lower wave height than the previous run. The most obvious effect of the reduced wave height on the roll motion is the increased time for the transition from linear to subharmonic response. The drift speed is

also slightly lower than in the previous run. Like run 67, the roll motion starts out with low amplitude, linear response, transitioning to subharmonic, and finally growing to 13-14 degree peak-to-peak roll excursions which is only half the previous run (#67). Run 68 was classified as a *combined* run on Fig. 15, mainly because of the long transition time (>25 sec.) from linear subharmonic rolling. The classification in this case is rather subjective, and could have been considered as a *yes* run type.

Runs 69 and 70, shown in Fig.26 and 27, exhibit faster subharmonic growth as well as the onset of a steady tilt (or mean roll) angle, with the port (lee) side down. In run 70 (Fig.27), the steady tilt appears to be increasing with roll amplitude, reaching nearly -4.0 degrees mean roll by the end of the run. Another observation in run 70 is that the drift velocity appears to slow down at the end of the run. The carriage is initially drifting at a steady rate, and then the mean sway starts to decrease rapidly toward end of run, as roll amplitudes and tilt get large. Run 70 was classified on Fig. 15 as a *combined* run since the transition from linear to subharmonic involved a few cycles of large amplitude combined response, however this run could have been considered either a *yes* or *combined* run type. The difference in this case is again rather subjective.

As wave height is increased further, Run 71 (Fig. 28) shows that the roll response again becomes linear (also with a steady tilt). At the beginning of the run, a slight transient subharmonic response can be seen, but dies out after the first few cycles.

Summary

The time histories presented above generally illustrate the trends of the experimental results. As should be apparent from these examples, the quantification of the results was extremely difficult due to the unsteady nature of the response and various other problems such as wave reflections. The impact of these and other difficulties with the experiment and the analysis are discussed further in the next section.

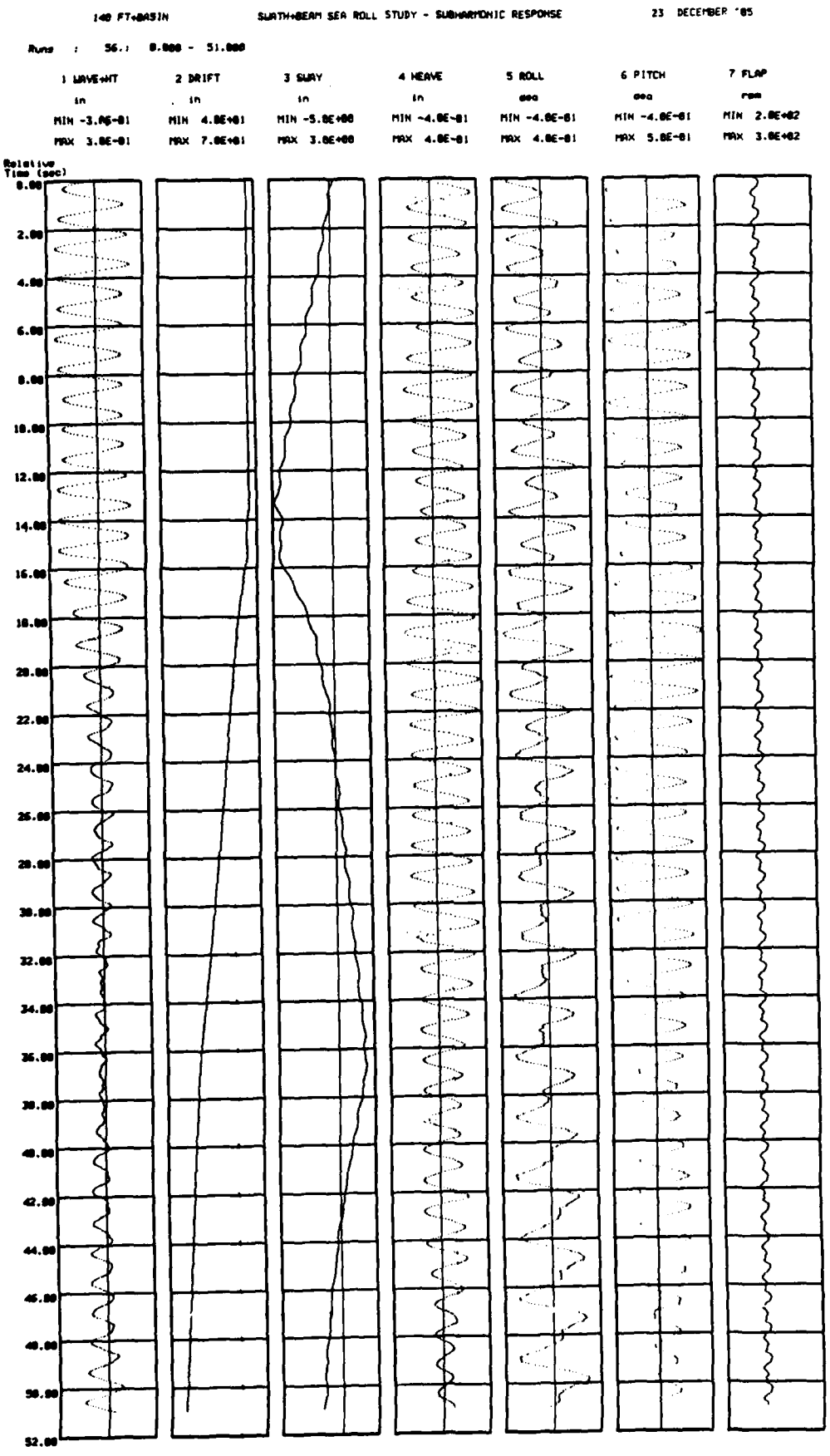

Fig. 17. Sample time history from Line D, Run 56 (Low wave amplitude transition to subharmonic roll).

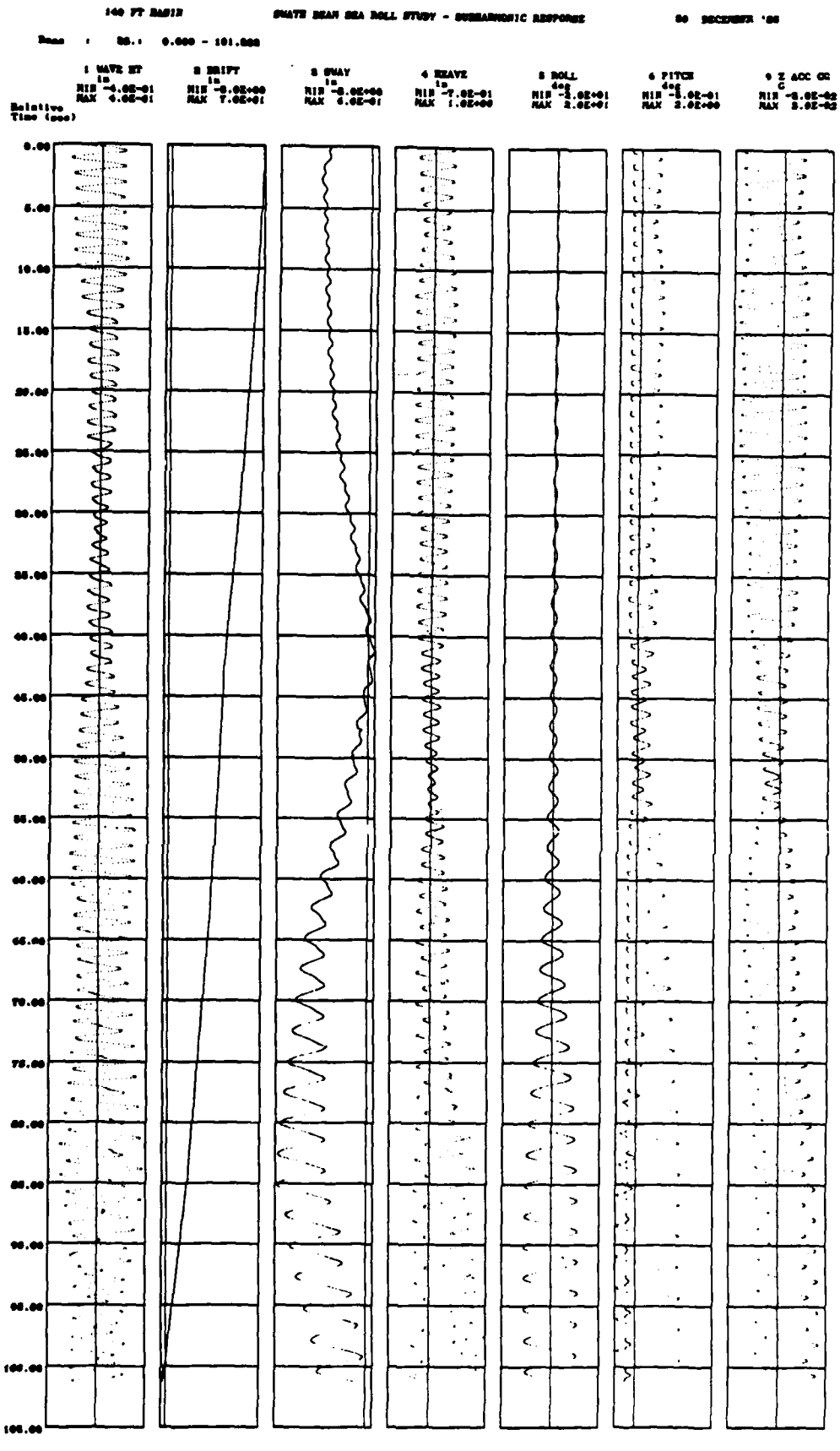

Fig. 18. Sample time history from Line D, Run 58 (Typical low wave amplitude *Yes* response).

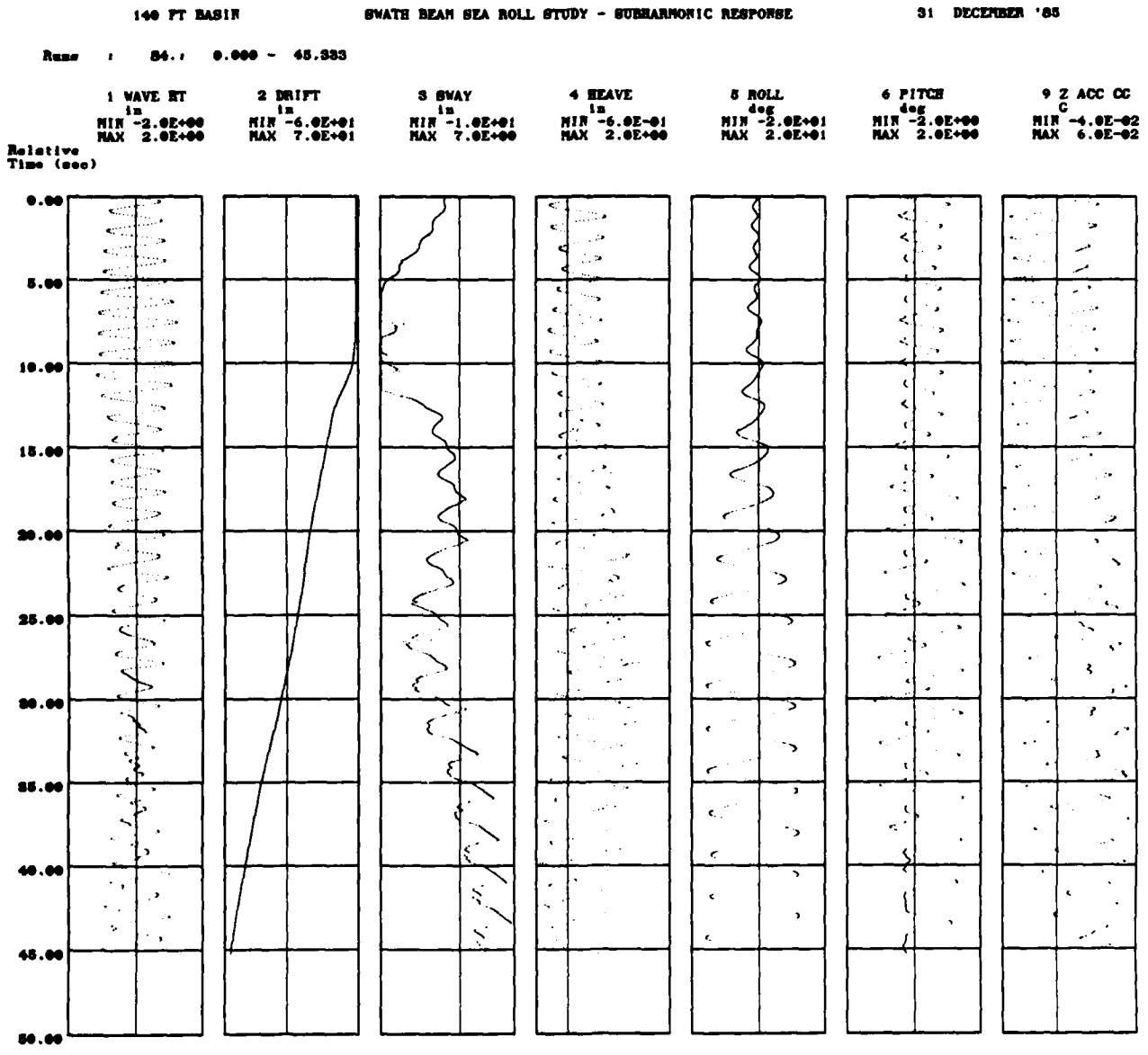

Fig. 19. Sample time history from Line E, Run 84 (Typical *Yes* response).

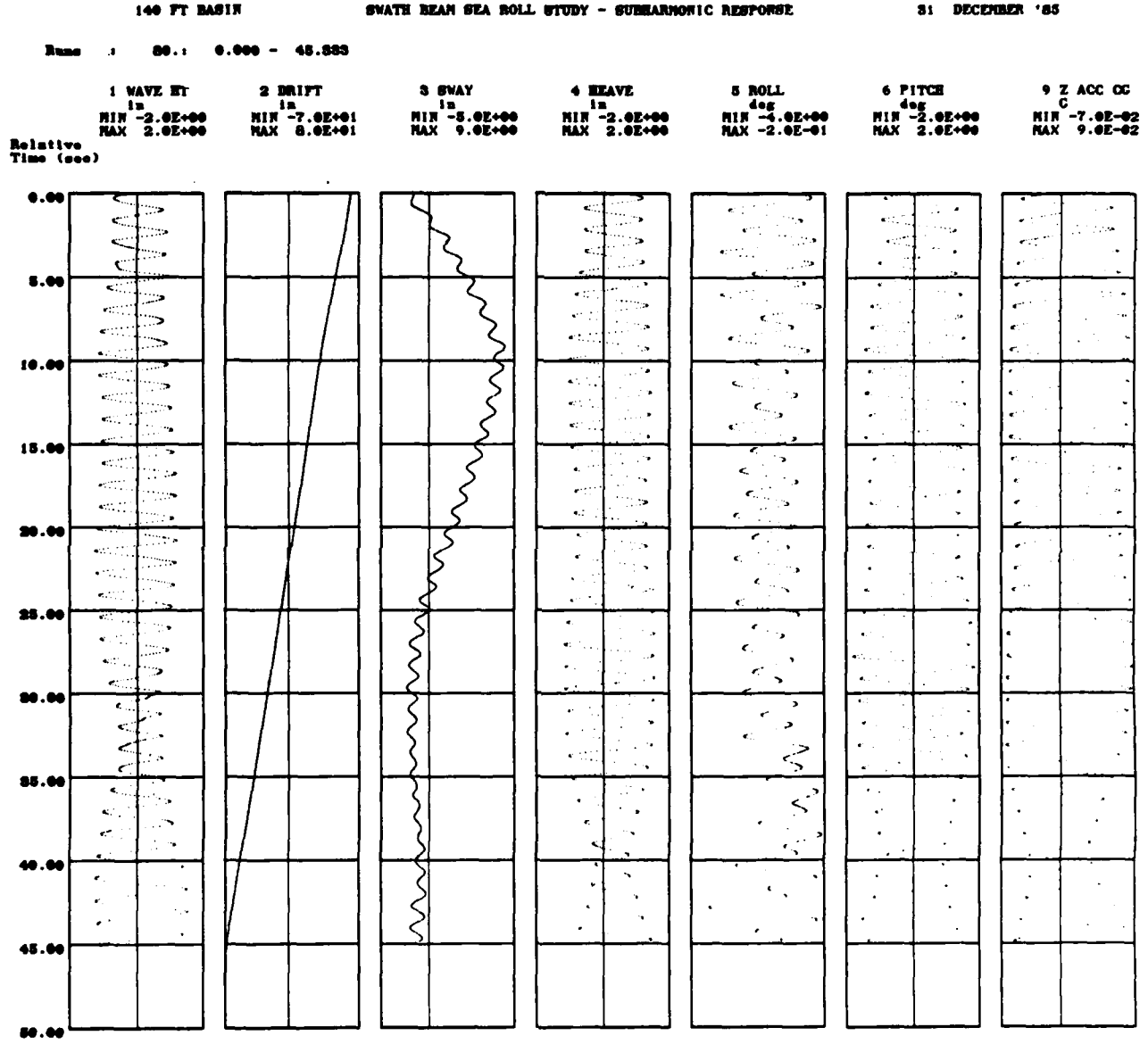

Fig. 20. Sample time history from Line C, Run 80 (Typical *Slight* response).

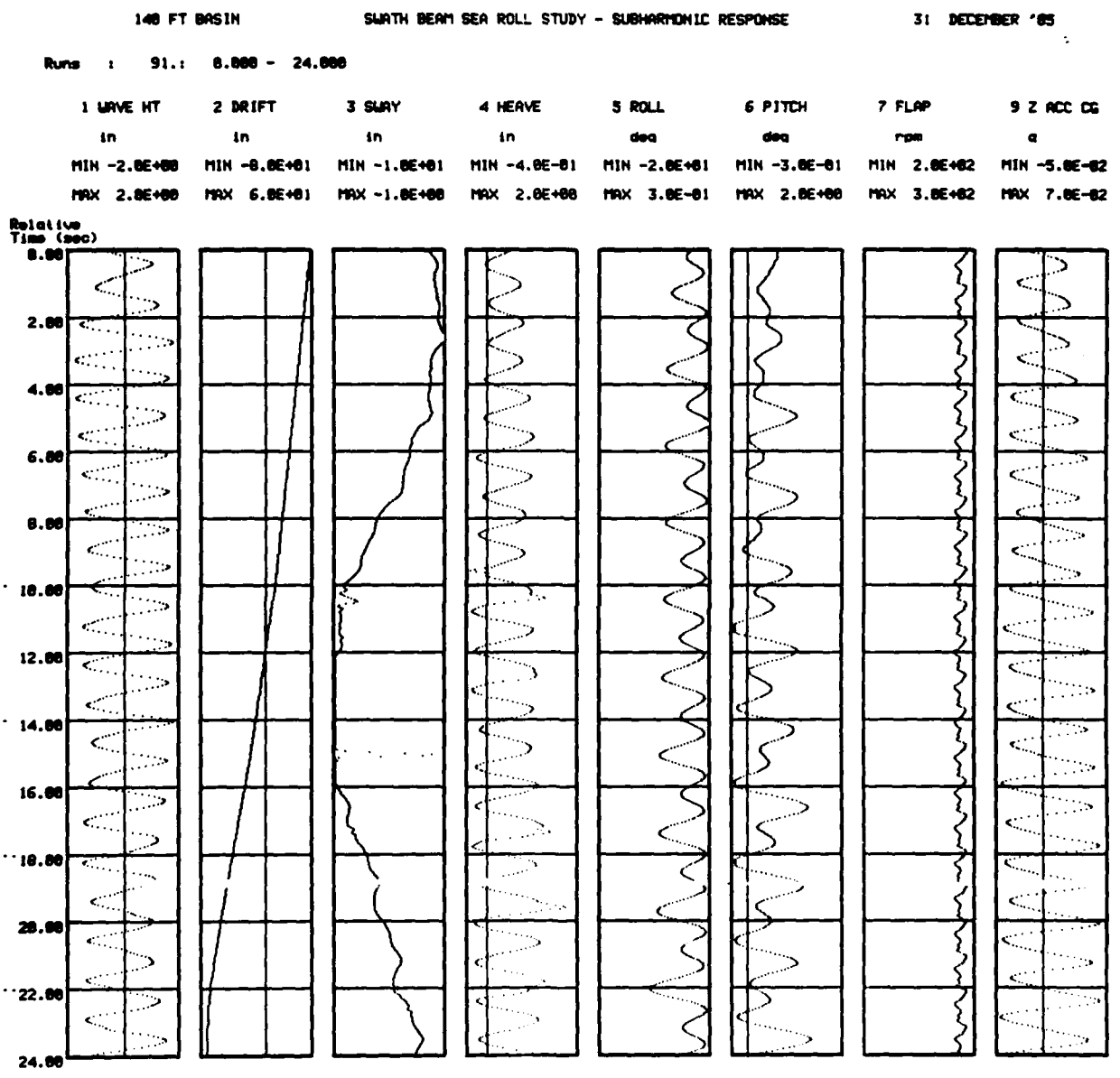

Fig. 21. Sample time history from Line I, Run 91 (Typical *Combined* response).

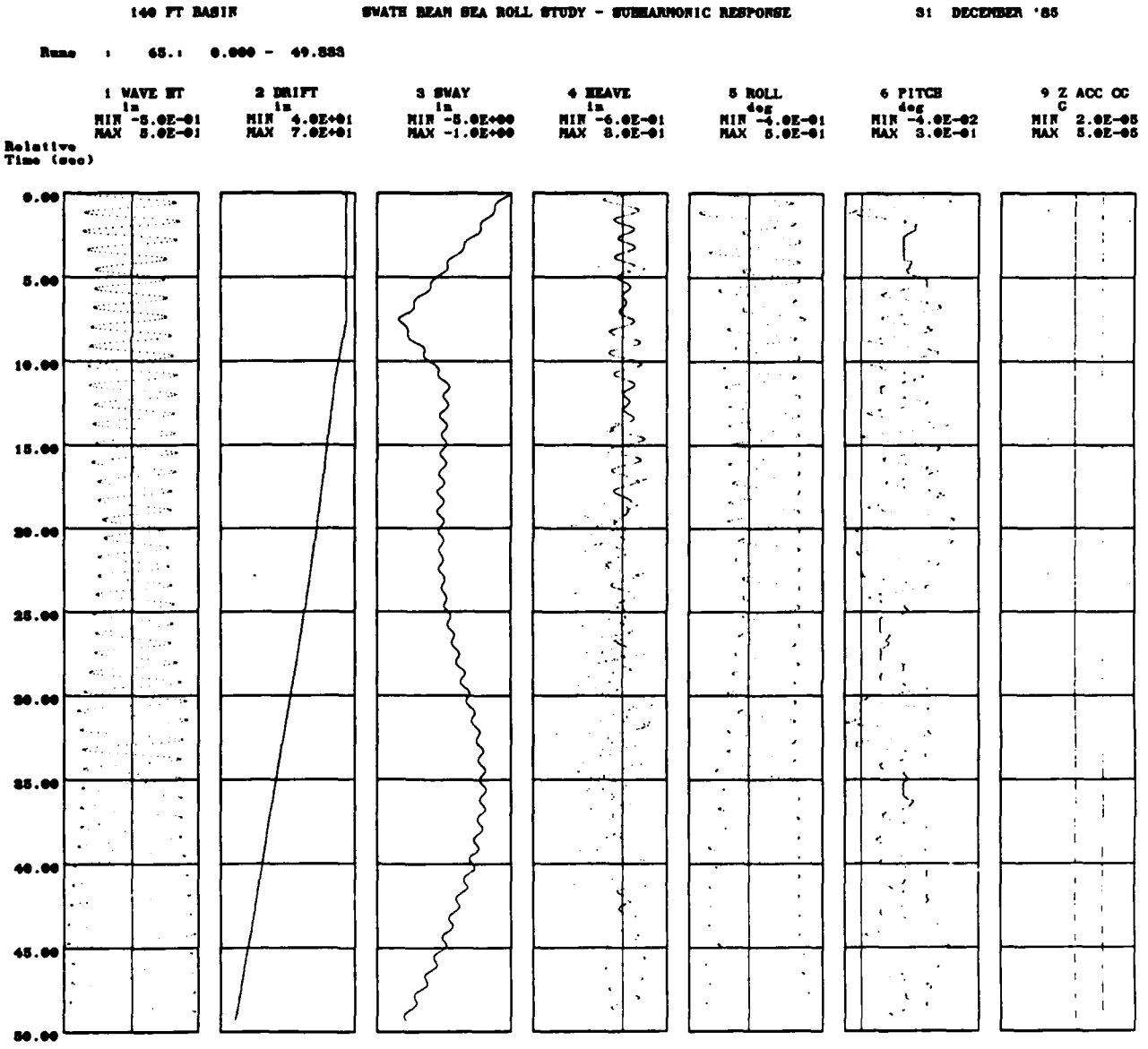

Fig. 22. Sample time history from Line G- Run 65.

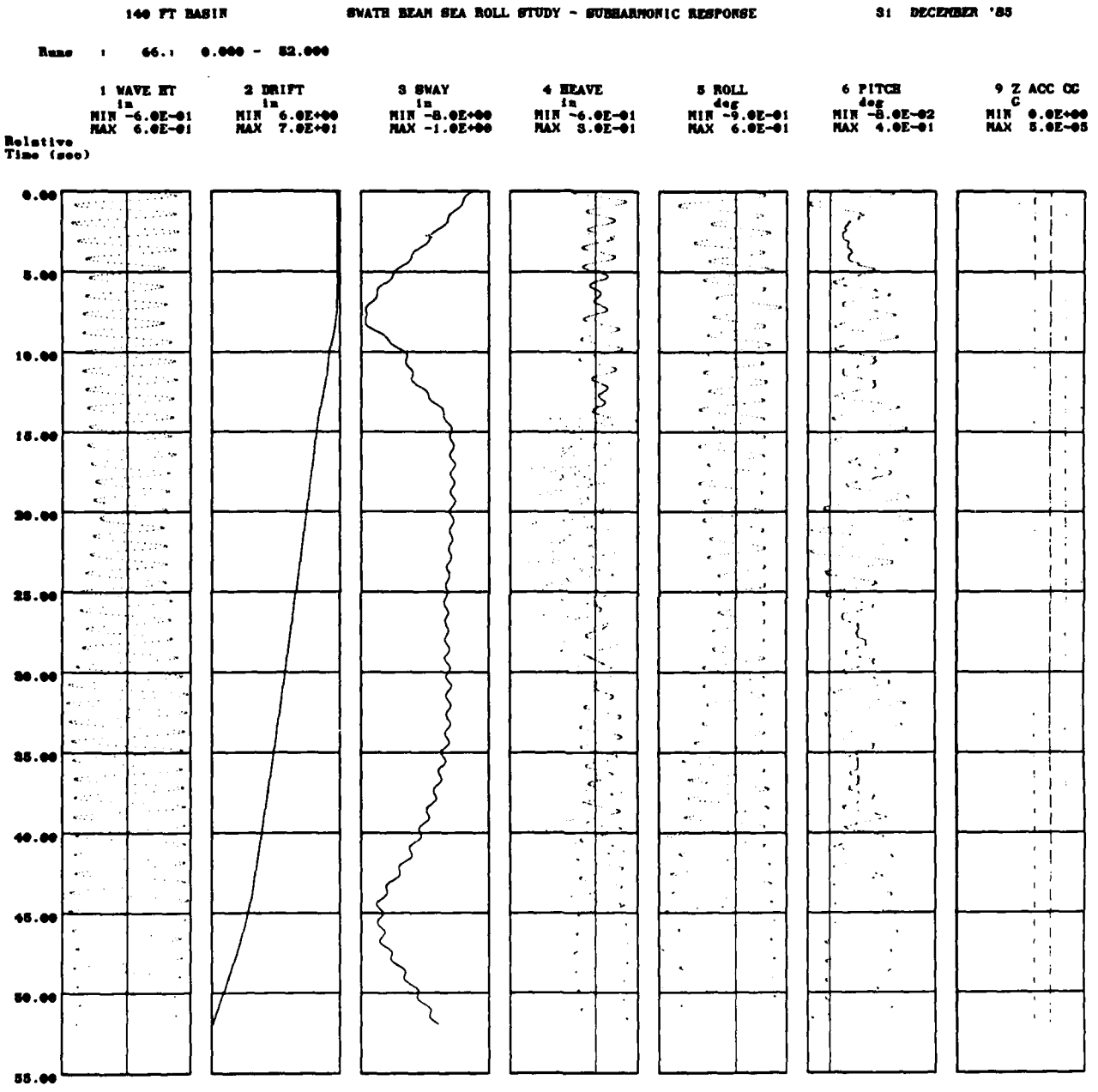

Fig. 23. Sample time history from Line G- Run 66.

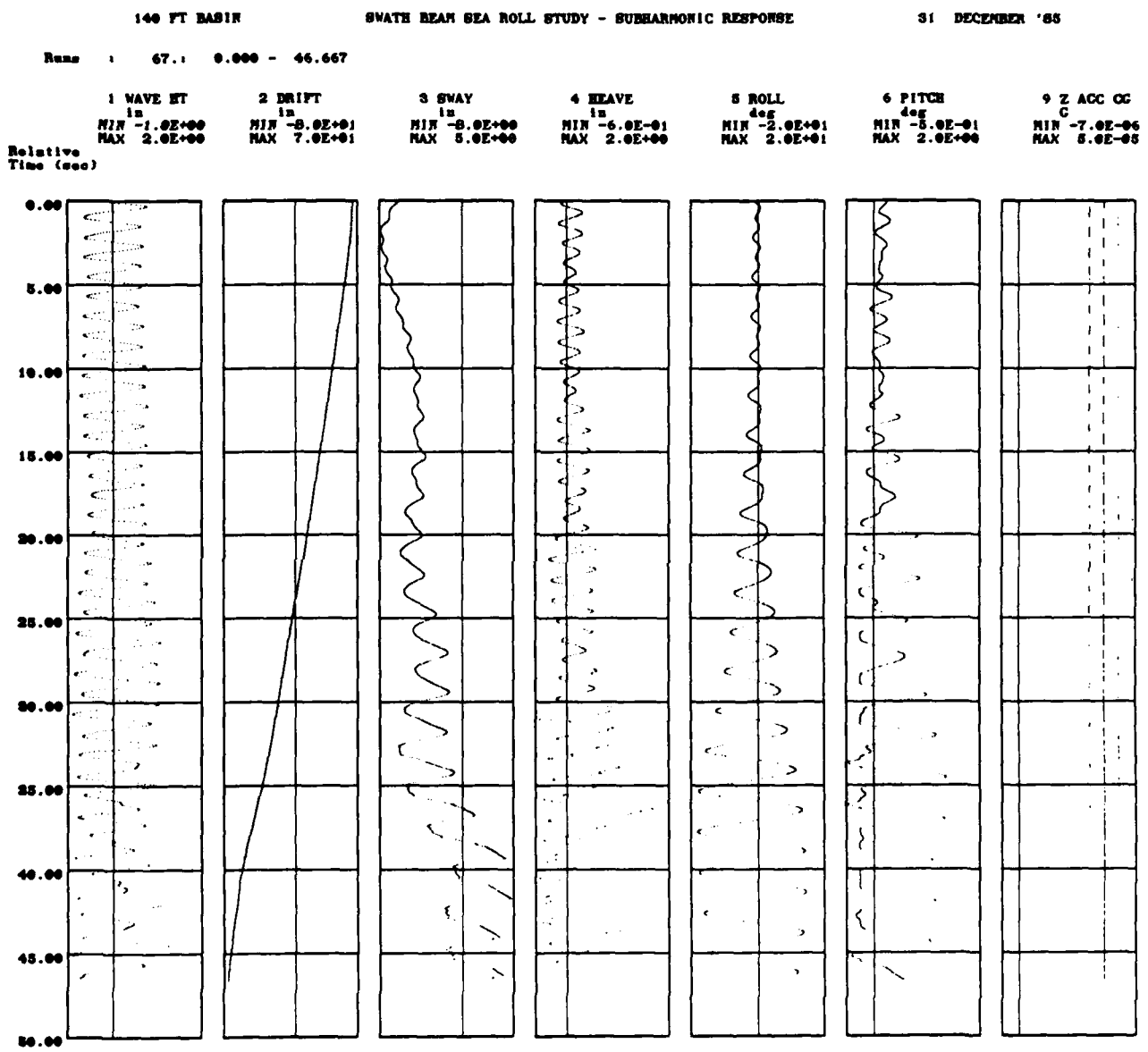

Fig. 24. Sample time history from Line G- Run 67.

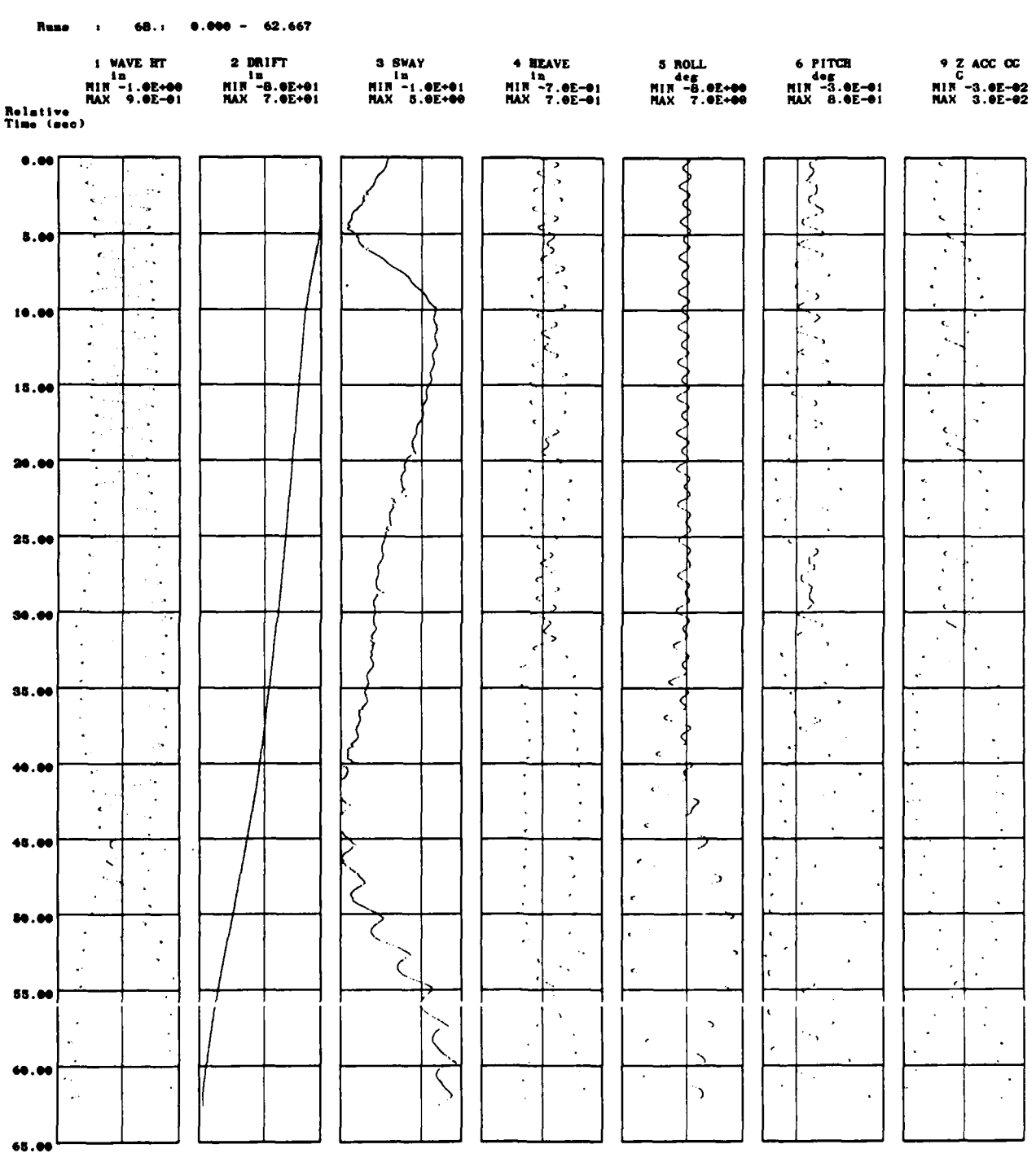

Fig. 25. Sample time history from Line G- Run 68.

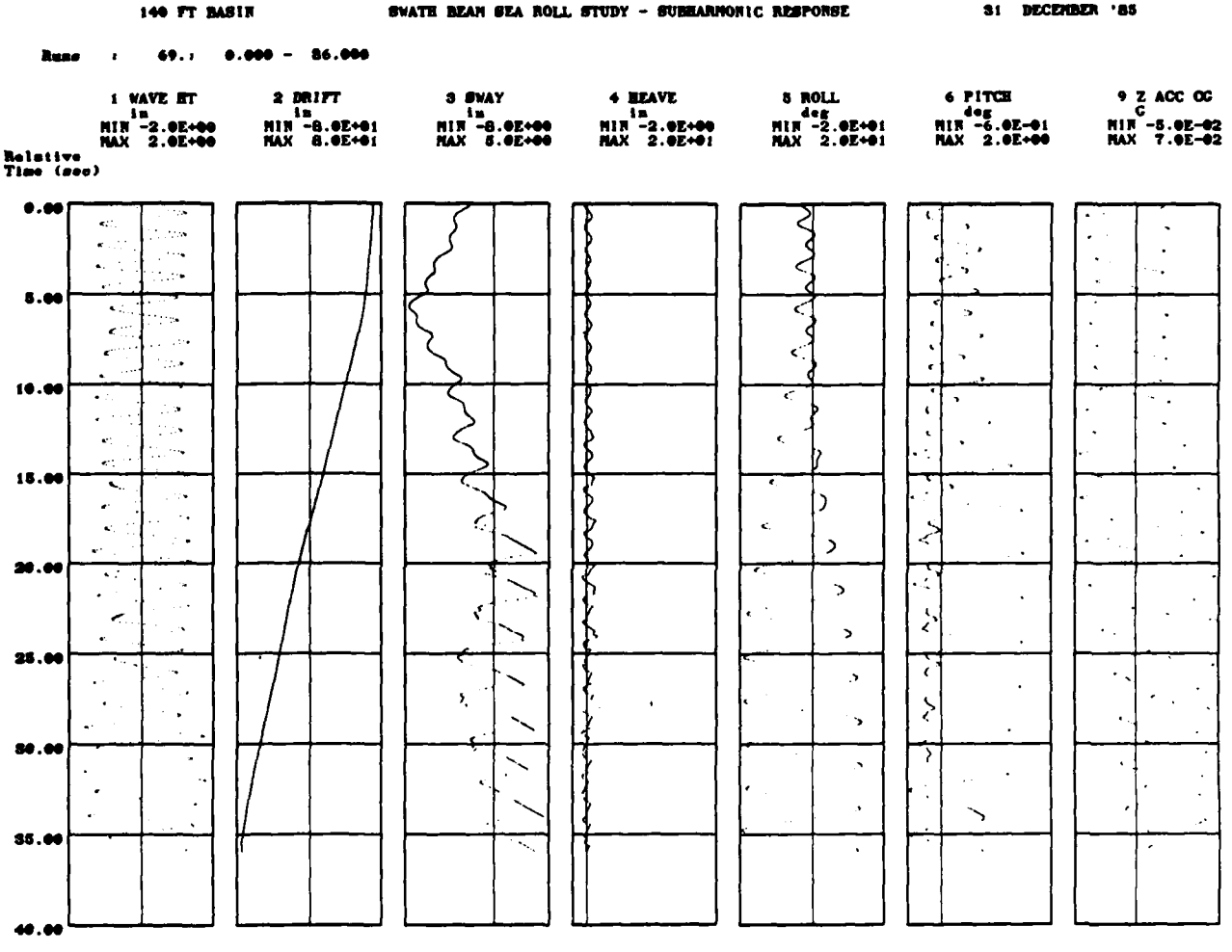

Fig. 26. Sample time history from Line G- Run 69.

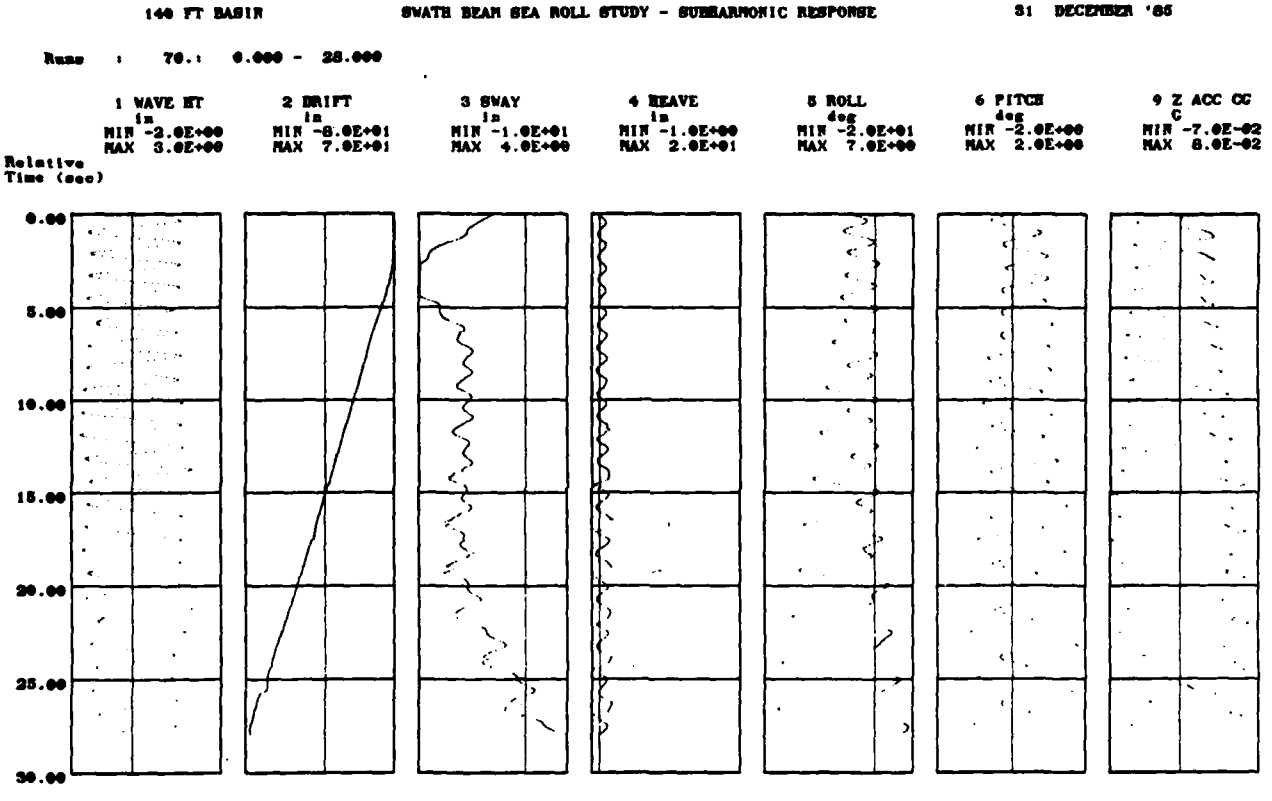

Fig. 27. Sample time history from Line G- Run 70.

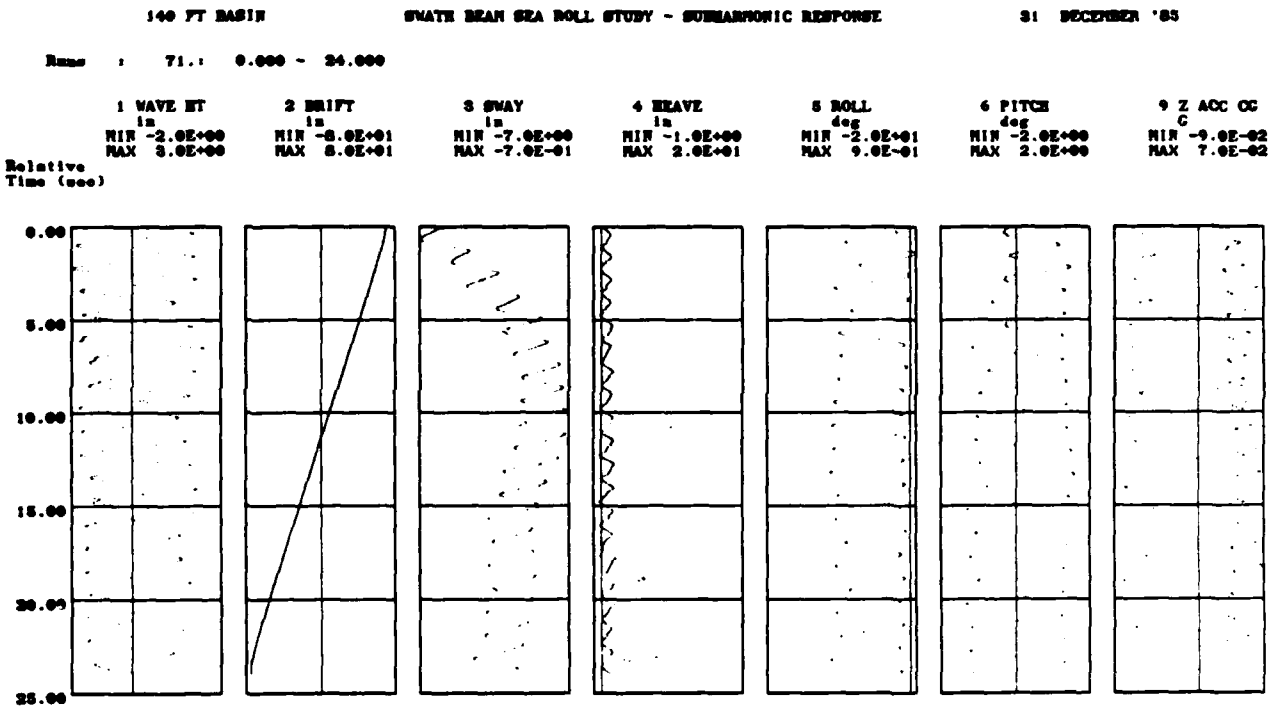

Fig. 28. Sample time history from Line G- Run 71.

DISCUSSION OF EXPERIMENTAL DIFFICULTIES

The purpose or philosophy of performing this experiment in a free to sway (drift) manner, was to provide the most realistic motions possible, to accurately assess the type of coupling that might induce nonlinear motions. This "realism" came at the expense of much control over the experiment. As mentioned, with the model free to heave, pitch, roll and sway (and only slightly restrained in yaw and surge) in this experiment, many problems arose in the quantification of the results. While measurement uncertainty can be addressed for the data channels, such as calibration, data collection /acquisition type of errors, the real uncertainties in this experiment are due primarily to two aspects, which were, the methods of analyzing/quantifying the nonsteady response of a free-to-drift model, and the effects of wave reflections in the small tank.

To illustrate some of the problems encountered in an unsteady test condition consider the following scenario:

> *The model is initially stationary. The wavemaker is started, and waves propagate toward the model . The model first starts to heave, and then begins to drift. The subharmonic roll begins to build and the model's drift rate increases. The carriage speed is adjusted to keep up with the model. The model starts rolling excessively and the deck edge starts to impact the wave surface which causes the model drift rate to slow down. The carriage then has to be slowed down. All the while, the wave probe is mounted to the carriage which is changing speeds throughout the run to match the model drift speed.*

In this typical scenario, each time the carriage or model speed changes, the encounter frequency is shifted, such that the wave height and frequency (for some runs) could not be determined accurately using harmonic analysis. Therefore quantifying or summarizing each run with a characteristic wave amplitude and frequency was difficult at best, and other means to get consistent and correct values had to be used. From the digital time histories, time segments were identified for each run, where the drift speed of the carriage and the mean of the sway channel were relatively constant (i.e. the wave probe was moving at the same speed

as the model). Then, these waveheights and frequencies were compared with estimates obtained from knowing the wavemaker set-up, and from hand calculations from the analog strip chart traces.

The issue of experimental accuracy gets further complicated when the unknown element of the reflected waves is considered. Even for the runs that were short enough not to be concerned with reflected waves affecting the model motions, the reflections from the model could potentially affect the wave height readings in only a matter of a few seconds. In runs with large roll or sway oscillations, the model either reflected or generated waves which traveled back to the wave probe and modified its output. Since the model only appeared to reflect significant waves at certain conditions, this again posed problems of developing a consistent approach to the analysis.

There were primarily two factors which limited the length of a given run. First, the range that the carriage could be drifted was only about 12 feet, and at the higher wave heights and frequencies, the model drifted faster, thereby limiting the amount of time to collect data. This means that for runs in which amplitudes may have still been growing or reaching equilibrium, the ultimate results are not known. The second limitation was the amount of time in which data could be collected before being corrupted with reflected waves. This factor also increased with wave height, as the model tended to reflect more waves back toward the wavemaker than was anticipated. The reflections from the model travel immediately back past the wave probe, causing a partial standing wave (or beating effect) at the probe. Using the group velocities listed in Table 4, some of the times for the expected wave reflections can be estimated. The time it takes for waves reflecting off of the model to reach the wave probe is typically only about 4 seconds. The time for reflected waves to travel from the model to the wavemaker and back is roughly 20 to 30 seconds for wave frequencies in the subharmonic region. Originally, runs limited to (or on the order of) 50 to

60 seconds were anticipated, since that is the approximate time for the waves reflected by the beach to return to the model.

While the above presents negative aspects of the experiment, it is thought that the types of variations observed in the results did not significantly affect the boundaries presented. A favorable aspect of the experiment is that the wavemaker was extremely consistent in repeatability of test conditions. During the experiment, the wave height and frequency output of the wavemaker was checked at several test conditions with the model lifted out of the water (to minimize reflections). In checking several repeated conditions, the agreement was excellent. It also should be pointed out that the transducers, calibrations, and data acquisition hardware were all up to top professional standards (eg. pre- and post- test calibrations were performed, with acceptable repeatability). The test method, combined with the nonlinear behavior, is what presented the most difficult analysis problems. If the model had not been allowed to drift, or one or more of the degrees of freedom had been held purely rigid (such as sway, pitch or yaw), the data no doubt would have been easier to analyze, but then the effects of locking out various degrees of freedom on the behavior would not have been known.

The following suggestions are given for future experiments of this nature. A possible alternative for reducing the effects of wave reflections is to test in a larger facility. This would allow longer run times for responses to steady out. If the sway velocity was steady, the calculations of encounter frequencies would be much easier and more accurate. Also, in a larger tank, the wave probe could be moved off centerline of the carriage to avoid direct reflections off of the struts. The range in which the carriage was able to be moved to follow the model was limited, and in some cases did not allow a sufficient time for the responses to stabilize. This was primarily a hardware problem (drift measurement), and could be rectified in future experiments. In any setup, an additional wave probe located off of the carriage would also be helpful in discerning the wave frequency from the encounter frequency,

particularly in the case of the carriage speed changing during the run. Another suggestion would be to perform a more thorough calibration of the wavemaker prior to the experiments. This might allow the direct use of the wavemaker settings to provide further resolution of the wave data, particularly in the case where the wave information at the probe was modified by reflected waves. The heave dropouts experienced using an ultrasonic transducer in this test seem to dictate the use of alternate instrumentation.

CHAPTER 6. ANALYTICAL APPROACH

BACKGROUND

The objective of this thesis was to investigate the extent (i.e. boundaries) of subharmonic roll motion of a SWATH ship in beam seas, and draw an analogy to a dynamic system with variable spring characteristics. In the previous chapter, the instability boundary has been documented. This boundary in fact appears generally similar to the instability regions discussed by Timoshenko[2] in mechanical vibrations as a consequence of a fluctuating or time dependent spring stiffness. As mentioned in the introduction, he showed that large vibrations could be built up in systems with variable spring characteristics for certain frequencies of stiffness fluctuation. By including spring stiffness as a periodic function of time in the differential equation of motion, he demonstrated good agreement with experiments in defining the boundaries of instability, and found that spring stiffness fluctuation at the natural frequency and half the natural frequency was of the most practical significance. One such system illustrated by Timoshenko is a pendulum, the length of which is varying at a frequency of twice the natural frequency of the system. This results in the build up of large amplitudes of motion at the natural frequency.

In the study of naval architecture, as early as 1863, William Froude observed that a ship would have undesirable roll characteristics if its natural frequency in pitch (or heave)

was twice its natural roll frequency. A classical work on the nonlinear coupling of ship motions resulting in unstable motions by Paulling and Rosenberg[7] sought to explain this phenomenon. While their work involved various modes of coupling in three degrees of freedom, they presented results of experiments carried out for a roll-heave system. In their experiments, a captive ship model (free only in roll) was tested by impressing a prescribed heave oscillation on the model, over a range of frequencies and amplitudes. The resulting instabilities were then compared to the unstable regions of a Mathieu equation. A standard form of the Mathieu Equation [Mathews and Walker[8]] is given by:

$$\frac{d^2y}{dx^2} + (\delta + \varepsilon \cos 2x)y = 0$$

By application of Floquet's theorem, solutions of the Mathieu equation can be derived (Mathieu functions) and plotted, showing the stable and unstable regions as a function of ε and δ. In the case of the ship analogy, however, there is an excitation term on the right hand side which is not present in the form above. Thus, the ship case can only be partially considered to be simulated by a homogeneous equation of Mathieu type. In this regard, Paulling and Rosenberg[7] note that "it has been shown ...that such equations have instabilities for the same values of the parameters ε and δ as the reduced homogeneous equations". On this basis, they present their stability boundary comparison, which showed reasonable qualitative agreement, but was quantitatively only fair. Their results were considered to be limited due to the omission of damping and to experimental concerns such as the prescribed heave (i.e. lacked realism compared to wave induced motions) and also problems with reflected waves.

More recent studies in the area of nonlinear ship dynamics presented by Nayfeh et al.[9] and Nayfeh[10] have sought to expand on the nonlinear coupling, providing more complex mathematical/analytical modeling techniques. However, very little in the way of experimental results exist, particularly for a SWATH.

In early SWATH seakeeping experiments, Kallio [11] observed the occurrence of subharmonic roll motion for one of three design variants of the SWATH 6 Series. The SWATH(6C) having the heave natural frequency near (but not equal to) twice the roll natural frequency, experienced a build up of large roll angles in waves near heave resonance. These observations may have prompted Numata's study[1] on the effects of variations in SWATH geometry on subharmonic roll at zero speed in beam seas. Of the four variants tested, the *Deep Draft* configuration exhibited the strongest subharmonic response, while the *Low KG* variant had the next strongest. Their ratios of heave to roll natural frequency were 2.06 and 1.82 respectively. The subharmonic roll was observed in both regular and irregular waves. Since only a few unstable points were identified for each configuration, the boundaries were not pinned down, however, a Mathieu like instability was suggested from the data.

DERIVATION

Therefore, with the quasi-stability diagram presented in the previous chapter, the hypothesis that this instability is caused by variable spring characteristics, was explored using a simple, semi-intuitive, modification to the single degree of freedom, linear roll equation, as follows.

Modified Single DOF Roll Equation

The standard linear uncoupled single degree of freedom equation for roll is given by

$$I\ddot{\phi} + N\dot{\phi} + \Delta\,\overline{GM}_t\,\phi = \Delta\,\overline{GM}_t\,\alpha_e \qquad (6.1)$$

where I = Roll Inertia
$\ddot{\phi}, \dot{\phi}, \phi$ = roll acceleration, velocity , and displacement.
N = damping coefficient
Δ = displacement
$\overline{GM}_t$ = transverse metacentric height
α_e = effective surface wave slope.

The effective wave slope, α_e, is often taken to be the slope of the envelope of the wave particle orbits at some effective depth below the mean free surface level. This approach has been followed in the present analysis, where the effective depth is taken to be the depth of the model center of buoyancy below the waterline, T_B.

Adopting the coordinate system shown in Figure 4c, and noting that the waves in the experiments propagate in the negative-y direction, the wave elevations in the tank may be written:

$$\eta = a \cos (ky + \omega t) \tag{6.2}$$

where a and ω are the wave amplitude and frequency and k=wavenumber in water depth of d, given by $\omega^2 = gk \tanh kh$.

Differentiating with respect to the y direction, and evaluating the result at the position of the model (y=0), the surface wave slope at the model becomes:

$$\alpha = -ka \sin (\omega t) \tag{6.3}$$

Approximating the effective wave slope as noted above, and assuming deep water waves ($\tanh kd \approx 1$), the effective wave slope is written:

$$\alpha_e = -\frac{\omega^2}{g} a e^{(-\omega^2 T_B / g)} \sin (\omega t) \tag{6.4}$$

Dividing through by I, Eq. 6.1 is often expressed as,

$$\ddot{\phi} + B \dot{\phi} + \omega_r^2 \phi = \omega_r^2 \alpha_e \tag{6.5}$$

where B = N/I, a damping coefficient, and

ω_r, ω_r^2 = roll resonant frequencies (same as ω_{ϕ_n} used in data presentation).

If the variation in spring constant is assumed to be due to the heave motion acting on the effective restoring moment, then it seems reasonable to express the restoration term at any given instant, as some function of heave and the static restoration moment in the form:

$$\Delta \overline{GM\,t}_{instant} \phi = \Delta \overline{GM\,t}_{static} \phi \{1 + \varepsilon (heave)\} \tag{6.6}$$

Epsilon, ε can be thought of as a percentage change in the restoration coefficient, due to heave, or

$$\varepsilon = \frac{\text{change in } \overline{GM\,t} \text{ per unit heave}}{\overline{GM\,t}|_{static}} \qquad (\approx 1/\text{length}). \tag{6.7}$$

Equation 6.5 can then be reduced to:

$$\ddot{\phi} + B\,\dot{\phi} + \omega_r^2\{1+\varepsilon\,(\textit{heave})\}\,\phi = \omega_r^2\,\alpha_e\,. \tag{6.8}$$

The *heave* in this case is a function of wave amplitude, a, and frequency, ω,

$$\textit{heave} = a\,|H(\omega)|\cos(\omega t+\zeta(\omega)), \tag{6.9}$$

where $H(\omega)$ and $\zeta(\omega)$ are the magnitude and phase of the heave transfer function. Substituting Eq. 6.9 into Eq. 6.8,

$$\ddot{\phi} + B\,\dot{\phi} + \omega_r^2\{1+\varepsilon\;a\,|H(\omega)|\cos(\omega t+\zeta(\omega))\}\,\phi = \omega_r^2\,\alpha_e. \tag{6.10}$$

Equation 6.10 represents the basic modification of the linear single degree of freedom roll equation with the time varying restoration coefficient due to heave response. It is therefore coupled with heave, and a function of both wave amplitude and frequency. This form of the roll equation provides the basis on which the theoretical correlation was performed.

For the purpose of providing an exploratory analytical model, the possibility of the restoring moment being a function of heave-squared was also investigated. Equation 6.6 was expanded as follows,

$$\Delta\,\overline{GMt}_{\,instant}\,\phi = \Delta\,\overline{GMt}_{\,static}\,\phi\,\{1+\varepsilon_1\,(\textit{heave})+\varepsilon_2\,(\textit{heave})^2\}. \tag{6.11}$$

Substituting Eq. 6.4 into Eq. 6.10, and expanding the form of the nonlinearites in accordance with Eq. 6.11, the dimensional roll equation becomes,

$$\ddot{\phi} + B\,\dot{\phi} + \omega_r^2\{1+ \varepsilon_1\, a\, |H(\omega)| \cos(\omega t+\zeta(\omega))+\varepsilon_2\,[a\,|H(\omega)| \cos(\omega t+\zeta(\omega))]^2\}\,\phi =$$

$$-\omega_r^2 \frac{\omega^2}{g}\, a\, e^{(-\omega^2 T_B/g)} \sin \omega t \,. \qquad (6.12)$$

Roll can then nondimensionalized by maximum wave slope, $\alpha_m = Ka = \frac{\omega^2 a}{g}$, such that $\varphi = \frac{\phi}{Ka}$ and Eq. 6.12 becomes,

$$\ddot{\varphi} + B\,\dot{\varphi} + \omega_r^2\{1+ \varepsilon_1\, a\, |H(\omega)| \cos(\omega t+\zeta(\omega))+ \varepsilon_2\,[a\,|H(\omega)| \cos(\omega t+\zeta(\omega))]^2\}\,\varphi =$$

$$-\omega_r^2\, e^{(-\omega^2 T_B/g)} \sin \omega t \,. \qquad (6.13)$$

This non-dimensional, heave-coupled roll equation was used to provide the analytical results for comparison with the model data, as described below. It contains the wave frequency and amplitude dependent heave response in the restoration term, and includes a linear damping term as well. It was assumed that wave and encounter frequencies are the same. While this analytical scheme is a rather non rigorous, semi-intuitive approach, it provided a means to perform exploratory analysis aimed at studying the origin of the observed instability.

Relative Heave Transfer Function

The driving mechanism of the variable spring characteristic was presumed to be a consequence of vertical or heave motion of the craft. It was not known however, whether the variable spring would be better modeled by using a heave or relative heave motion transfer function. While relative heave was not specifically measured, the magnitude and phase of the heave transfer function, Z(t) were known, and the relative heave motion, R(t) could then be derived in the form

$$R(t) = a\,|R(\omega)| \cos(\omega t+\varepsilon_r(\omega)) \qquad (6.14)$$

where $|R(\omega)|$ and $\varepsilon_r(\omega)$ are the magnitude and phase of the relative heave as a function of wave frequency. By expressing R(t) as the difference between the heave motion and wave profile, $\eta(t)$,

$$R(t) = Z(t) - \eta(t)$$

where $\eta(t) = a \cos \omega t$, and

$$Z(t) = a\,|H(\omega)| \cos(\omega t + \zeta(\omega))$$

it can be shown that

$$|R(\omega)| = \left[|H(\omega)|^2 + 1 - 2\,|H(\omega)|\,\cos\zeta(\omega)\right]^{1/2}, \quad \text{and} \tag{6.15}$$

$$\varepsilon_r(\omega) = \tan^{-1}\left(\frac{-|H(\omega)|\sin\zeta(\omega)}{|H(\omega)|\cos\zeta(\omega) - 1}\right). \tag{6.16}$$

Unfortunately, the heave data in the desired frequency range were particularly messy due to the sonic drop-outs, caused by large subharmonic roll angles. By analyzing good segments of each run, with harmonic analysis, and using some hand calculated data from time histories, the heave transfer function was extended through the subharmonic region. It was not possible to define the transfer function for all runs, but most of the non-subharmonic runs in the region could be used, such as the runs at very low and very high wave heights. This probably contributed somewhat to the scatter (particularly phase), but nevertheless, the trends were fairly clear. The magnitude and phase of the extended heave transfer function are presented in Figure 29, and the calculated relative heave transfer function (Eqs. 6.15 & 6.16) is given in Fig. 30. Also shown in Figs. 29 and 30 are the interpolated data (summarized again in Table 7) which were incorporated into the analytical model to allow the differences in response characteristics to be explored using either absolute or relative heave.

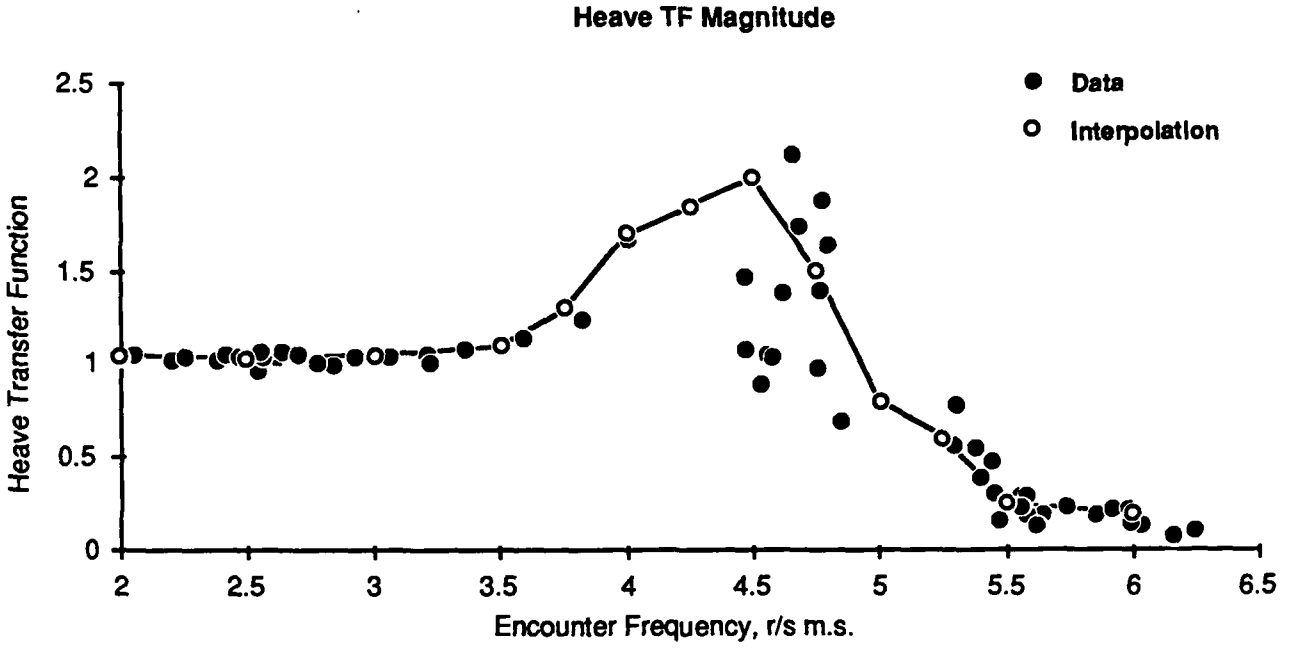

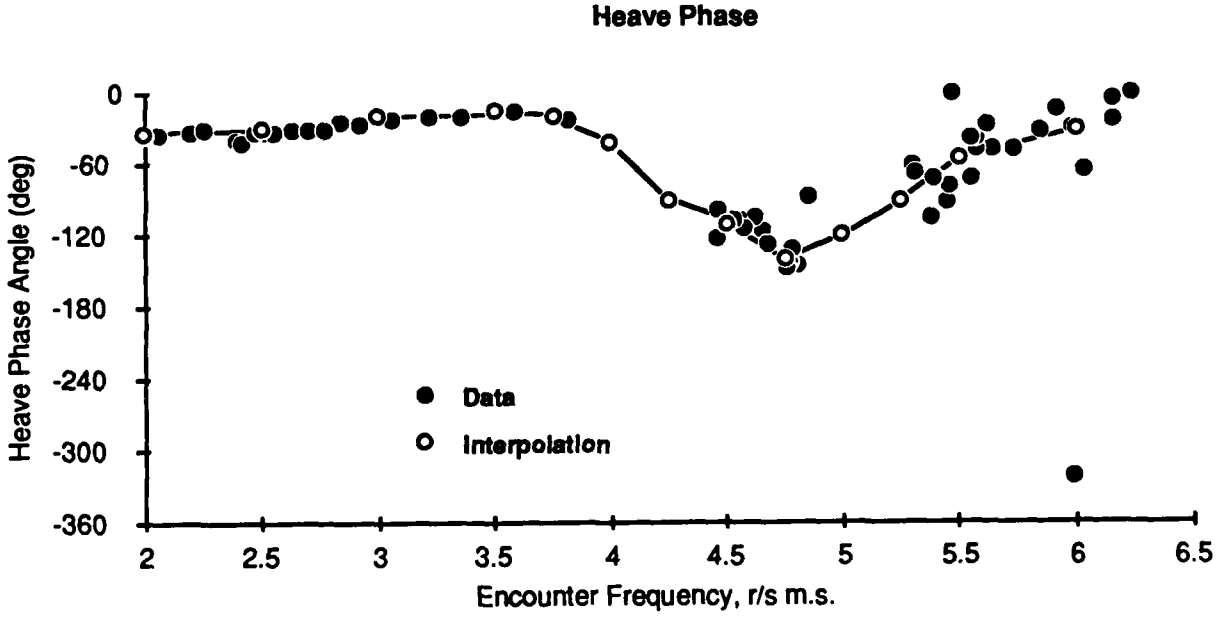

Fig. 29. Heave transfer function magnitude and phase plot in subharmonic region.

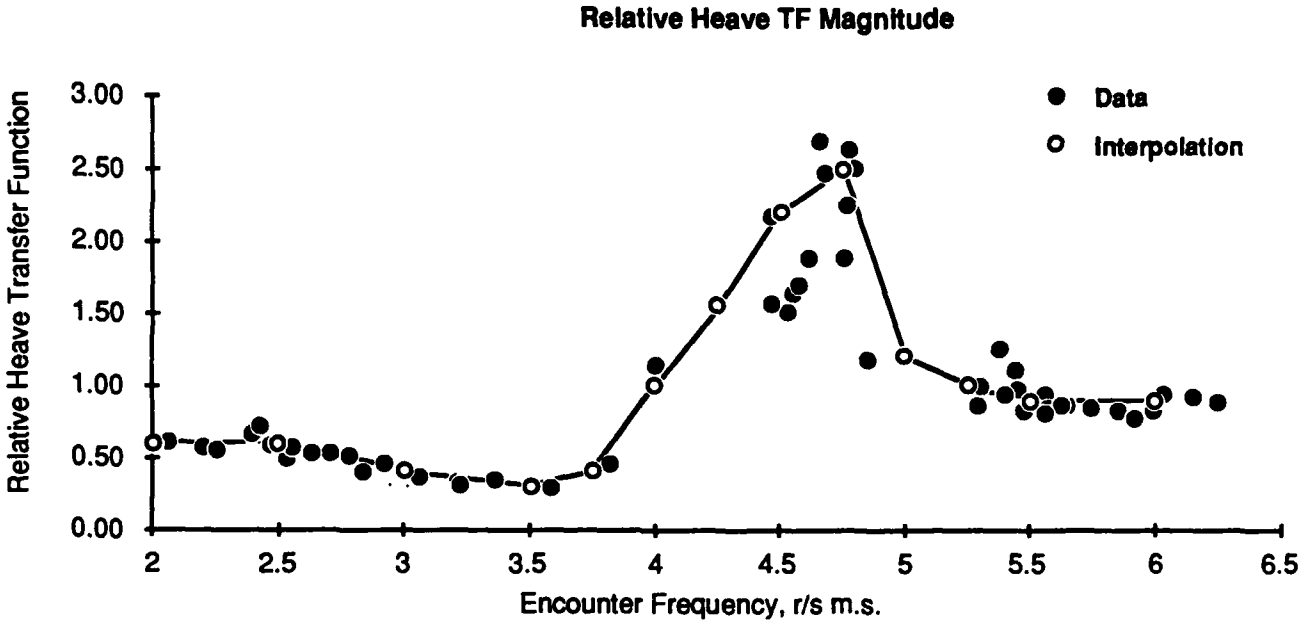

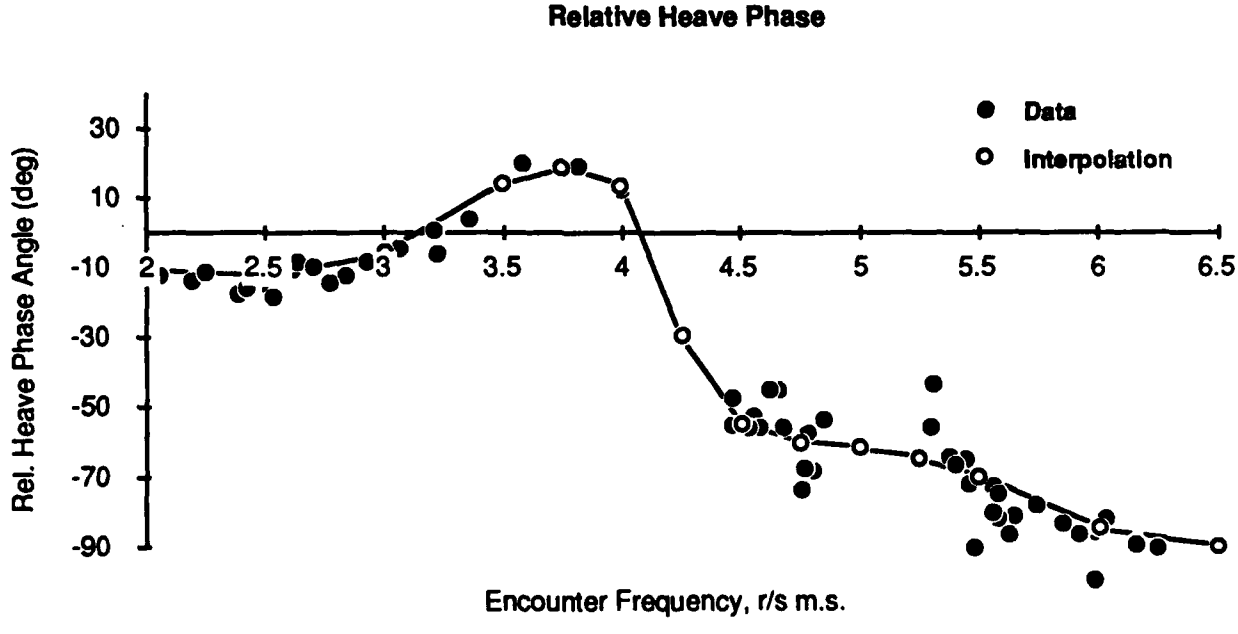

Fig. 30. Relative heave transfer function magnitude and phase plot.

Table 7. Relative and absolute heave transfer function look-up table.

Estimated/ Extrapolated from Model Data				
Encounter Frequency	Heave TF	Heave Phase deg	Relative Heave TF	Relative Heave Phase(deg)
2	1.05	-34	0.6	-11
2.5	1.03	-31	0.6	-13
3	1.05	-20	0.4	-5.5
3.5	1.1	-16	0.3	14
3.75	1.3	-20	0.4	19
4	1.7	-42	1	13
4.25	1.85	-90	1.55	-30
4.5	2	-110	2.2	-55
4.75	1.5	-140	2.5	-60
5	0.8	-120	1.2	-62
5.25	0.6	-90	1	-65
5.5	0.25	-55	0.9	-70
6	0.2	-30	0.9	-85
6.5	0.1	-3	0.95	-90

ANALYTICAL PROGRAM

Description

The hypothesis of this project was based on the assumption that a variable spring characteristic exists on a SWATH and is driven by either heave or *relative* heave motion. Therefore, Equation 6.13 was solved numerically in the time domain, using a fourth order Runga-Kutta integration scheme with zero initial conditions (start time = 0). The computer program ran on a DEC MicroVax II, and provided graphical time histories of the solution (i.e. roll angle) based on the following main input parameters.

Fixed Input Parameters:	Natural Roll frequency, ω_r, Draft to Center of Buoyancy, T_B , and Damping Factor, B.
Variable Input Parameters:	Relative vs Absolute heave selection, ε_1 and/or ε_2, wave amplitude and frequency.

The relative and absolute heave transfer functions were built into the program in the form of a look-up table, and needed only to be selected upon program start-up. The value of damping function used (B=.453), was calculated from the linear solution of the roll equation corresponding to the peak of the transfer function (rather than from decay tests). Figure 31 shows the comparison between the linear solution of roll (solving Eq. 6.5), and the test data. The analytical program was run for ε_1 and $\varepsilon_2 = 0$, to check the linear solution. Figure 32 shows the time history output of the program, at the frequency corresponding to the peak of the linear roll transfer function.

The program was run much the same as the model experiment. That is, for a given value of ε_1 or ε_2, and using either the relative or absolute heave transfer functions, an array of amplitudes and frequencies were applied and the time histories of the solutions were generated. The time histories were then used to define the boundaries of the unstable region. An unstable condition was characterized by a diverging, or exponentially growing solution,

in which the roll was oscillating at its natural frequency. In general, the faster the solution diverged (high growth rate), the further it was from the boundary (into the unstable region). Stable or linear responses were harmonic with magnitudes and frequencies corresponding to the expected linear response.

After a reasonable amount of testing of the program, it appeared that using ε_1 provided better qualitative agreement of the stability of the solutions with model data, than using ε_2 or combinations of ε_1 and ε_2. Therefore, the program was exercised over a range of frequencies and amplitudes, primarily using values of ε_1 only, and the following description of results is limited accordingly.

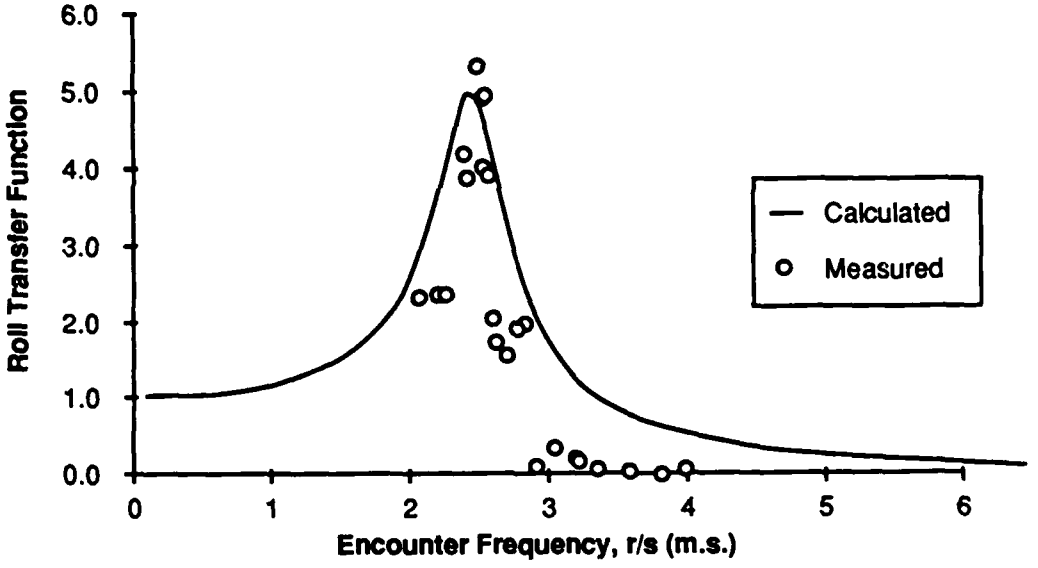

Fig. 31. Comparison of linear roll transfer function- calculated vs. experiment.

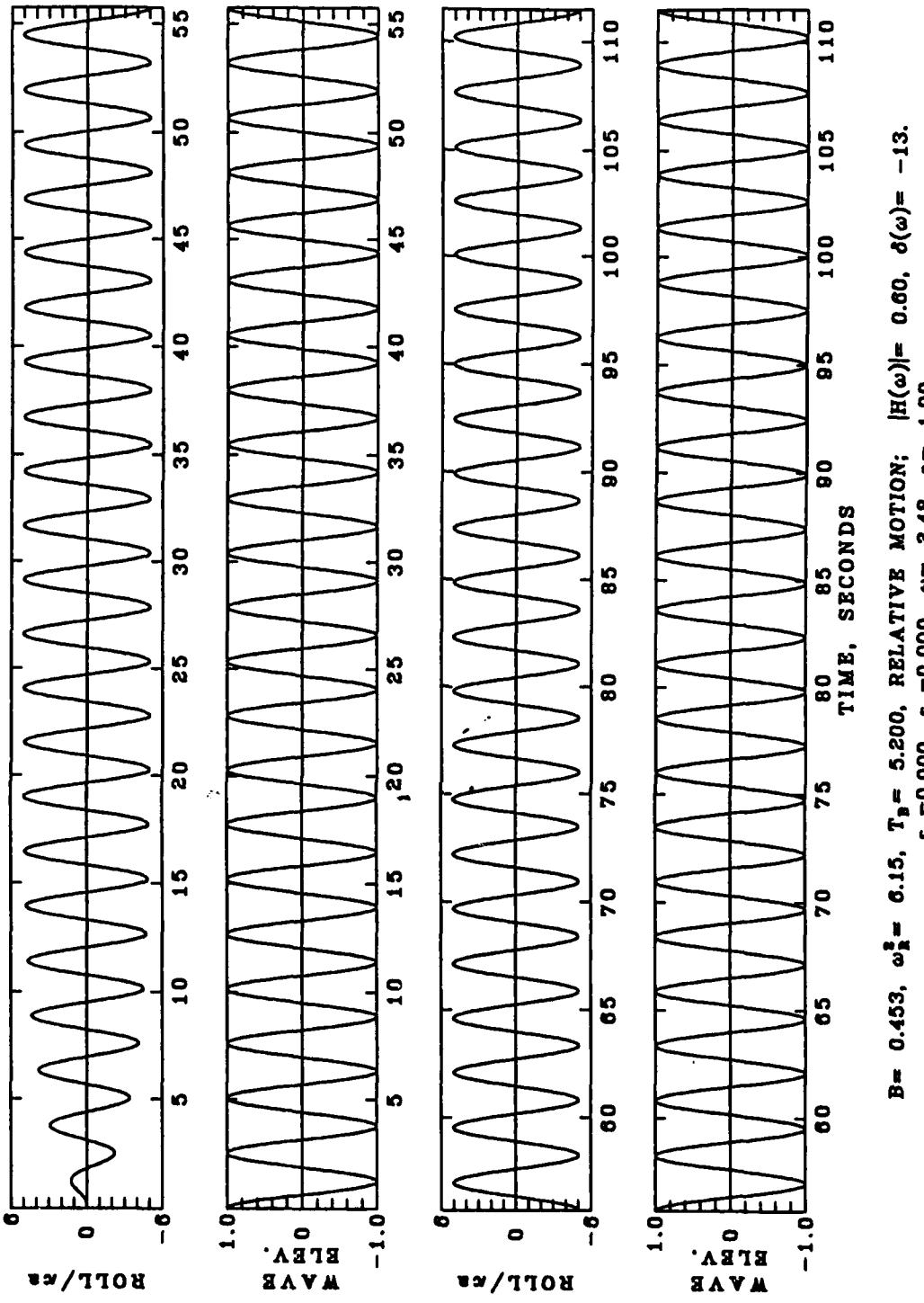

Fig. 32. Time history showing linear response at the peak of the roll transfer function.

Sample Time Histories

Specific time histories generated by the analytical program exhibit trends that are remarkably similar to the test data. Some of these trends include: various growth rate characteristics, transitions from linear roll motion to subharmonic rolling, combined linear and subharmonic response, as well as, some qualitative similarities in behavior near the stability boundaries. Figures 33 to 41 show several time histories (in model scale units) generated using the *relative* heave transfer function and $\varepsilon_1 = 0.5$. In these figures, roll is nondimensionalized by wave slope, ka, and is given as a function of time in model scale seconds, along with the time history of the wave (excitation) amplitude.

In Figures 33 to 37, the effects on roll motion response of successive increases in wave amplitude are shown, for a constant wave frequency of 4.96 radians/second, corresponding to a frequency ratio of one (i.e. excitation at 2 times roll natural frequency). In Figure 33, the time history is given for a wave amplitude of 0.25 inches. In this case, the roll response is linear, and has a transfer function of about 0.3, which is approximately what would be expected from the linear roll equation. With an increase of wave amplitude to 0.5 inches, it can be seen in Fig. 34 that the response begins to exhibit a slight subharmonic component. This behavior is not unlike the experimental time history of run 80, given in Figure 20. In Figure 35, the wave amplitude is increased to 0.6 inches, and the transition from linear to subharmonic rolling can clearly be seen. This time history qualitatively resembles several of the experimental time histories, such as runs 56, and 67 to 69 presented in Chapter 5 (Figs. 17, 24 to 26). In each of these examples, the roll response begins as primarily linear motion and then transitions to subharmonic rolling with increasing amplitudes. As wave height is increased further, the rate at which the roll goes unstable also appears to increase. The transition of the roll frequency from linear to subharmonic is less evident, but the growth rate of the roll amplitude in the subharmonic frequency increases

significantly. This can be seen in Figures 36, and 37, for which the corresponding wave amplitudes are 0.7 and 0.75, respectively. In general, the analytical program required a slightly greater wave amplitude than did the experiments, to induce subharmonic rolling.

Figures 38 to 40 are at a frequency of 5.2 r/sec, and show the combined nature of the roll responses at a higher frequency ratio, as a function of wave height. Figure 38 begins as a combined transient response which, over the course of the run, slowly transitions back toward a linear response. The amplitude of roll is again close to the linear magnitude expected at this frequency. In Figure 39, the wave amplitude is increased from 0.75 inches to 0.85, and again the roll response is of a combined nature, only in this run the transition is moving toward subharmonic response. With an increase of wave amplitude to 0.95 inches, the analyitcal time history in Fig. 40, is combined at the beginning, but quickly transitions to a pure subharmonic roll of increasing amplitude. These characteristics were similar to the experimental results in that the roll more often tended to be of a combined nature on the high frequency boundary, than on the low frequency boundary.

Fig. 41 shows a steady-combined response such as was observed at higher wave frequencies in the experiments. At a frequency of 5.46 radians/second, or a frequency ratio of 1.1, this time history is very similar to the experimental response for Run 91 (also at a ratio of 1.1, but with a slighly greater wave amplitude), shown in Fig. 21.

Boundaries of instability were determined from the analytical time histories, as the point at which an increase in wave amplitude at a given wave frequency would cause the roll response to go unstable (subharmonic), much the same way as the experimental boundaries. These boundaries are compared to the experimental results in the next section.

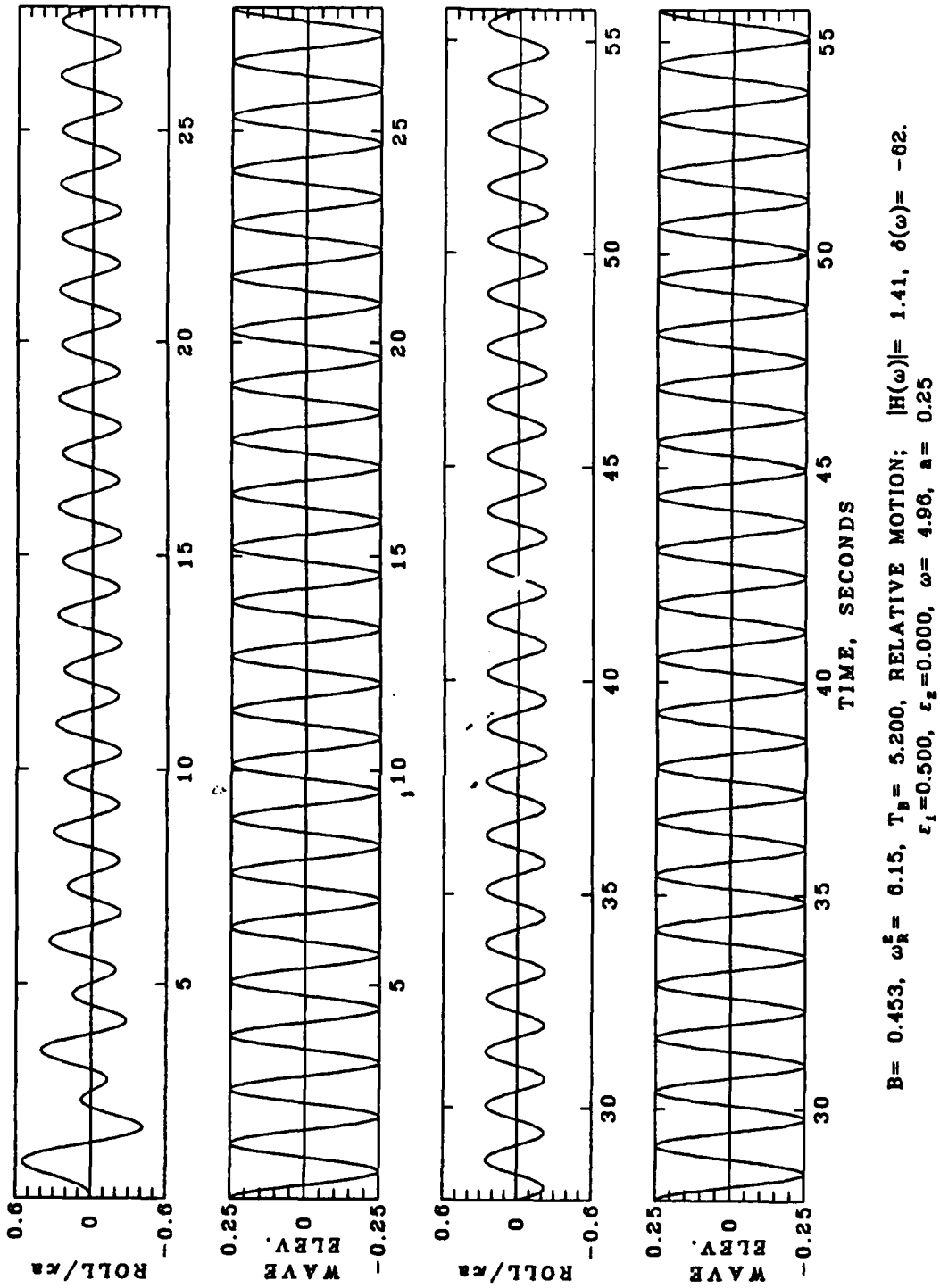

Fig. 33. Analytical time history for epsilon 1= .5, using relative heave at $\omega = 4.96$, and a wave amplitude of 0.25 inches.

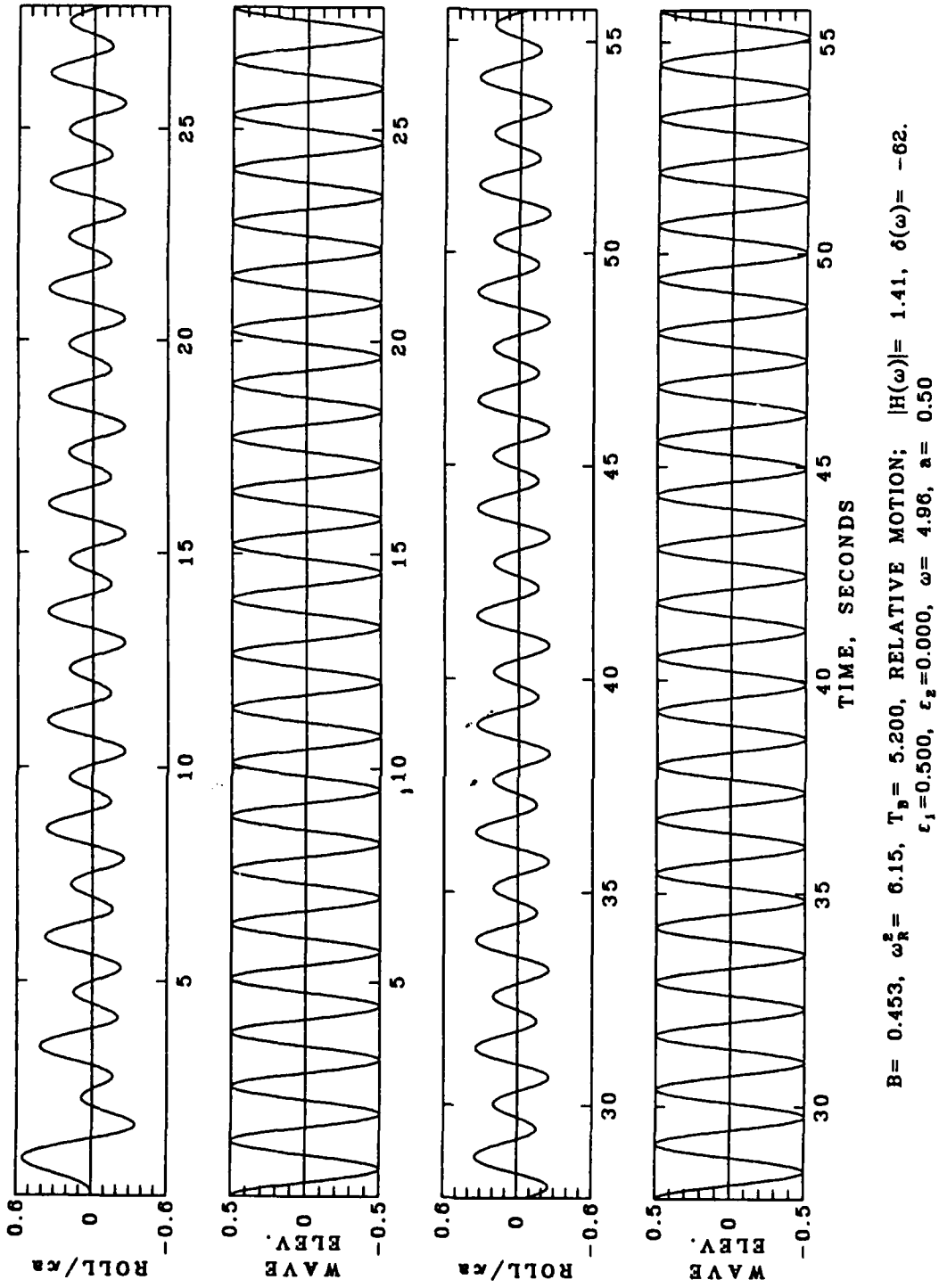

Fig. 34. Analytical time history for epsilon 1= .5, using relative heave at $\omega = 4.96$, and a wave amplitude of 0.5 inches.

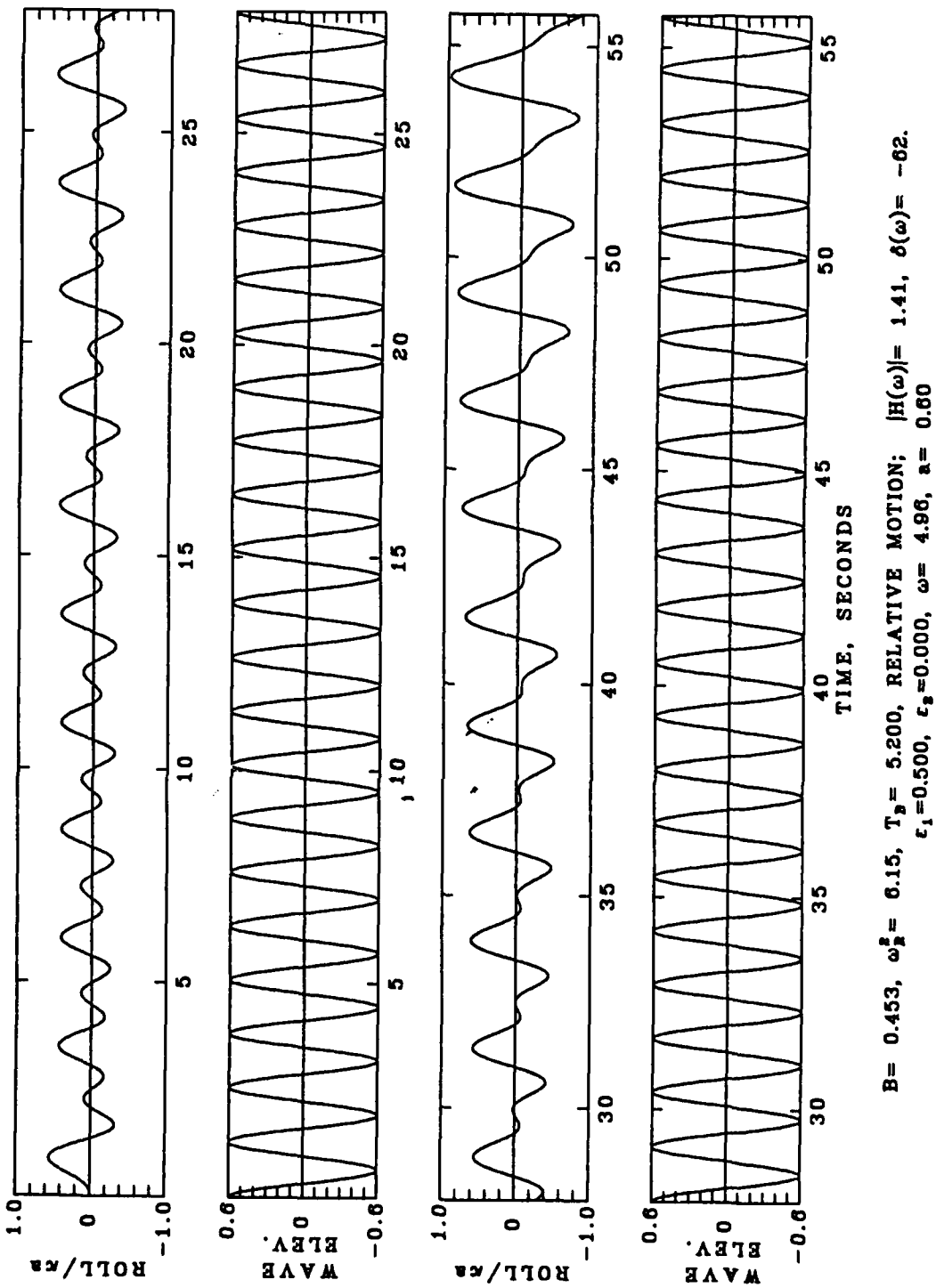

Fig. 35. Analytical time history for epsilon 1= .5, using relative heave at $\omega = 4.96$, and a wave amplitude of 0.6 inches.

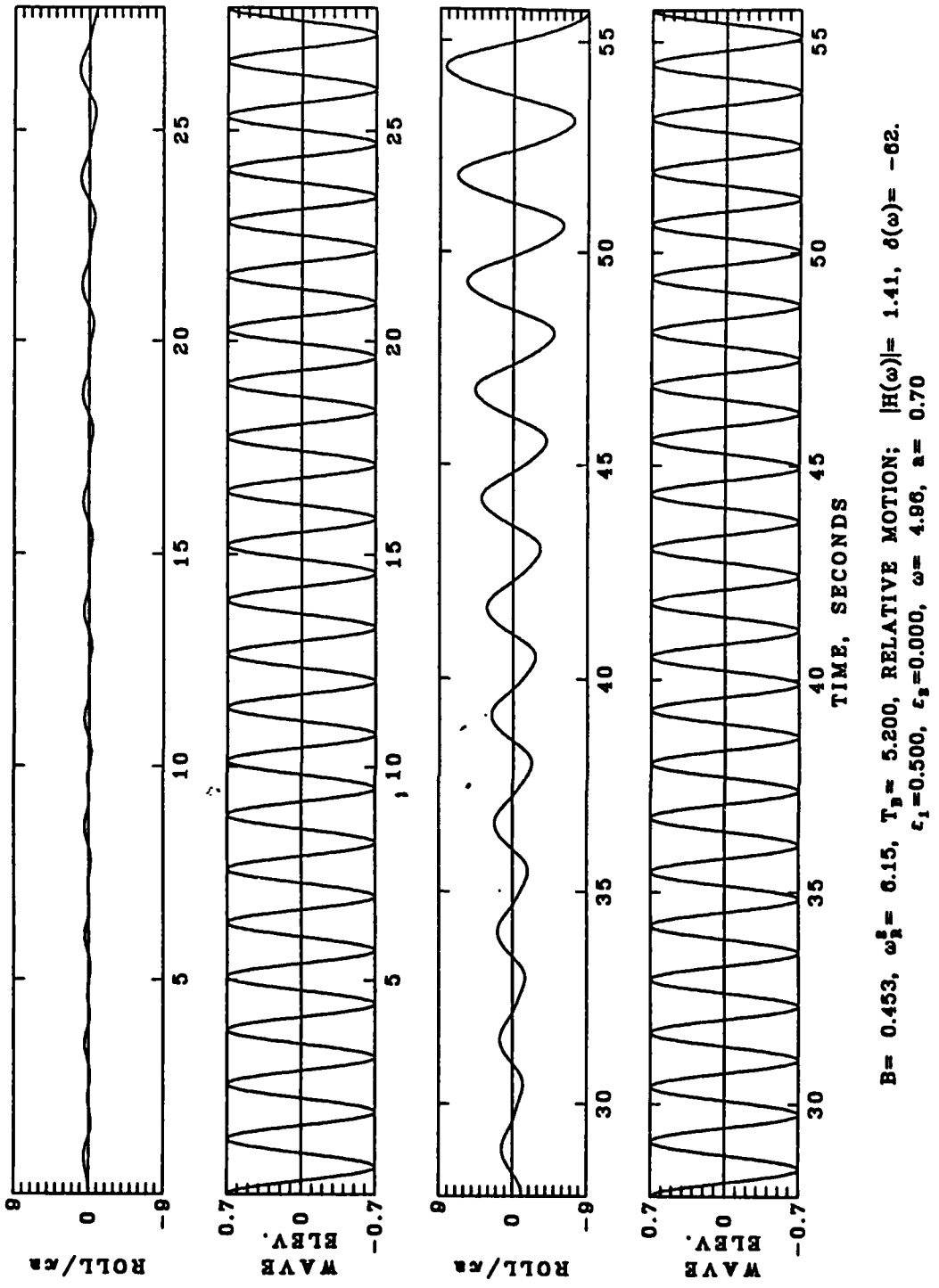

Fig. 36. Analytical time history for epsilon 1= .5, using relative heave at $\omega = 4.96$, and a wave amplitude of 0.7 inches.

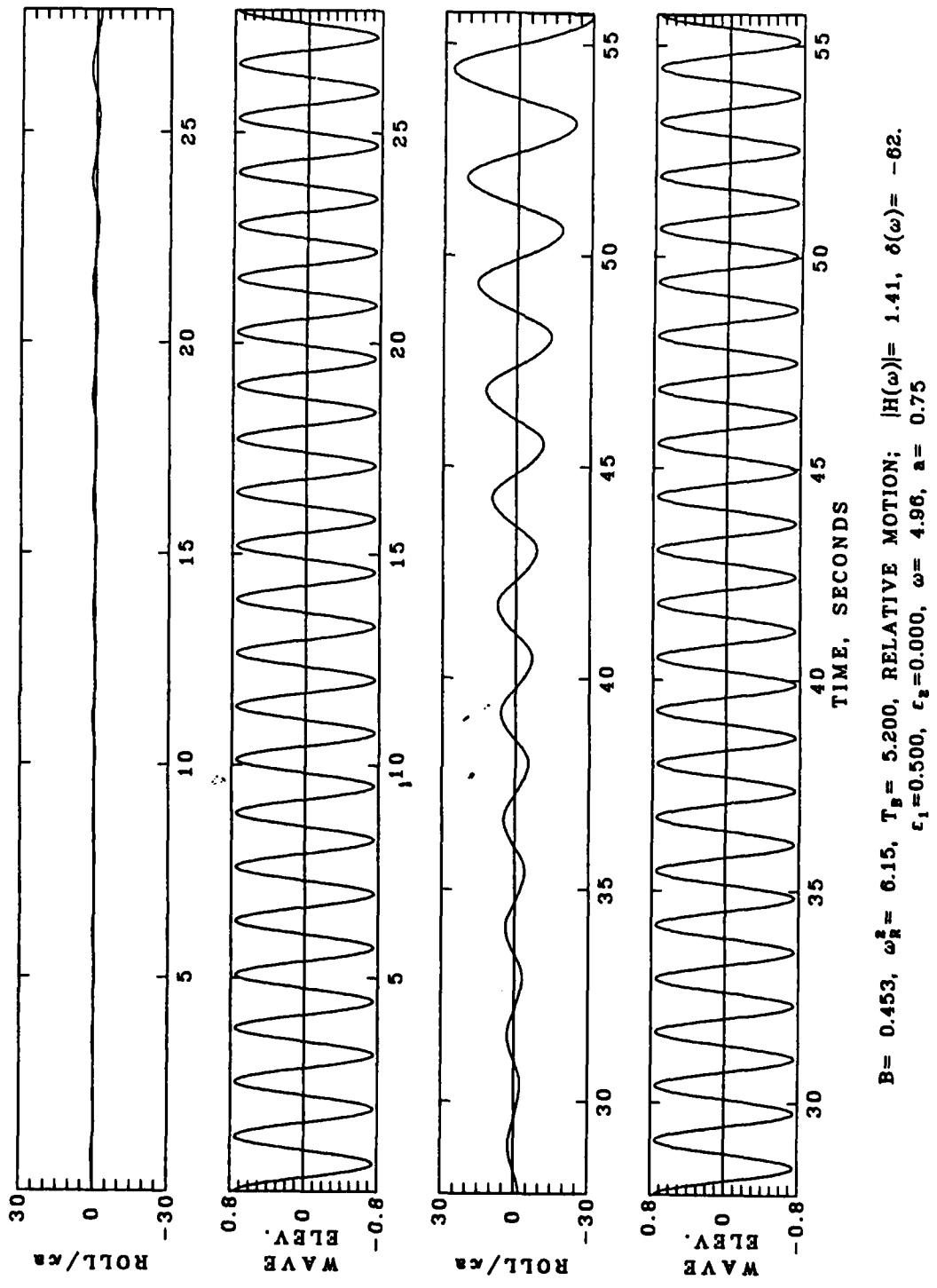

Fig. 37. Analytical time history for epsilon 1= .5, using relative heave at ω = 4.96, and a wave amplitude of 0.75 inches.

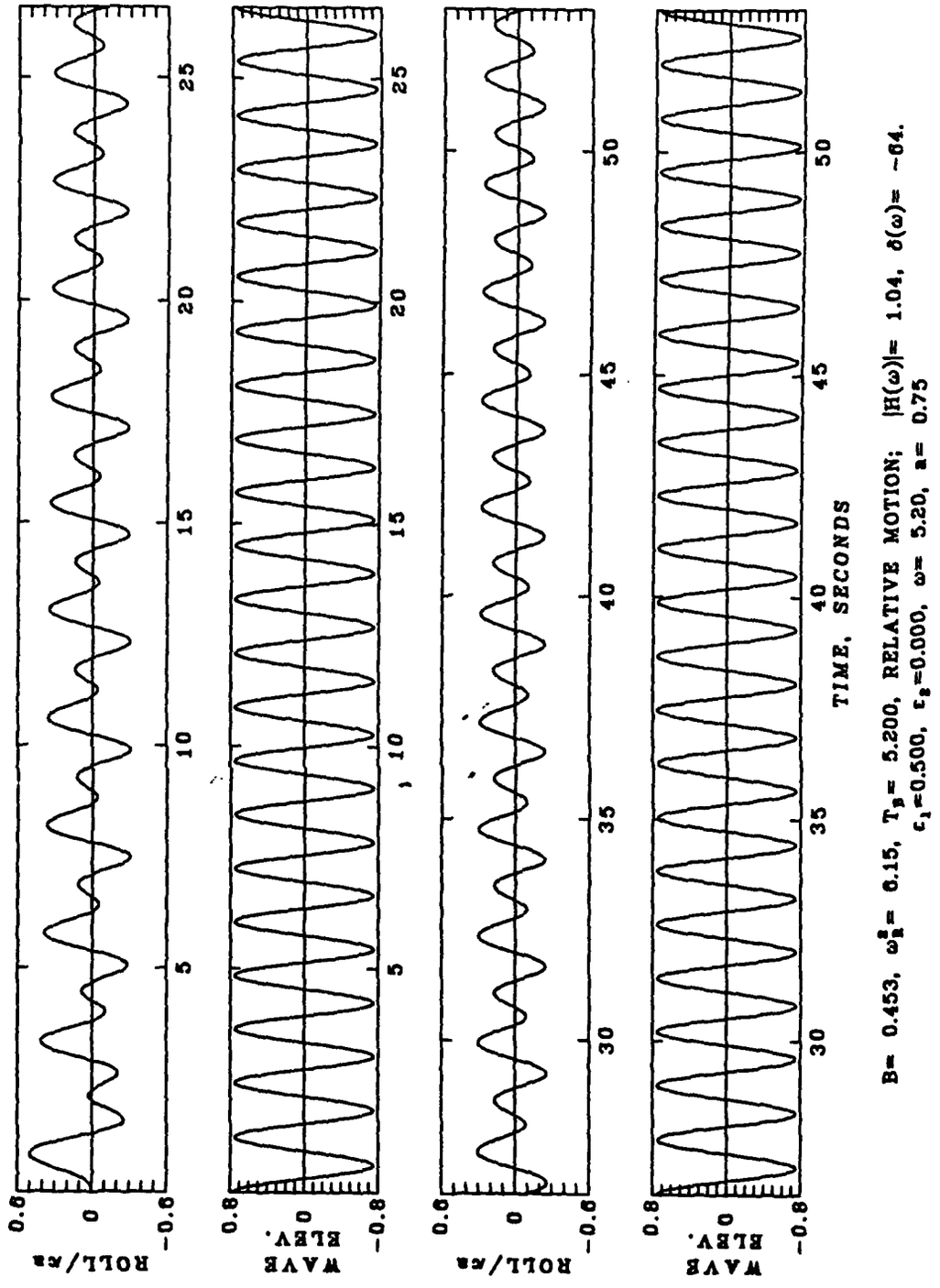

Fig. 38. Analytical time history for epsilon 1= .5, using relative heave at $\omega = 5.20$, and a wave amplitude of 0.75 inches.

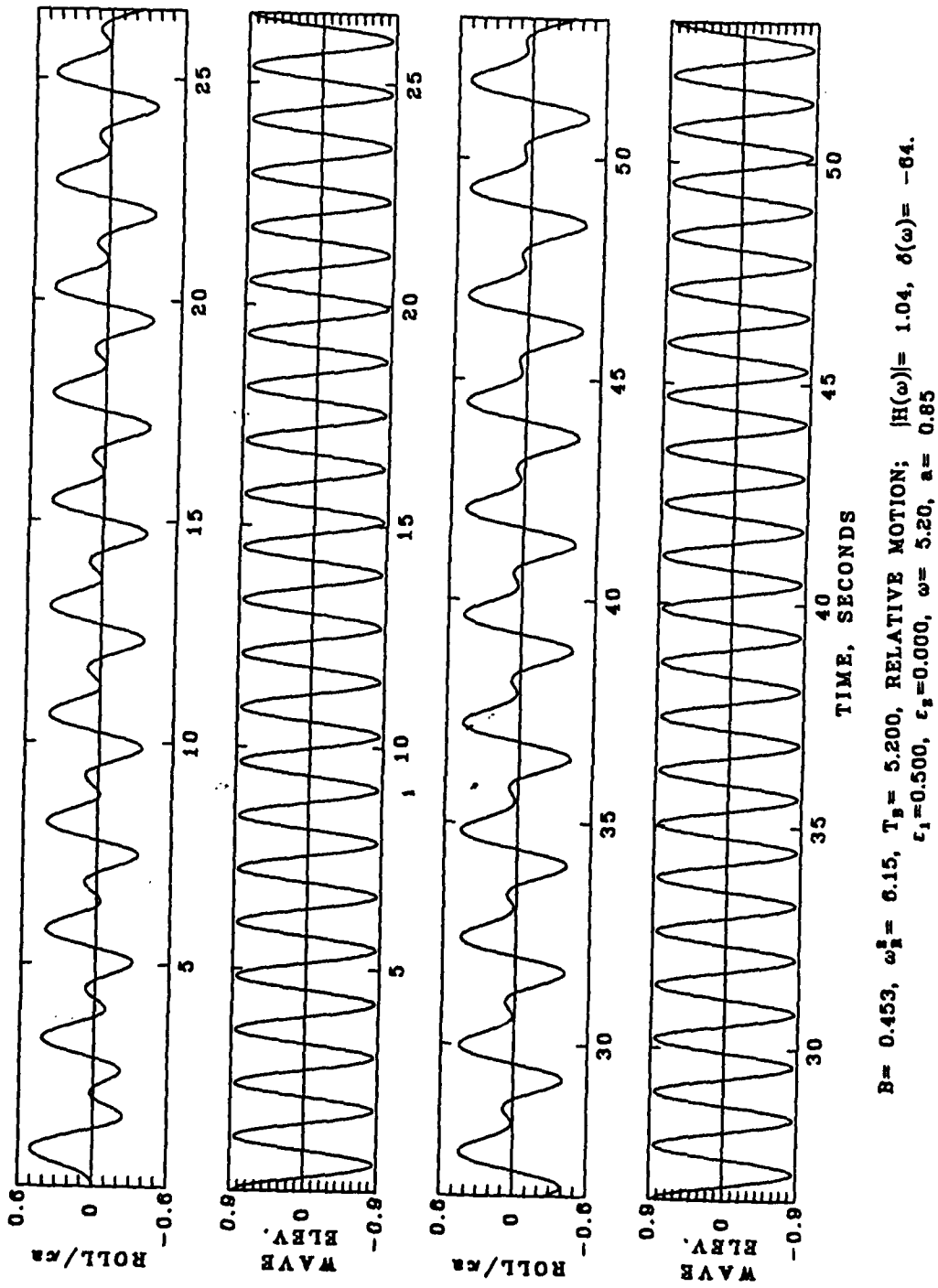

Fig. 39. Analytical time history for epsilon 1= .5, using relative heave at $\omega = 5.20$, and a wave amplitude of 0.85 inches.

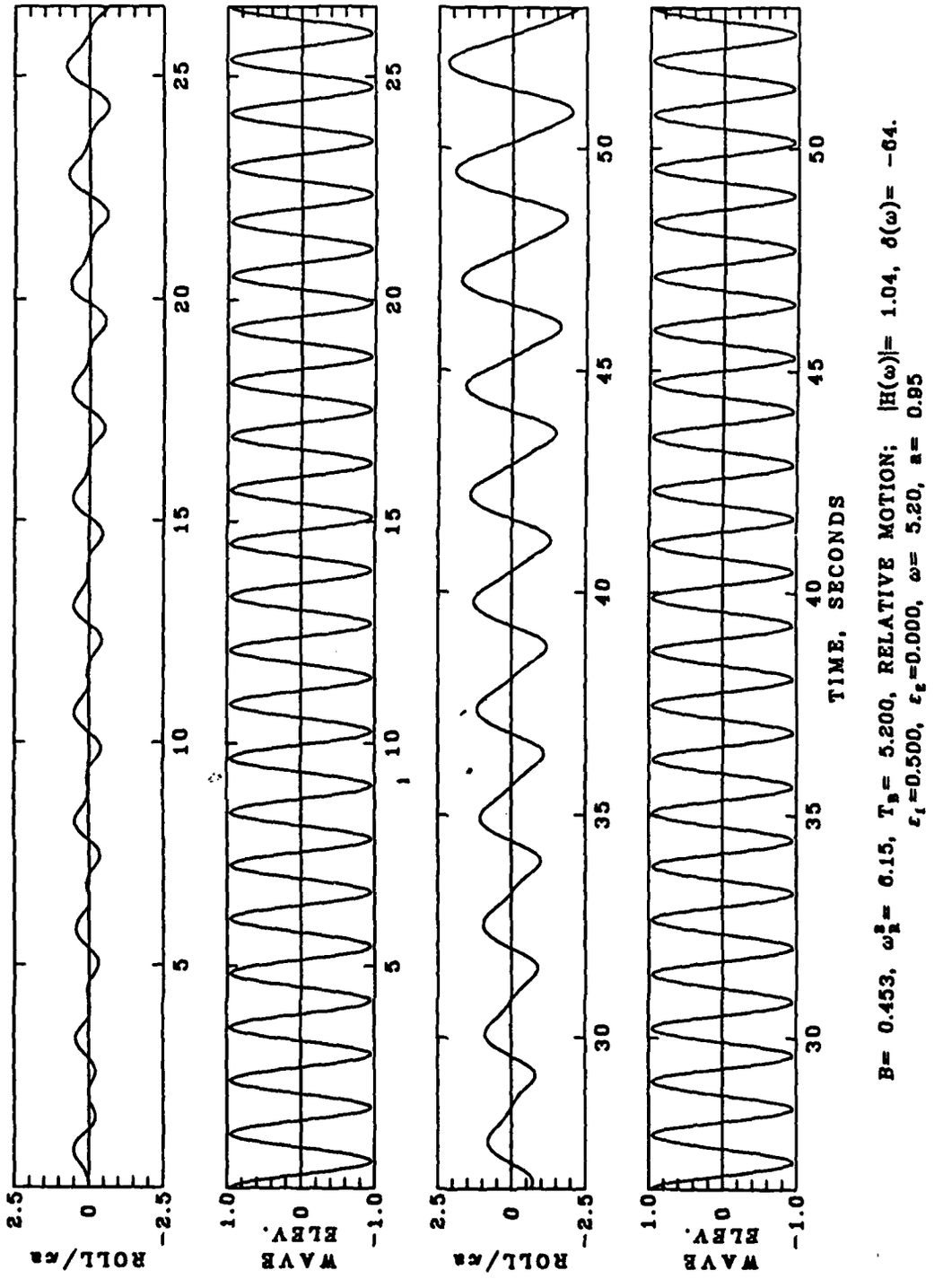

Fig. 40. Analytical time history for epsilon 1= .5, using relative heave at $\omega = 5.20$, and a wave amplitude of 0.95 inches.

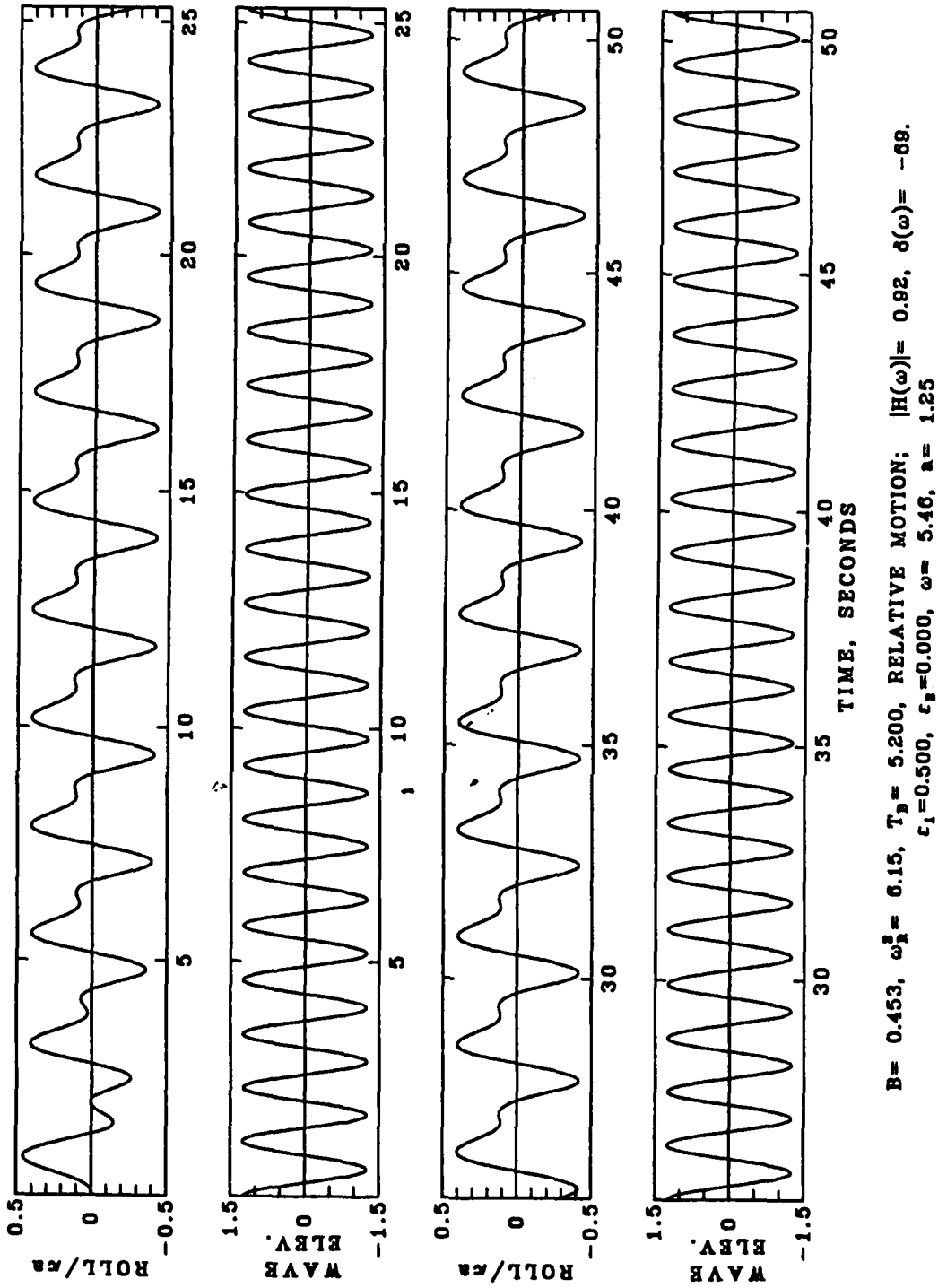

Fig. 41. Analytical time history for epsilon 1= .5, using relative heave at $\omega = 5.46$, and a wave amplitude of 1.25 inches.

Analytical Boundaries

The boundaries of instability were approximated for ε_1 values of 0.25, 0.5 and 1.0 with both the heave and relative heave transfer functions, using the same subjective criteria as with the experimental work. The predicted boundaries for ε_1 values of 0.25, 0.5 and 1.0 using the relative heave transfer function are shown in Fig. 42, and are shown in Fig 43 using the absolute heave transfer function. The approximate boundaries for the absolute and relative heave at $\varepsilon_1 = 0.5$, are compared with the experimental boundary in Fig. 44. The use of the relative heave transfer function has the general effect of causing the subharmonic roll to occur at a lower wave amplitude and shifts the boundaries toward higher frequencies. The bucket of the subharmonic region is lower for the experimental data than for any of the simulated conditions. This might be due to the observed drop in experimental damping at lower oscillation amplitudes. Each of the analytical stability boundaries (all epsilons, relative and absolute heave), appear to be centered at a frequency ratio of 0.95 rather than at 1.0 (observed in experiments). Also, the simple model is clearly unable to explain the recursive nature of the low frequency side experimental boundary. That is, the experimental boundary on the low frequency side curves back on itself, such that there can be multiple values for a given excitation frequency. In any case, the overall results of the analysis show some qualitative agreement.

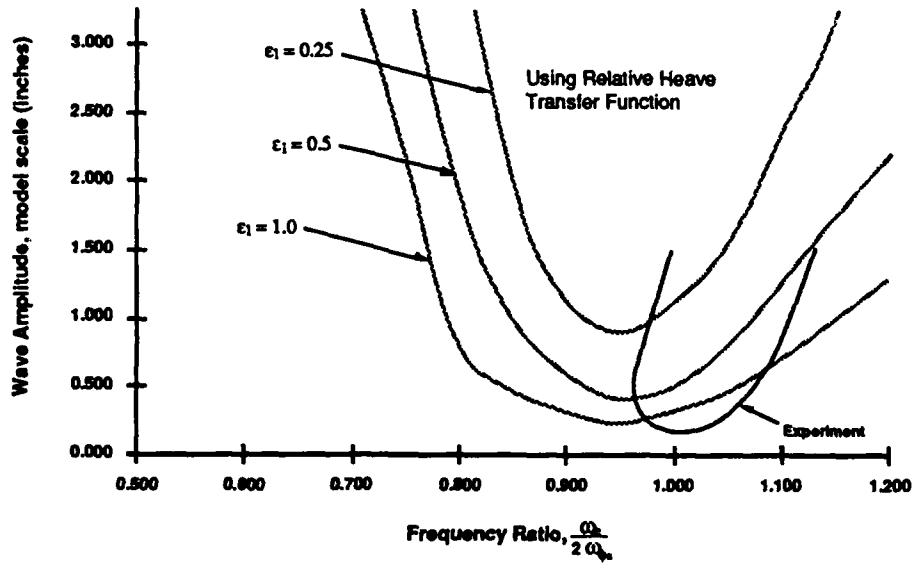

Fig. 42. Approximate stability boundary for epsilon1= .25,.5, and 1.0. using relative heave transfer function.

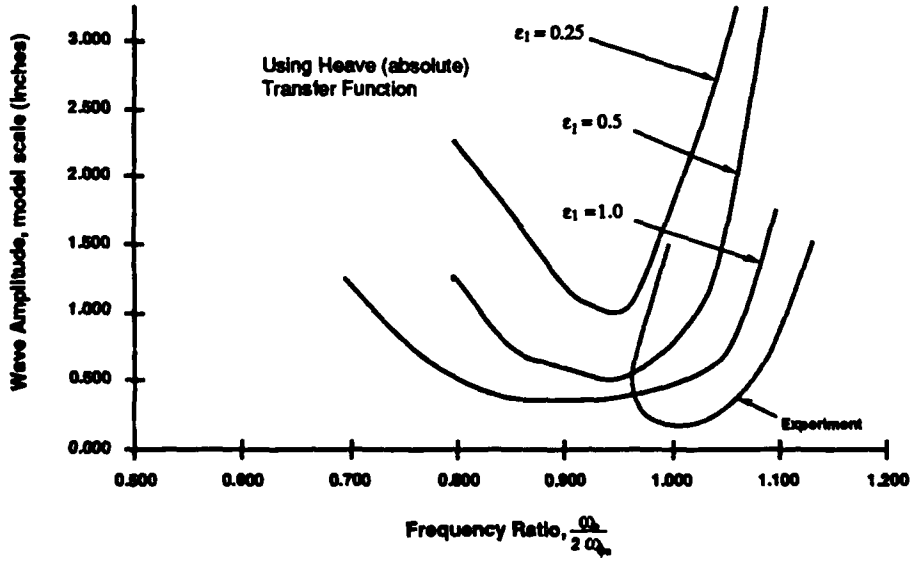

Fig. 43. Approximate stability boundary for epsilon1= .25,.5, and 1.0. using absolute heave transfer function.

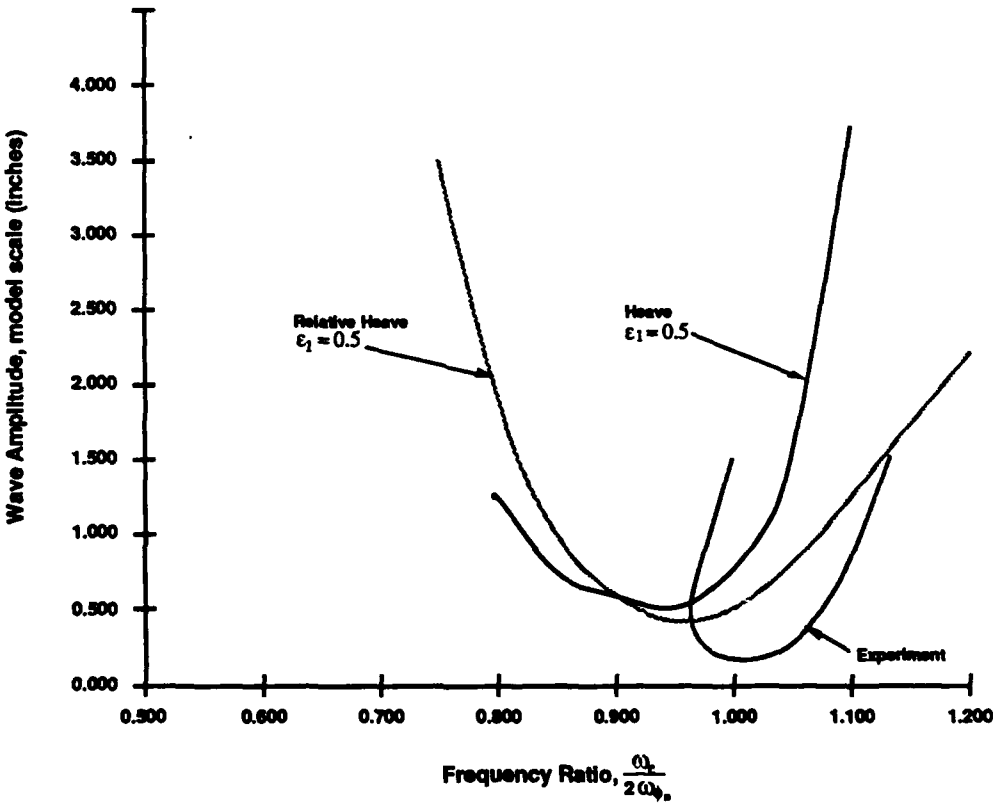

Fig. 44. Comparison of the experimental stability boundary with the approximated boundary for epsilon1= .5, using the absolute and relative heave transfer functions.

ANALYTICAL GMT CALCULATIONS FOR VARIOUS DRAFTS

Ship geometry and mass characteristics were entered into a SWATH hydrostatics program that allowed calculation of the GMt and ship displacement as a function of draft. This was done to provide a quantitative measure of the possible fluctuation of the restoration coefficient as a function of heave motion. The program was run for full scale drafts ranging from 16 ft (4.8 m) above to 11 feet (3.4 m) below the design waterline. Figure 45 presents the ship GMt as a function of draft and the results of the hydrostatics program are also summarized in Table 8.

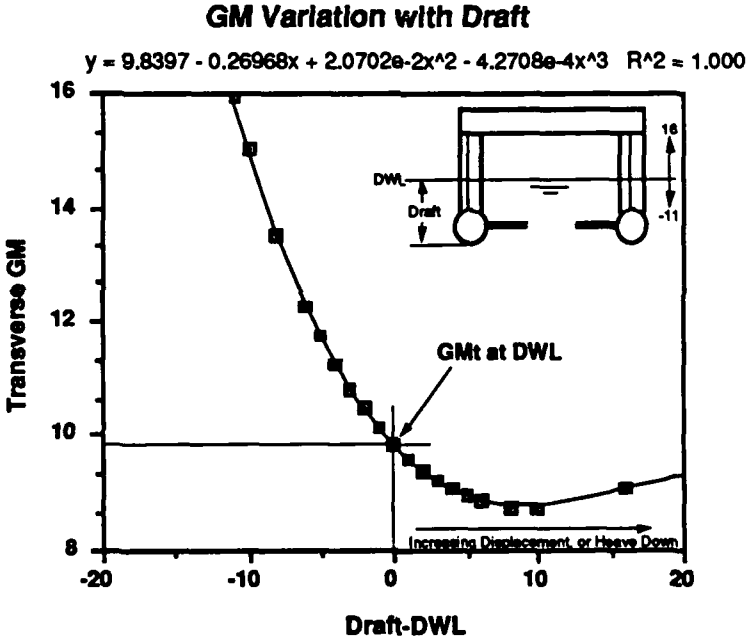

Fig. 45. Transverse metacentric height, GMt, as a function of ship draft.

A calculation of the change in GMt at each draft, as a percentage of the design GMt, is given in Table 9. Also given in Table 9 is the calculation of the percentage change in the restoration moment, as a function of draft. This includes the variation of ship displacement as well as the variation in GMt with draft. The inertial force of a heaving ship in regular waves, however, may cancel out this variation in displacement.

Therefore, as a estimate of an epsilon-like value, the variation in GMt with draft can be obtained from the slope of the curve in Fig. 45. Normalized by static (design) GMt, this calculation yeilds an estimate of epsilon (linear portion) on the order of 0.1 (in model scale, units of 1/inches). For the purpose of this project, the order of magnitude can be considered as "reasonable" correlation with the range of values used in the analysis presented in the previous section.

Table 8. GMt versus draft results from hydrostatics program.

Draft Feet	Displacement L Tons	Max Draft-DWL Feet	GMt Ft.
15.47	2119.20	-11.00	15.93
16.47	2191.40	-10.00	15.03
18.47	2335.79	-8.00	13.50
20.47	2480.19	-6.00	12.26
21.47	2552.39	-5.00	11.73
22.47	2624.59	-4.00	11.26
23.47	2696.78	-3.00	10.84
24.47	2768.98	-2.00	10.47
25.47	2841.18	-1.00	10.15
26.50	2915.54	0.03	9.86
27.47	2985.58	1.00	9.62
28.47	3057.77	2.00	9.41
29.49	3131.42	3.02	9.22
30.47	3202.17	4.00	9.08
31.47	3274.37	5.00	8.96
32.47	3346.56	6.00	8.87
34.47	3490.96	8.00	8.76
36.47	3635.36	10.00	8.73
42.47	4068.54	16.00	9.10

Table 9. Calculations of the change in delta GMt versus draft .

Draft Feet	Displacement L Tons	Max Draft-DWL Feet	GMt Feet	Δ GM, f.s. Dyn.,ft-lbs	$\frac{\Delta GMt-\Delta_o GMt_o}{\Delta_o GMt_o}$	$\frac{GMt-GMt_o}{GMto}$	Max Draft-DWL in, m.s.
15.47	2119.20	-11.00	15.93	75,619,837.4	0.000	0.000	-3.75
16.47	2191.40	-10.00	15.03	73,778,302.1	-0.024	-0.056	-3.41
18.47	2335.79	-8.00	13.50	70,634,289.6	-0.066	-0.153	-2.73
20.47	2480.19	-6.00	12.26	68,111,969.9	-0.099	-0.230	-2.05
21.47	2552.39	-5.00	11.73	67,064,557.7	-0.113	-0.264	-1.71
22.47	2624.59	-4.00	11.26	66,198,357.9	-0.125	-0.293	-1.36
23.47	2696.78	-3.00	10.84	65,482,133.2	-0.134	-0.320	-1.02
24.47	2768.98	-2.00	10.47	64,940,334.1	-0.141	-0.343	-0.68
25.47	2841.18	-1.00	10.15	64,597,068.5	-0.146	-0.363	-0.34
26.50	2915.54	0.03	9.86	64,393,782.7	-0.148	-0.381	0.01
27.47	2985.58	1.00	9.62	64,335,666.3	-0.149	-0.396	0.34
28.47	3057.77	2.00	9.41	64,452,899.2	-0.148	-0.409	0.68
29.49	3131.42	3.02	9.22	64,672,591.0	-0.145	-0.421	1.03
30.47	3202.17	4.00	9.08	65,129,576.1	-0.139	-0.430	1.36
31.47	3274.37	5.00	8.96	65,717,915.6	-0.131	-0.438	1.71
32.47	3346.56	6.00	8.87	66,492,131.3	-0.121	-0.443	2.05
34.47	3490.96	8.00	8.76	68,469,734.5	-0.095	-0.450	2.73
36.47	3635.36	10.00	8.73	71,090,191.9	-0.060	-0.452	3.41
42.47	4068.54	16.00	9.10	82,933,119.4	0.097	-0.429	5.46

Where Δ and GMt are the displacement and transverse GM at each draft, and Δ_o and GMt_o are the design displacement and transverse GM at the DWL, respectively.

CHAPTER 7. SUMMARY AND CONCLUSIONS

The primary objective of this report was to present the results of experiments conducted to identify the boundaries of subharmonic roll response, and to investigate the analogy to the instability displayed by systems having variable spring characteristics. The following comments and conclusions are offered.

1. For the most part, the roll instabilities were observed to be qualitatively what might be expected from a dynamic system with time varying restoration. That is, large amplitude subharmonic rolling occurred at wave excitation frequencies of approximately twice the natural roll frequency (which corresponded roughly to the heave resonance).

2. Certain aspects of the nonlinear behavior were much more complicated than expected.

   a . A *cap* on the stability diagram was observed. For a given fixed frequency, the instability disappears for high excitation amplitudes. This does not accord with the behavior of parametrically excited systems represented by Mathieu's equation or similar equations.

   b. *Steady tilt*, or non zero mean response was observed for high excitation amplitudes. This is also not explainable by the present theory (although it has been observed in previous experiments), and is probably associated with nonlinearity.

   c. The shape of the low frequency side of the experimental stability diagram is dissimilar to that predicted by the simple theory, since it bends in the high frequency direction at the higher excitation amplitudes (i.e. recursive), thus implying stability can be restored at higher wave amplitudes for any given unstable frequency. This is probably related to items 2a, 2b.

   d. Observed roll responses such as, transitions from linear to unstable rolling, growth rates, and steady tilt angles, varied significantly depending on the area of excitation, relative to the stability boundaries. For example, higher frequency and amplitudes of excitation were more likely to result in a combined linear/subharmonic roll response, than at low amplitude-mid-frequency excitation, which resulted typically in large amplitude pure subharmonic response. Also, the increase in roll amplitude varied dramatically depending on the position in the unstable region.

3. This investigation was a first serious attempt to define stability boundaries for the roll motion of a SWATH ship. A number of experimental difficulties were encountered:

a. Unsteady drift rates had an adverse effect on the measurement of encounter frequency, and on the use of harmonic analysis to characterize the model motion responses (as did the growth rate characteristics of subharmonic roll).

b. Wave reflections from the model back toward the wave probe, affected the wave height and frequency measurements. A larger facility and/or the use of an additional wave probe, located off of the carriage might alleviate some of the difficulties caused by reflections.

c. Instrumentation problems were encountered using an ultrasonic transducer for measuring heave, particularly during large amplitude rolling. Alternate methods should be considered.

d. The range in which the towing carriage was able to drift with the model was limited, and in some cases did not allow a sufficient time for the responses to stabilize. A longer range in which to monitor the sway velocity and roll response would be advisable in future studies.

e. The wide variety of observed roll responses (linear, combinations of linear and subharmonic, various amplitudes, growth rates, and steady tilt angles...) made it difficult to form an approach to quantifying, characterizing, and presenting the experimental results in a clear and consistent manner.

4. The semi-intuitive analysis attempted here was qualitatively successful in the sense that it reflected some of the characteristics of the observations in the time domain quite well. It does not predict the experimental stability boundaries too well, probably because of the unexpected behavior noted above (Item 2), and possibly because of neglect of coupling with sway. The order of magnitude of the coupling between heave motion and the time varying part of the roll restoration implied by the simple theory is reflected by hydrostatic computations for the model.

5. A much more realistic analytical model will be required to fully describe or explain SWATH motion behavior. Nevertheless it is believed that the analysis has confirmed the initial speculations that observed subharmonic rolling is connected with heaving motions.

ACKNOWLEDGEMENTS

The author wishes to acknowledge those who contributed significantly to the completion of this project;

- My advisor, Mr. John Dalzell, at DTRC, whose expertise, patience, guidance and effective instruction were much appreciated throughout the stages of this project, and were vital to accomplishing this research.

- Dean Feir, of George Washington University, for his support, encouragement, and involvement throughout the graduate study program, and particularly, for his understanding of the demands on those balancing academic studies with full-time employment at DTRC.

- Dr. Dave Moran and Mr. Steve Callanen of DTRC, for providing facility support during the experiments in the 140 Foot Basin.

- Mr. Jim Fein, manager of the Office of Naval Research (ONR) Applied Hydrodynamics Program, for his support and interest in this work.

- Mr. Ed Numata, formerly of the Stevens Institute of Technology's Davidson Laboratory (retired), for his assistance in providing background information and the SWATH model used in the experiments.

- Coworkers, Mr. Martin Dipper, Mr. Jim Hickok, and Mr. Dan Hayden for providing assistance with the data acquisition system used in the experiments.

- Mr. William Dixon and Mr. Daniel Huminik of DTRC, for providing guidance and assistance in the area of electronics and signal conditioning equipment used in the experiments.

- Machinists, Mr. John Wasko, Mr. Earl Merson, and Mr. Marty Monier, of DTRC, for the guidance and shop support they provided during the experiments.

- and in particular, my wife, Susan, for her patience, support, encouragement, and understanding, as many hours were spent away from home.

BIBLIOGRAPHY

1. Numata, E.,"Experimental Study of SWATH Model Rolling in Beam Seas," SIT-DL-81-9-2200, Davidson Laboratory, Stevens Institute of Technology (August 1981).

2. Timoshenko,S., *Vibration Problems in Engineering*, 3rd ed., D.Van Nostrand Company Inc., Princeton, N.J. (1955).

3. Dean , R. G. and Dalrymple, R. A., *Water Wave Mechanics for Engineers and Scientists*, Prentice-Hall Inc., Englewood Cliffs, NJ (1984).

4. Roberts, J. B., "Estimation of Nonlinear Ship Roll Damping From Free-Decay Data," *Journal of Ship Research*, Vol. 29, No. 2 (June 1985).

5. Dalzell, J. F., "A Note on Form of Ship Roll Damping," *Journal Of Ship Research*, Vol. 22, No. 3 (Sept 1978).

6. Spouge, J. R., "Non-Linear Analysis of Large-Amplitude Rolling Experiments," *Intl. Shipbuilding Progress*, 35, no. 403 (1988).

7. Mathews, J. and Walker, R. L., *Mathematical Methods of Physics*, 2nd ed., W. A. Benjamin, Inc., Menlo Park, California (1970).

8. Paulling, J.R. and Rosenberg, R. M., "On Unstable Ship Motions Resulting from Nonlinear Coupling," *Journal Of Ship Research*, Vol. 3 (1959).

9. Nayfeh, A. H., Mook D. T., and Marshall, L. R., "Nonlinear Coupling of Pitch and Roll Modes in Ship Motion," *Journal of Hydronautics*, Vol. 7 (1973).

10. Nayfeh, A. H., "On Undesirable Roll Characteristics of Ships in Regular Seas," *Journal of Ship Research,* Vol. 32, No. 2 (June 1988).

11. Kallio, J. A., "Seaworthiness Characteristics of a 2900 Small Waterplane Area Twin Hull (SWATH)," DTNSRDC SPD-620-03, David Taylor Research Center (Sept 1976).